Reprogrammable and tunable actuation in multiblock copolymer blends

Cumulative Dissertation
zur Erlangung des akademischen Grades
“Doktor der Naturwissenschaften”
(Dr. rer. nat.)

in der Wissenschaftsdisziplin “Materialwissenschaft”
eingerichtet an der
Mathematisch-Naturwissenschaftlichen Fakultät
der Universität Potsdam
von
Victor Izraylit

Berlin, 2021

Disputation 7.September 2021, Potsdam, Deutschland

Helmholtz Graduate School Macromolecular Bioscience

Universität Potsdam

Helmholtz-Zentrum Geesthacht
Zentrum für Material- und Küstenforschung

Betreuer:	Prof. Dr. Andreas Lendlein	Universität Potsdam
	Prof. Dr. Dieter Neher	Universität Potsdam
Gutachter:	Dr. Jonnathan Blaker	University of Manchester
	Prof. Dr. Jukka Seppälä	Aalto University

Published online on the
Publication Server of the University of Potsdam:
https://doi.org/10.25932/publishup-51843
https://nbn-resolving.org/urn:nbn:de:kobv:517-opus4-518434

Statement of authenticity

I, Victor Izraylit, formally submit my PhD dissertation entitled “Reprogrammable tunable actuation in physically cross-linked multiblock copolymer blends” to the Institute of Chemistry of the Faculty of Mathematics and Natural Sciences at the University of Potsdam in Germany for acquirement of the academic degree of Doctor of Natural Sciences (Dr. rer. nat.) in the Department of Chemistry.

I hereby declare that the work presented in this dissertation is my own original work based on the research carried out at Helmholtz-Zentrum Geesthacht, Institute of Biomaterial Science in Teltow, Germany, from October 2015 to September 2020 under the supervision of Prof. Dr. Andreas Lendlein. To the best of my knowledge and belief, this dissertation does not contain any work previously published or written by another person, except where due reference is made in it. No portion of this work has been previously submitted in the support of any other degree to another university or institute. Any contribution made by others to this research is explicitly acknowledged in the dissertation.

Victor Izraylit

Acknowledgments

At the final sprint of my PhD thesis, I would like to acknowledge everyone who has provided me with their support on this journey and has contributed to its successful completion. First, I would like to thank the advisor of my work Prof. Andreas Lendlein for giving me such an amazing opportunity to pursue my academic title at one of the best facilities in the world. His supervision has welcomingly unveiled to me the world of science with its wonders and miracles. I would like to express my further gratitude to people who daily supervised my work, to my mentor Dr. Karl Kratz, to Dr. Tobias Rudolph and Dr. Oliver Gould. Thank you for being there when I needed an experienced advice.

My special acknowledgement goes to the reviewers of my thesis Dr. Jonny Blaker and Prof. Jukka Seppälä, and the defence committee of Prof. Yan Lu, Prof. Dieter Neher, and Prof. Svetlana Santer for showing your interest in my research.

The completion of my thesis would have never been possible without my colleagues Johan Bäckemo, Dr. Muhammad Farhan, Dr. Matthias Heuchel, Yue Liu, Dr. Ulrich Nöchel, Mark Schröder, Wing Tai Tung, and Wan Yan who were always ready to lend me a hand in the lab and develop new ideas in our fruitful discussions. Thank you Manuela Keller, Yvonne Pieper, Daniela Radzik, and Susanne Schwanz for your invaluable technical support that you have provided to my work. I would also like to express my appreciation to my colleagues Dr. Rainhard Machatschek, Dr. Natalia Tarazona, and Dr. Stephen Quinn. Your work had never explicitly intersected with my thesis, but you were always there to cheer me up.

I would like to mention wonderful coordinators of our PhD programme Patricia Ebel, Dr. Michael Schroeter, and Dr. Anne Schöne, who showed their best at organising the events and communications.

I am saying thank you to my dearest friends Dmitry Cherkasov, Anton Hähnel, Dr. Ivan Lemesh, and Dr. Pavel Yudin, who have showed me their support during these long and labourious years. I am much appreciated for all the joy we shared and your hard work keeping me intact in the hardest periods of this project. Finally, I want to thank my family, especially my father Vladimir Izraylit for your both wise and debatable advises.

I am grateful to the Helmholtz Association for providing its financial support to my project through the programme-oriented financing.

Table of Contents

Abstract

Soft actuators have drawn significant attention due to their relevance for applications, such as artificial muscles in devices developed for medicine and robotics. Tuning their performance and expanding their functionality are frequently done by means of chemical modification. The introduction of structural elements rendering non-synthetic modification of the performance possible, as well as control over physical appearance and facilitating their recycling is a subject of a great interest in the field of smart materials. The primary aim of this thesis was to create a shape-memory polymeric actuator, where the capability for non-synthetic tuning of the actuation performance is combined with reprocessability. Physically cross-linked polymeric matrices provide a solid material platform, where the *in situ* processing methods can be employed for modification of the composition and morphology, resulting in the fine tuning of the related mechanical properties and shape-memory actuation capability.

The morphological features, required for shape-memory polymeric actuators, namely two crystallisable domains and anchoring points for physical cross-links, were embedded into a multiblock copolymer with poly(ε-caprolactone) and poly(*L*-lactide) segments (PLLA-PCL). Here, the melting transition of PCL was bisected into the actuating and skeleton-forming units, while the cross-linking was introduced via PLA stereocomplexation in blends with oligomeric poly(*D*-lactide) (ODLA). PLLA segment number average length of 12-15 repeating units was experimentally defined to be capable of the PLA stereocomplexes formation, but not sufficient for the isotactic crystallisation. Multiblock structure and phase dilution broaden the PCL melting transition, facilitating its separation into two conditionally independent crystalline domains. Low molar mass of the PLA stereocomplex components and a multiblock structure enables processing and reprocessing of the PLLA-PCL / ODLA blends with common non-destructive techniques. The modularity of the PLLA-PCL structure and synthetic approach allows for independent tuning of the properties of its components. The designed material establishes a solid platform for non-synthetic tuning of thermomechanical and structural properties of thermoplastic elastomers.

To evaluate the thermomechanical stability of the formed physical network, three criteria were appraised. As physical cross-links, PLA stereocomplexes have to be evenly distributed within the material matrix, their melting temperature shall not overlap with the thermal transitions of the PCL domains and they have to maintain the structural integrity within the strain ε ranges further applied

in the shape-memory actuation experiments. The fulfillment of the morphological criterion was derived from the microphase structure, consisting of isolated PLA domains within PCL continuous phase with average domain spacing d_0 = 12 – 19 nm. The melting transitions of PCL and PLA stereocomplexes were not overlapping fulfilling the thermal criterion. The structural stability of PLA stereocomplexes was evaluated in a detailed study of the mechanical properties in the single elongation, strain recovery and stress relaxation experiments. At temperature T_{prog} = 70 °C, used at the programming step of the shape-memory actuation, PLA stereocomplexes maintain integrity in the engineering strain range ε < 850%, while limiting PLA stereocomplexes content to φ_c < 6±0.6 wt% broadens ε ranges to up until breakage of the samples. This allows for characterising the PLLA-PCL / ODLA blends as thermomechanically stable physical networks in these composition and ε ranges. These findings provide a valuable design criteria for thermoplastic elastomers and the basic knowledge of the structure-to-property relationship of polymeric matrices cross-linked with PLA stereocomplexation.

Assigning PCL the function of the skeleton-forming and actuating units, and PLA stereocomplexes the role of physical netpoints, shape-memory actuation was realised in the PLLA-PCL / ODLA blends. The selected temperature profile was as follows: the lowest temperature in the shape-memory actuation cycle was set to T_{low} = 0 °C, where PCL reaches its highest crystallinity. The highest temperature in the shape-memory actuation cycle was experimentally optimised as T_{high} = 55 °C. At T_{prog} = 70 °C, the PCL domains were completely molten, but PLA stereocomplexes were below the onset of their melting. Sufficient for shape-memory actuation molecular orientation was achieved at programming strain ε_{prog} > 300%. Further increase of ε_{prog} resulted in no significant within the error of the measurements changes in the actuation capability ε'_{rev}. Further, ε'_{rev} was found to be a function of PLA stereocomplex φ_c, i.e. physical cross-linking density, with a maximum ε'_{rev} = 13.4 ± 1.5% at φ_c = 3.1±0.3 wt%. In this way, ε'_{rev} can be tuned via adjusting the composition of the PLLA-PCL / ODLA blend. This makes the developed material a valuable asset in the production of cost-effective tunable soft polymeric actuators for the applications in medicine and soft robotics.

Zusammenfassung

Weiche Polymer-Aktuatoren haben, dank ihrer Bedeutung bei Anwendungen wie z.B. als künstliche Muskeln in Geräten oder in Medizin und Robotik, maßgeblich Aufmerksamkeit erregt. Das Einstellen ihrer Leistung und die Erweiterung ihrer Funktionalität werden oft mittels chemischer Modifizierung durchgeführt. Die Einführung struktureller Elemente, die durch nicht-synthetische Prozesse hervorgerufene Einstellung von Eigenschaften, sowie die Kontrolle der physikalischen Parameter und die Möglichkeit, das Material erneut zu verarbeiten, sind von besonderem Interesse für das Design von intelligenten Werkstoffen. Das Ziel dieser Doktorarbeit war es einen polymeren Formgedächtnis-Aktuator zu entwickeln, der die durch nicht-synthetische Prozesse hervorgerufene Einstellung der Aktuator Parameter mit erneuter Formgebung kombiniert. Physikalisch vernetzte Polymermatrizen stellen dafür eine solide Materialbasis dar, wobei *in situ* Verarbeitungsmethoden zum Ändern der Zusammensetzung und der Morphologie verwendet werden können. Die Folge davon ist eine präzise Einstellung der entsprechenden mechanischen Eigenschaften und der Formgedächtnis-Aktuator-Leistung.

Die morphologischen Elemente, die für die polymeren Formgedächtnis-Aktuatoren benötig werden, nämlich zwei kristallisierbare Domänen und Verankerungspunkte für die physikalischen Cross-Links, wurden in einem Multiblock-Copolymer aus Poly(ε-Caprolakton) und Poly(*L*-Lactid) Segmenten (PLLA-PCL) integriert. Der Schmelzübergang von PCL wurde auf die aktuierenden und die skelettbildenden strukturellen Einheiten verteilt. Die Cross-Links wurden durch PLA-Stereokomplexe in Blends mit Poly(*D*-Lactid) Oligomer (ODLA) geformt. Eine mittlere Länge der PLLA-Segmente von 12 bis 15 Wiederholeinheiten wurde experimentell als ausreichend zur Formierung von Stereokomplexen bestimmt, aber als zu kurz um isotaktische Kristallisation einzugehen. Die Multiblock-Struktur und Phasendurchdringung verbreitern den Schmelzübergang von PCL und ermöglichen dessen Aufteilung in zwei voneinander unabhängige kristalline Domänen. Das niedrige Molekulargewicht der PLA Stereokomplexe und die Multiblock-Struktur von PLLA-PCL ermöglichen Verarbeitung und auch Wiederverarbeitung von den PLLA-PCL / ODLA Polymerblends mittels üblicher zerstörungsfreier Methoden. Die Modularität der PLLA-PCL Struktur und der synthetische Ansatz ermöglichen die unabhängige Einstellung der Eigenschaften der einzelnen Komponenten. Das entwickelte Polymer-Material bildet eine solide Basis für die durch nicht-synthetische Prozesse hervorgerufene Variation der thermomechanischen und strukturellen Eigenschaften der thermoplastischen Elastomere.

Um die thermomechanische Beständigkeit der hergestellten physikalischen Vernetzung einzuschätzen, wurden drei Kriterien bewertet. Als physikalische Cross-Links müssen die PLA Stereokomplexe gleichmäßig innerhalb des Materials verteilt sein, ihr Schmelzen darf sich nicht mit thermischen Übergängen von PCL Domänen überschneiden, und sie müssen ihre strukturelle Integrität innerhalb des Dehnungsbereichs ε in den Formgedächtnis-Aktuatorexperimenten behalten. Die Erfüllung des morphologischen Kriteriums wurde aus der Mikrophasenstruktur abgeleitet. Diese bestand aus einer kontinuierlichen PCL Phase und den isolierten PLA Domänen mit einem durchschnittlichen Domänenabstand von d_0 = 12 – 19 nm. Die Schmelzübergänge von PLA Stereokomplexen und PCL überschnitten sich nicht, womit das thermische Kriterium erfüllt wurde. Die strukturelle Beständigkeit der PLA Stereokomplexe wurde in einer detaillierten Untersuchung der mechanischen Eigenschaften mittels Zug-, Dehnungsrückstellungs- und Spannungsrelaxationsversuchen nachgewiesen. Bei T_{prog} = 70 °C, der Temperatur für den Programmierungsschritt im Formgedächtnistest, behielten die PLA Stereokomplexe ihre strukturelle Integrität im Dehnungsbereich ε < 850%. Ein PLA Stereokomplexgehalt unter φ_c < 6±0.6 wt% erweitert diesen Bereich bis zur Bruchdehnungsgrenze der Probe. Damit können die PLLA-PCL / ODLA Polymerblends in diesen Dehnungs- und Zusammensetzungsbereichen als thermomechanisch stabile physikalische Netzwerke betrachtet werden. Die Ergebnisse stellen wertvolle Design-Kriterien für thermoplastische Elastomere dar und liefern Grundlagen für die Struktur-Eigenschafts-Beziehung von polymeren Mehrphasensystemen, die mit PLA Stereokomplexen vernetzt sind.

Indem PCL die skelettbildende und die Aktuatorfunktion zugeordnet wurde, und die PLA Stereokomplexe die Rolle des physikalischen Netzwerks übernehmen, lassen sich in den PLLA-PCL / ODLA Polymerblends Formgedächtniseffekte ausführen. Dazu wurde folgendes Temperaturprofil gewählt: Die niedrigste Temperatur des Formgedächtnis-Aktuatorzyklus war T_{low} = 0 °C, dabei hat PCL seine größte Kristallinität. Die höchste Temperatur des Formgedächtnis-Aktuatorzyklus wurde experimentell zu T_{high} = 55 °C optimieret. Bei T_{prog} = 70 °C war die PCL Domäne ganz geschmolzen, jedoch erreichten die PLA Stereokomplexe noch nicht den Anfangspunkt ihres Schmelzbereichs. Die ausreichende molekulare Orientierung für die Formgedächtnis-Aktuation wurde erst ab einer Programmierungsdehnung ε_{prog} > 300% erreicht. Eine weitere Erhöhung von ε_{prog} führte, innerhalb der Fehlergrenze, zu keiner erheblichen Änderung der Formgedächtnis-Aktuation ε'_{rev}. Des Weiteren wurde festgestellt, dass ε'_{rev} eine

Funktion des Gehalts an PLA Stereokomplex φ_c ist, d.h. von der Dichte der physikalischen Cross-Links abhängt. Das Maximum der der Formgedächtnis-Aktuation von ε'_{rev} = 13,4±1,5% wurde bei φ_c = 3,1±0,3 wt% erreicht. Dadurch könnte ε'_{rev} im PLLA-PCL / ODLA System mittels Variation der Zusammensetzung eingestellt werden. Dies verschafft dem entwickelten Polymermaterial ein wertvoller Vorteil bei der Herstellung von kosteffektiven, skalierbaren polymeren Formgedächtnis-Aktuatoren für Anwendungen in der Medizin und der Robotik.

Abbreviation and symbols

AFM	Atomic force misroscopy
DIPC	*N,N′*-Diisopropylcarbodiimide
DMA	Dynamic mechanical analysis
DMAP	Dimethylaminopyridine
DSC	Differential scanning calorimetry
$Đ$	Dispersity
d_0	Average domain spacing
$\Delta\sigma(t)$	Stress decay in relaxation process
E	Young's modulus
ε	Engineering strain
ε_{break}	Elongation at break
ε_A	Shape-memory actuator deformation at T_{high}
ε_B	Shape-memory actuator deformation at T_{low}
ε_H	Hencky strain
ε_e	Elastic contribution to deformation
ε_p	Plastic contribution to deformation
ε_{prog}	Shape-memory actuator programming strain
ε'_{rev}	Reversible elongation
φ_c	Crystal content
G	Shear modulus
GPC	gel-permeation chromatography
λ	Extension ratio
M_n	Number average molar mass
M_w	Weight average molar mass
σ	Stress
σ_{break}	Ultimate tensile strength
σ_c	Stress stored in the elasto-plastic component of the three-component model
σ_n	Stress stored in the elastic component of the three-component model
σ_r	Stress stored in the viscoelastic component of the three-component model

σ_{true}	True stress
σ_0	Reference stress
t	Time
tan(δ)	Loss tangent
T	Temperature
T_g	Glass transition temperature
T_{high}	Highest temperature in the shape-memory actuation cycles
T_{low}	Lowest temperature in the shape-memory actuation cycles
T_m	Melting temperature
T_{onset}	Onset temperature of melting transition
T_{prog}	Programming temperature of shape-memory actuation
τ_r	Relaxation characteristic time
ω	Frequency
PCL	Poly(ε-caprolactone)
ODLA	Poly(*D*-lactide) oligomer
PLA	Polylactide
PLLA	Poly(*L*-lactide)
PLLA-PCL	Multiblock copolymer with PLLA and PCL segments
pTSA	*p*-Toluene sulfonic acid
Q_{eff}	Deformation fixation
SAXS	Small-angle X-ray scattering
TEM	Transitional electron microscopy
w	Mass content
WAXS	Wide-angle X-ray scattering
χ_c	Relative crystallinity

List of figures:

Chapter 1 – Introduction

Soft polymeric actuators

Emerging trends in medicine and robotics emanate the demand for miniaturising of active mechanical elements and embedding multiple functions into a single structural component. The material class, which can actively contract, expand or rotate in response to an external stimulus, playing the actuator role in a dynamic mechanical system, can be consolidated with an umbrella term of artificial muscles.[1] This term was initially introduced by Robert Hooke in 1670s for a gunpowder-actuated piston-based mechanism. Since then, the image of an artificial muscle came a long way from pneumatic or hydraulic pistons and inflatable bladders confined with braided elastic sleeves, e.g. McKibben artificial muscle,[2] to the modern perception of this term as an actuator material. An overview of artificial muscle actuation principles is given in Figure 1.

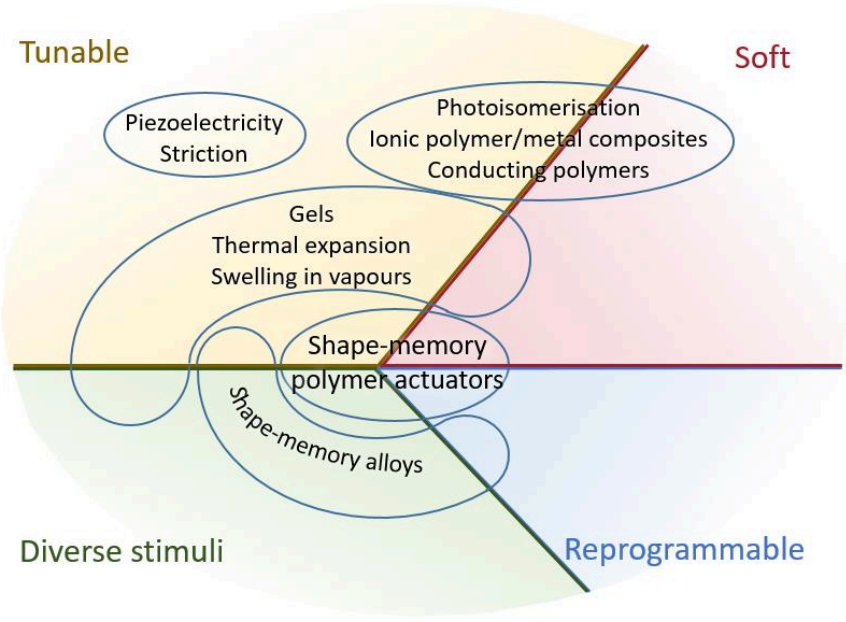

Figure 1. Classification of artificial muscles actuators according to their operation principle and key characteristics.

The physical phenomena underlying actuation in materials can be organised into three principle categories. The first one is based on the mass exchange with the surrounding medium. A typical example of this mechanism would be swelling and deswelling of polymers upon the exposure to

humidity or solvent vapours.[3, 4] Multimaterial design of the actuator, composition gradient or inhomogeneous exposure to the absorbate facilitate tuning of the direction and amplitude of the actuation.[5, 6] Temperature actuation trigger can be realised in gels, where the transition through the upper or lower critical solution temperature switches the material's ability to absorb the medium.[7, 8] One of the most studied material of this category is poly(*N*-isopropylacrylamide) (PNIPAM) based hydrogels. Gel-based actuators typically demonstrate very high actuation strains up to 90%, but very slow response and generate stresses in the order of 1 MPa. Further, absorption of the medium can be activated by an electric potential in conducting polymers such as polypyrrole or polythiophene.[9, 10] Electron exchange between the polymer and an electrode in an electrochemical cell leads to the appearance of an electric charge in the polymer. To neutralise this charge, ions of the electrolyte diffuse into the polymer. The result of this process is a volumetric expansion of polymers, which allows their application as soft-actuators. Despite high amplitudes and manifold possible shapes, actuators based on mass exchange are limited in applications due to the strict requirements to the medium.

The actuation principle of the materials from the second category is the mass transfer inside the material. For example, applying potential difference to an ionic polymer triggers a flux of cations to the cathode. This mass transfer causes swelling of the cation-rich domains and shrinkage of the other volume. The actuation based on this mechanism can be realised in ionic polymer / metal composites.[11-13] Here ionically conductive membrane of a synthetic polymer, such as sulfonated tetrafluoroethylene, or a natural one, such as chitosan or cellulose derivatives, is sandwiched between two electron-conductive electrodes of noble metals or carbon nanostructures. A very high actuation rate of these structures is however counterbalanced by modest generated stresses, instability of the electrolyte, and actuation limited to bending. An interesting, but narrow selection of materials are capable of displacement of the atoms in their lattices under an external field. Such materials are called electrostrictive (e.g. lead magnesium niobate ceramics, poly[(vinylidene fluoride)-*co*-trifluoroethylene], etc.),[14, 15] magnetostrictive (e.g. nickel, $Tb_xDy_{1-x}Fe_2$ alloy, etc.)[16, 17] and photostrictive (e.g. lead zirconate titanate, chalcogenide glasses, etc.).[18, 19] Low actuation strains in order of 1% are offset by high excitation rates in order of 1 μs or even 1 ns.

The third group of the actuator materials generates the macroscopic shape shift via changes in their microscopic structure. Some organic molecules, e.g. azobenzene, undergo *cis-trans* isomerisation upon irradiation with a high-energy photon. Integrating them into oriented polymer chains allows

for creating a directional actuation force.[20, 21] Actuation amplitude in such materials is limited by the differences in dimensions between *cis*- and *trans*-isomers. Certain crystalline structures, e.g. perovskite, ZnO, etc., possess non-zero charge in a unit cell. This property allows these materials for generating mechanical stress subjected to an electric field. This phenomenon is called piezoelectricity.[22, 23] Here, actuation strains generated by this effect are rarely higher than 1%, which is compensated by large generated stresses of >100 MPa and very high energy efficiency up to 90%. Thermal expansion is another phenomenon employed in the design of soft actuators. Anisotropy of the shape change, required for actuation, can be achieved with different approaches. One of them is uneven infiltration of a structural material with a guest material characterised with high thermal expansion coefficient, e.g. paraffin wax.[24] Another approach is based on different thermal behaviour of the crystalline and amorphous domains in oriented polymer fibers.[25, 26] The crystalline domains undergo conventional thermal expansion, while the amorphous domains tend to entropic contraction resulting in an anisotropic shape change of the material. Actuation strain can be enhanced up to 50% by vowing the fibers into a yarn or twisting them.

The term "shape-memory polymer" was initially introduced for polymeric materials, which can memorise and recover their initial shape, the one-way shape-memory effect. The temporary shape is imposed with the programming procedure, where the material is deformed at elevated temperatures or during the cold drawing. The molecular orientation is fixed with supramolecular structures of reduced mobility, remaining beneath the glass transition (T_g) or melting temperature (T_m). The shape recovery effect is achieved due to tendency of the polymer chains to release the stored entropic energy after surpassing the thermal transition point (T_g or T_m).[27-29] The further development of this principle, the shape-memory actuation in polymers is based on entropic contraction of oriented amorphous chains of the actuating units after melting at T_{high} and their oriented crystallisation after cooling to T_{low}. The direction of the shape change is defined at the programming step and maintained by the crystalline skeleton-forming units.[30, 31] A detailed explanation of the mechanism is illustrated in Figure 2. Of note, the described mechanisms for the one-way shape-memory effect and shape-memory actuation are realizable in free-standing articles. Putting a sample under a permanent stress, excludes the requirement for shape-fixating or skeleton-forming units, because the molecular orientation is maintained by external forces. The externally supported molecular orientation in shape-memory actuation experiments under stress typically allows for higher reversible deformations.[32] Comparing to the other physical effects underlying

artificial muscles, shape-memory actuation in polymers is notable for diversity of possible programmable shapes and ability to reprogram the actuation pathway.[33, 34] The generated stresses are typical for the soft polymeric actuators and lie within tens of megapascal. As all temperature-controlled actuators, shape-memory polymer actuators are characterised with modest energy efficiency and their response time is strongly dependent on their thermal conductivity, thickness and thermal capacity of the energy-exchange medium.[35] Although shape-memory actuation in polymers is a temperature transition base phenomenon, the heating can be performed via interaction of a nano-sized filler with e.g. oscillating electromagnetic field,[36, 37] visible light[38] or by transferring energy to the polymer with focused ultrasound.[39]

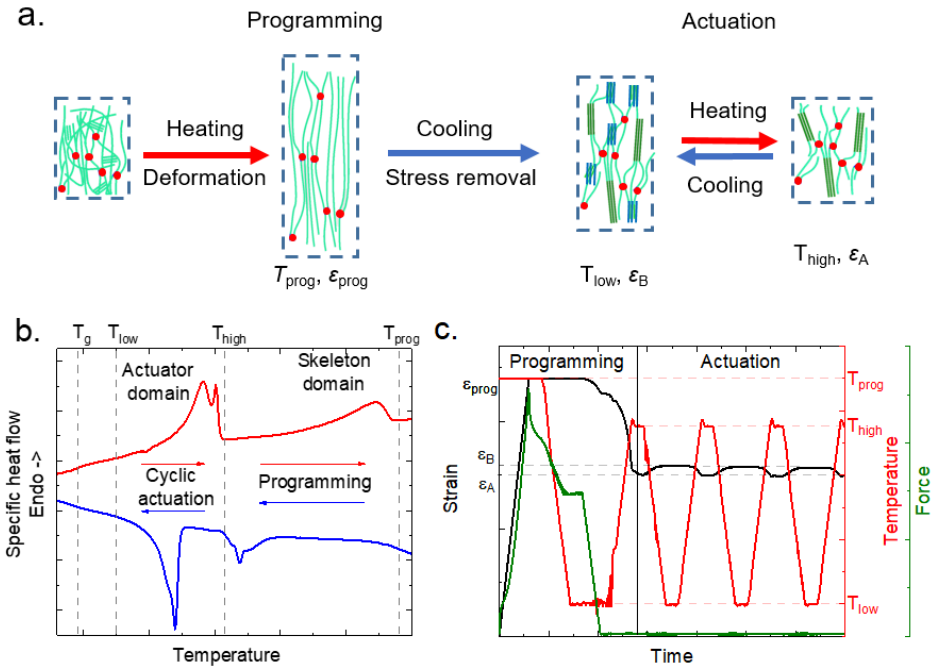

Figure 2. (a) Schematic representation of the morphological changes in a shape-memory actuator matrix during the programming step and cyclic reversible actuation. Melted at T_{prog} sample is elongated to ε_{prog} and crystalised in a deformed state. Macroscopic deformation is transferred to the orientation of the molecular chains with cross-linked network (red dots). The crystalline skeleton domains (green) maintain the orientation of the actuator domains (blue) throughout cyclic temperature change between T_{high} and T_{low}. Melting and crystallisation of the actuator domain drive the reversible shape change. (b) Exemplary DSC curves of a shape-memory actuator. Red – heating, blue – cooling. (c) Evolution of the strain, temperature, and inflicted force through the programming procedure and actuation cycles in a zero-force shape-memory actuation experiment.

Shape-memory actuation is evaluated with efficiency of deformation fixation Q_{eff} and reversible elongation ε'_{rev} calculated with formulae:

$$Q_{eff} = \frac{\varepsilon_A}{\varepsilon_{prog}} \cdot 100\% \quad (1)$$

$$\varepsilon'_{rev} = \frac{\varepsilon_B - \varepsilon_A}{\varepsilon_A + 100} \cdot 100\% \quad (2)$$

where ε_A and ε_B are engineering strains at T_{low} and T_{high} respectively and ε_{prog} is the programming strain (Figure 2c).

The described mechanism can be realised in a polymeric material fulfilling a number of morphological requirements.[32] To avoid corrupting the structural integrity of the skeleton during the cooling-heating shape-memory actuation cycles, the functional domains should possess separate melting transitions. This leads to a phase separation between the constituents of the matrix, where the size of morphological features depends on the miscibility of the polymers.[40] In case of an incompatible dyad, the separation is observed on the micron scale, which nevertheless can provide sufficient interconnection of the domains for realisation of shape-memory actuation.[41] Synthesis of (multi)block copolymers allows reducing the size of morphological features to micrometer or even nanometer scale, which provides even distribution of the skeleton and actuator within the volume of the material.[42] Compatibilisation of the matrix elements can be alternatively achieved by using a material, where one chemical entity with a broad melting transition plays the role of both types of structural units.[43-45] In this case however crystallites with melting temperature closely to T_{high} can be constantly be transferred between domains causing gradual deterioration in the degree of molecular orientation and actuator performance with each subsequent cycle.[43]

Entropic form-transformation mechanism requires presence of an amorphous domain with a glass transition T_g lying in the lower temperature ranges than shape-memory actuation cycle $T_{low} - T_{high}$. Miscible components of the actuation matrix possess a single glass transition of a mixed amorphous phase. Here, mixed T_g can be tuned by the adjustment of the matrix composition following the Fox equation:

$$\frac{1}{T_g} = \frac{w_1}{T_{g,1}} + \frac{w_2}{T_{g,2}} \quad (3)$$

where w_1 and w_2 are the weight content of the constituents in the amorphous matrix and $T_{g,1}$ and $T_{g,2}$ are their glass transition temperatures.

Nonetheless, even if T_g attributed to one of poorly miscible polymers overlaps with the actuator melting transition range, the corresponding change in thermal capacity and mobility of the molecular chains do not exclude the capability of shape-memory actuation.[46]

The cross-linking in shape-memory polymer actuators is traditionally performed with chemical bonds synthetically or by irradiation. Covalent netpoints are evenly distributed within a polymer matrix, possess high activation energy, [47] and their density can be precisely tuned via changing the precursor structure, reaction conditions or irradiation parameters.[48, 49] Although reversible chemical bonds have been reported,[50] covalent networks generally cannot be reprocessed. In terms of shape-memory actuation, this means that the permanent shape and the corresponding actuation pathways of an article are defined at the synthesis step and cannot be further altered. In lieu of the chemical bonding, weaker physical interactions can be used, which can be parted by elevated temperatures or dissolving the material, whereby allowing its reprocessability.[51]

Thermoplastic elastomers

Interactions responsible for physical cross-linking in polymers have to remain stable in the thermomechanical ranges of the material's application. Further, matrix elements responsible for these interactions have to be as small as possible. This would ensure their even distribution in the bulk and increase the relative content of the shape-memory functional domains. Physical interactions between polymer molecules, providing sufficient stability to form a network capable of shape-memory actuation, can be hydrogen bonding,[52-54] e.g. between urethane segments in the backbone of e.g. poly(3*S*-*iso*butylmorpholin-2,5-dione),[46] or ionic interactions[55, 56] formed via e.g. neutralisation of ionasable side methacrylic acid groups with sodium.[57] Besides this, a broad variety of polymers having thermally and mechanically stable crystals provides a wide selection of candidates for the role of physical cross-links.[58, 59]

Some polymers having a stereocentre in their backbone are capable of forming a special type of a regular crystalline structures between their opposite enantiomers called stereocomplex.[60] The driving forces of stereocomplexation are as a rule stronger than the one of the isotactic crystallisation and are comparable with hydrogen bonding,[61, 62] van der Waals forces[63] or ionic interactions.[64] For instance, in situ FTIR analysis shows presence of existence hydrogen bonding between $CH_3\cdots O{=}C$ and $C_\alpha H\cdots O{=}C$ in PLA stereocomplex.[65, 66] This leads to higher crystallisation rates and higher crystallinities than for isotactic crystals. Stereocomplexation results

in an energetically preferable supramolecular configuration characterised by a denser packing of the molecules. This can be derived from an increased comparing to isotactic semicrystalline and amorphous polymer spin lattice relaxation time in NMR.[67] Stronger intermolecular bonds and denser unit cell packing in stereocomplexes effects improved thermal and mechanical properties in comparison with isotactic crystals.[68, 69] High molar mass polymers reinforced with stereocomplex demonstrate resistance to solvents and hydrolysis.[70-72] Those enhancements allow for their utilisation as physical netpoints.[73, 74] Suppositionally, all stereoactive crystallisable polymers can form stereocomplex under appropriate conditions. In practice, achieving the required optical purity can be complicated, hence the reported stereocomplex crystals are limited.

Representative examples of stereocomplexable polymers can be found among aliphatic polyesters,[75-77] polycarbonates,[61, 78] polyamides[79, 80] or polyketones.[81] Stereocomplex formation occurs not necessarily between homopolymers of different optical conformation of one polymer. It can happen between cyclic molecules,[82, 83] copolymers[84, 85] or oppositely configured different polymers.[86, 87] Poly(methyl methacrylate) was the first polymer reported to undergo specific interactions between its forms of opposite tacticities.[88, 89] Nowadays, polyester stereocomplexation gains significant attention due to sustainability of their production, renewability of the resources, degradability of the materials, and diversity of their applications. [60] Whereas long-known polyesters capable for stereocomplexation, like poly(2-hydroxybutanoic acid)[76] and poly(2-hydroxy-3-methylbutanoic acid)[90] are undeservedly poorly studied, polylactide (PLA) stereocomplexes gain significant attention due to broad availability of the raw material, its easy manufacturing, and outstanding for biodegradable polymers properties.[91, 92] Its substitutes are capable of bearing functional side-groups, e.g. azide, alkyl, benzyl, etc., changing its reactivity or physical behaviour, nonetheless retaining a stereocentre in the backbone, thus the capability for stereocomplexation.[93-95]

Besides having an optically active carbon, the CH_3-group in a PLA repeating unit can be oriented co- or anti-directional with the C(O)-O vector subdividing them into upward and downward respectively. (Figure 3a) The most common conformation of PLA isotactic crystals is the α form packed as the pseudo-orthorhombic unit cell.[96] Here, the upward and downward helical chains of the same stereo-form are packed in the centre and corners of the cell respectively. This conformation of PLA shows disorder in the domain level and gives no energetically stable arrangements of the chains.[96]

The most recent view on the crystalline structure of PLA stereocomplex suggests that it consists not necessary of equimolar ratio of *L*- and *D*-enantiomers, but their content can vary from 30/70 to 70/30.[97] Its trigonal unit cell exists in a space group of a low symmetry *P*3, where one lattice site can be occupied by the upward *L*- or downward *D*-lactide chain and another by the downward *L*- or upward *D*-lactide chain depending on the *L*/*D* ratio of the blend. A schematic of PLA stereocomplex crystalline lattice is presented in Figure 3b.

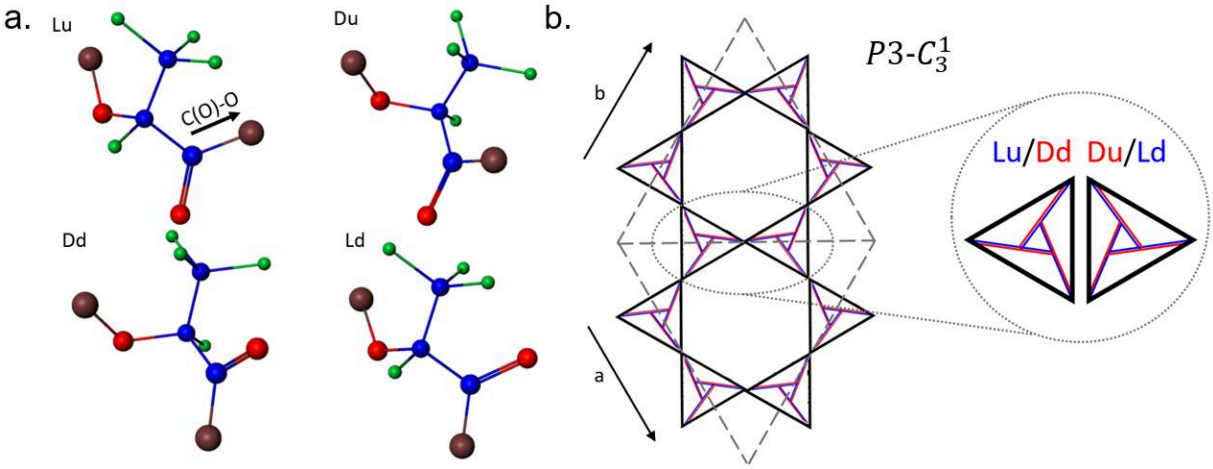

Figure 3. (a) Spatial conformations of a PLA repeating unit of different tacticity (*L*/*D*) and orientation of the CH_3 group along the +*c*-axis (C(O)-O vector) (u/d). Brown – further polymer chain **(b)** Schematic representation of the PLA stereocomplex crystalline structure in projection along *c*-axis. The lattice is occupied with *L*- and *D*-LA repeating units, where the probability of the couple composition equals to PLLA/PDLA ratio, but lies within 70/30 – 30/70 ratio. Blue – *L*-lactide repeating units, red – *D*-lactide repeating units representing possibility of having either of them in the lattice.

PLA stereocomplex is formed in procedures typical for polymer crystals. Being a more energetically preferable conformation than isotactic crystals, PLA stereocomplex has preference during crystallisation. PLA stereocomplex crystallites have been reported to require shorter PLA molecule length than isotactic crystals (7 against 11 repeating units).[98] Shorter polymer molecules engaged into crystallite formation favour smaller sizes of these crystallites. This allows reducing the size of physical netpoints beneficial for shape-memory actuation. Due to high activation energy

PLA stereocomplex consisting of high molar mass polylactides typically cannot be dissolved.[99] However, decrease of the molar mass of the components or incorporation of the PLA constituent chains into a copolymer decreases PLA stereocomplex T_m and significantly improves its solubility.[98]

Improved thermomechanical stability of PLA stereocomplex elaborates its application as physical cross-links in hydrogel production[100-102] and in bulk.[103, 104] Formation of a network can be demonstrated as a transition between rheological liquid- and solid-like behaviour of asymmetric PLLA/PDLA blends.[105, 106] Providing firm physical network, PLA stereocomplex at certain conditions and matrix composition grants a material without covalent cross-links an elastic rubber-like behaviour.[107-109] Combination of elastomeric mechanical properties and processing flexibility of thermoplastics named this class of materials thermoplastic elastomers.[110] However, as all crystallites PLA stereocomplexes undergo a multi-step elasto-plastic process upon macroscopic deformation of the material, which can divorce them from being firm network junctions.[111]

Deformation of semi-crystalline polymers

The crystalline domains in an undeformed semi-crystalline polymer are dispersed within the amorphous matrix. They consist of lamellae organised into larger spherulites, which experience elasto-plastic structural changes induced by macroscopic deformation passing through several strain threshold (Figure 4a).[111, 112] Initially, the deformation is purely elastic and the crystallites are not affected. [113] After reaching the true elastic limit, the stresses stored in the amorphous domains become large enough and begin being redistributed to the crystallites, causing random effects of shear, slip and rotation within the spherulites. As the stress gradually increases, the plastic movements inside the crystallites are set into the collective motion at the elastic limit. Macroscopically, the elastic limit is associated with the yielding behaviour and neck initiation.[114] Further stretching causes disintegration of the crystallites through fibrillation, accompanied by partial loss of crystallinity and subsequent strain-induced crystallisation.[115-117] Finally, the stresses accumulated in the amorphous matrix become so high that disentangling happens and the material loses memory of its initial shape.[118] Transition between these deformation regimes causes changes in microscopic mechanical behaviour of a polymer, namely different contributions of elastic ε_e and plastic ε_p deformation of the amorphous and crystalline domains respectively.[119] At the onset of fibrillation, crystallites including PLA stereocomplexes fail to preserve structural integrity and can

no longer provide firm cross-linking to the matrix. The attribution of the strain ranges to different deformations mechanisms determines elongation limits, at which crystallites maintain structural integrity.

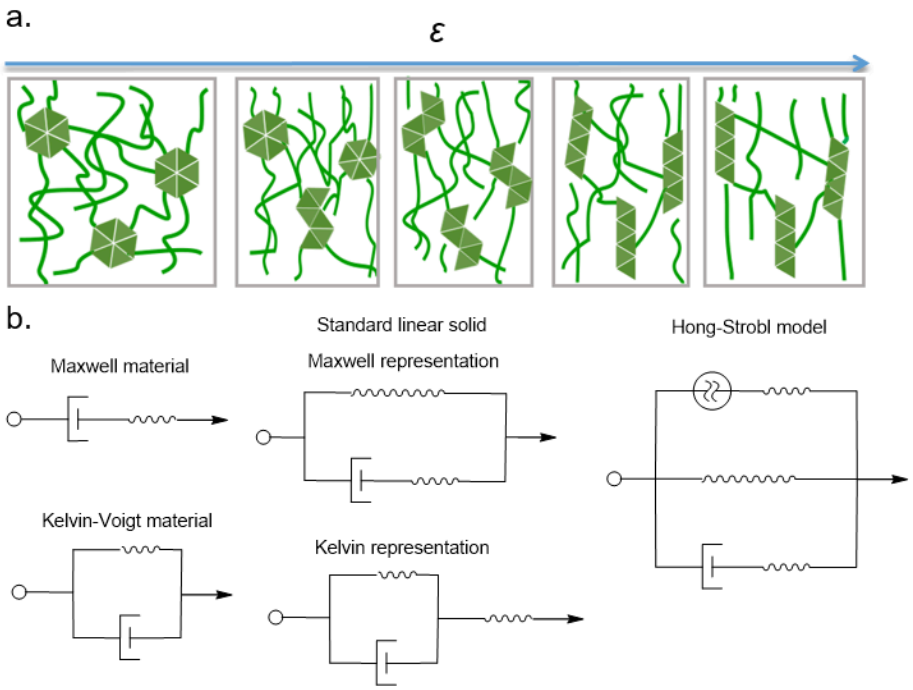

Figure 4. (a) Schematic illustrating changes in the microscopic structure of a semi-crystalline polymer during the deformation going through the elastic matrix stretching, crystallite sliding, fibrillation and amorphous network disentangling. **(b)** Generalised models of solid materials.

The viscoelastic deformation of polymers is often described with generalised models for linear solid materials. (Figure 4b) The Maxwell and Kelvin-Voigt models visualise material deformation behaviour with a spring and dashpot connected in series or in parallel respectively.[120] These models have created a solid platform for characterisation of materials' mechanical behaviour. However, the Maxwell model fails to describe creep and recovery, and the Kelvin-Voigt model does not explain relaxation. Their further development, the Zener model or the standard linear solid model, manages both phenomena, giving a basis for description of the elastic and viscoelastic behaviour of materials including thermoplastic polymers.[121, 122] For instance, Haward and Thackray proposed an assumption, in which at the limit of high strains, stresses stored in the amorphous network of a semi-crystalline polymer become predominant.[123] The material behaves as an ideal rubber and the

plot of true stress as the function of extension ratio $\sigma_{true}(\lambda^2 - \lambda^{-1})$ reaches its asymptotic limit. This model allows for calculating stresses distributed over the amorphous network as:

$$(1 - \varphi_c)\sigma_n = (1 - \varphi_c)G(\lambda^2 - \lambda^{-1}) \quad (4)$$

where φ_c in the crystalline content, σ_n in the stress stored in the amorphous network, G is the shear modulus, and λ is the extension ratio.

The process of viscoelastic stress relaxation in polymers is typically described with Eyring viscosity equation.[124-126] However, complexity of polymer systems makes it practically unsolvable without numerous assumptions. One of the recent stress relaxation model derived from Eyring's law of viscosities in relation to a Maxwell material was proposed by Hong *et al.*[127]:

$$\Delta\sigma(t) = \sigma_r(0) - 2\sigma_0 \operatorname{atanh}\left[\tanh\left(\frac{\sigma_r(0)}{2\sigma_0}\right)\exp\left(-\frac{t}{\tau_r}\right)\right] \quad (5)$$

where $\Delta\sigma(t) = \sigma_r(t = 0) - \sigma_r(t)$ is the stress decay in a relaxation process, σ_0 is the Eyring's reference stress and τ_r is the relaxation characteristic time. Three fitting parameters are involved in this equation: $\sigma_r(0)$ – the stress that will relax in infinite time, σ_0 is the characteristic stress representing the slope of the stress relaxation curve in $\Delta\sigma_r(\ln t)$ coordinates and the characteristic time of the process τ_r.

The deformation process of the crystalline domains is typically described phenomenologically. An elastoplastic component was added to the Maxwell representation of the Zener model by Strobl's group.[127, 128] In this instance, the reaction of the crystalline domains to the deforming stress is the residual of subtraction of the elastic and viscoelastic components from the aggregated stress. With this approach, forces responsible for crystallite, i.e. physical netpoints, deformations can be estimated at each applied strain.

Chapter 2 – Aims and strategy

The majority of shape-memory polymer actuators are fixed to a single permanent shape. Furthermore, tuning of the actuator performance is often related to chemical modifications of the material. The primary aim of this thesis was to design and create a physical interaction for a shape-memory polymer actuator matrix, allowing for its reprocessability and non-synthetic tuning of its actuation performance.

A multiblock copolymer architecture provides a flexible platform for embedding anchoring points for physical cross-linking into a shape-memory polymer actuator. Further, the network junctions can be introduced into the material by addition of a cross-linking moiety with an *in situ* processing method. The reversibility of the intermolecular interactions facilitates a reset of the sample thermal history and geometry with non-destructive processing techniques. The cross-linking density regulated by the concentration of the low molar mass additive orchestrates the morphology, structure, the related thermal and mechanical properties, and actuation performance of the designed material.

The work has been divided into three consecutive steps. At the first step, a polymeric material fulfilling the morphological requirements for shape-memory polymeric actuators has been created. Further, the designed physical interaction was examined to fulfill the morphological, thermal and mechanical criteria for stable physical cross-links. Explicitly, whether their physical properties permit them to maintain structural integrity in the thermal and deformational ranges of the shape-memory transitions, and whether it is possible to reduce netpoints sizes, maximising the content of the functional shape-memory units. Finally, the shape-memory actuation in the developed materials was studied and the approaches for its tuning were analysed. The realisation of their concept has been approached with the following strategies:

1. The multiblock copolymer would consist of immiscible PCL and PLLA. Here, phase dilution typical for multiblock copolymers provide PCL with a broad melting transition, which can be bisected into two distinct crystallisable domains with a separation temperature. PLLA acts as the anchoring point for PLA stereocomplexation in blends with PDLA oligomer. The multiblock structure and short length of the multiblock copolymer segments ensure presence of the mixed amorphous phase, where T_g can be adjusted by the multiblock copolymer composition.

2. Multiblock structure would contribute to formation of nano-scale PLA domains limiting the size of PLA stereocomplexes to these domains, which leads to their even distribution in the matrix. Comparatively short length of PLA chains required for stereocomplexation allows for reducing their sizes as physical netpoints and maximising the content of the skeleton-forming and actuating units. High difference in melting temperatures between PCL crystallites and PLA stereocomplexes prevents the melting of the latter during the thermal transitions of the first. PLA stereocomplexes' microscopic structural transformations upon the macroscopic deformation of the blends can be investigated with the methodology of the adopted three-component model. The strain and compositional ranges, where PLA stereocomplexes maintain integrity as physical netpoints of the matrix, can be defined as the conditions, at which the deformation behaviour of the materials cannot be attributed to fibrillation or amorphous matrix disentanglements. Deformation regimes at lower strains are followed by rotation, shear and slipping of the crystallites and do not reach the threshold, at which PLA stereocomplexes fail as the network junctions.
3. PCL crystallites would bear the function of both the skeleton and actuator. PLA stereocomplexes would provide a physically cross-linked network. The effect of the adjustment of thermomechanical treatment and blend composition on shape-memory actuation would be studied.

Attributing the desired functions to the segments of the multiblock copolymer PLLA-PCL requires a precise control over their length. Moreover, a large amount of chain entanglements corresponding to high molar masses is required to reach higher elasticity and deformation stability of polymeric materials. A multiblock copolymer with the designed molecular architecture will be synthesised via self-polycondensation reaction of diblock macromonomers of PCL and PLLA. Here PCL will be used as initiator in a ring-opening polymerisation of *L,L*-dilactide. High rates of *L,L*-dilactide polymerisation will reduce the reaction time, which would prevent the undesidred transesterification reactions. The self-polycondensation reaction will be conducted at ambient temperature in solution using dimethylaminopyridine *p*-toluenesulfonate as a catalyst and *N,N′*-diisopropylcarbodiimide as an activating agent. The molecular structure of the synthesised copolymer will be studied with proton magnetic resonance spectroscopy (^{1}H NMR) and gel-permeation chromatography (GPC). Further, the PLLA-PCL / ODLA blends will be prepared as solution casted films. The formation of PLA stereocomplex and its crystallinity will be

investigated with wide-range X-ray scattering (WAXS) and differential scanning calorimetry (DSC). The thermal properties of the pure PLLA-PCL and its ODLA blends, namely PCL melting and crystallisation transition and presence of the PCL / PLA mixed glass-transition temperature, will be investigated with dynamic mechanical analysis (DMA) and DSC. The phase morphology of the synthesised materials, as morphological feature size and distribution of the constituents in the material matrix will be studied with transmission electron microscopy (TEM), atomic force microscopy (AFM) and analysis of the small-angle X-ray scattering (SAXS) correlation function.

The effect of PLA stereocomplex concentration on the mechanical properties of the synthesised materials will be investigated in a series of single elongation experiments. Further, the stability of stereocomplexes will be investigated with techniques proposed by the three-component model for mechanical deformation of semi-crystalline polymers as follows: The stress-strain curves will be decomposed into reversible and irreversible contribution in the step-cycle experiment. A sample is stretched to a certain elongation and then the stress is removed to 0. In each following cycle the sample is stretched to a higher strain. The recovered ε_e and unrecovered ε_p deformation is compared as the curves $\varepsilon_{e,p}(\varepsilon_H)$ or $\varepsilon_{e,p}(\sigma_{true})$. The points of simultaneous abrupt change in the profile of the curves signify the transition between the macroscopic deformation behaviour attributed to different microscopic deformation mechanisms of crystallites. Initiation of fibrillation is assumed to be the strain limit for PLA stereocomplex structural integrity. The relaxation behaviour of the pure PLLA-PCL and its ODLA blends will be studied to calculate the viscoelastic reaction of the materials to the applied stress. The reaction of the purely elastic network will be calculated in the ideal rubber approximation. The distribution of the stresses between the viscoelastic, elastic and elasto-plastic components of the adopted model in a range of strains and compositions will be used to understand the limits for network-like behaviour of the PLA stereocomplex cross-linked matrix.

The actuation performance will be investigated in cyclic thermomechanical experiments. The programming parameters T_{prog} and ε_{prog} as well as T_{low} will be determined with DSC and the tensile studies to determine how they influence shape-memory actuation capability. The PCL crystallinity will be bisected by T_{high} into the actuating and skeleton-forming units. Variation of T_{high} will be used to change the ratio of actuating to skeleton-forming units, and to optimise the thermomechanical treatment to maximise ε'_{rev}. Further, the ratio of PLLA-PCL and ODLA in the composition of the blend will be changed to adjust the PLA stereocomplex content. The effect of the PLA stereocomplex content, i.e. physical cross-linking density on ε'_{rev} will be studied.

Chapter 3 – Organisation of the thesis

This cumulative dissertation aims to design, create and characterise a shape-memory polymeric actuator system, where an in situ technique of controlling the physical cross-linking density allows for reconfiguring the material geometry and tuning the actuation performance with non-destructive processing methods. The content of the incorporated chapters is outlined below.

Chapter 1 titled 'Introduction' is a description of the research background prior to the start and its significant developments during the completion of PhD project.

Chapter 2 titled 'Aims and Strategy' describes motivation aims, the hypothesis formulated, and strategies employed in this thesis.

Chapter 3 titled 'Organisation of the Thesis' presents the organisational structure of the thesis.

Chapter 4 titled 'Investigating the phase-morphology of PLLA-PCL multiblock copolymer / PDLA blends cross-linked using stereocomplexation' – Appendix I.

Chapter 5 titled 'Strain recovery and stress relaxation behaviour of multiblock copolymer blends cross-linked with PLA stereocomplexation' – Appendix II.

Chapter 6 titled 'Controlling actuation performance in physically cross-linked polylactone blends using polylactide stereocomplexation' – Appendix III.

Chapter 8 titled 'Discussion' is an overall discussion of the findings of this work.

Chapter 9 titled 'Summary and Outlook' summarises the results of this work and potential future prospects.

Chapter 4 – Investigating the phase morphology of PLLA-PCL multiblock copolymer / PDLA blends cross-linked using stereocomplexation

Summary

In this publication, we investigate the morphological structure of physically cross-linked PLLA-PCL / PDLA blends. The effects of the blend composition and the PLLA-PCL molecular structure on the morphology are elucidated with AFM, TEM and SAXS. We identify the formation of a lattice pattern, composed of PLA domains within a PCL matrix, with an average domain spacing d_0 = 12–19 nm. The size of the PLA domains were found to be proportional to the block length of the PCL segment of the copolymer and inversely proportional to the PDLA content of the blend. By elucidating the phase structure and thermal character of the multifunctional PLLA-PCL / PDLA blends, we illustrate how composition affects the internal structure and thermal properties of multicomponent polymeric materials.

Contribution to the publication

- Literature review
  - Phase morphology of polymer blends and copolymers
  - Compatibilisation of immiscible or poorly miscible multi-material polymeric matrices
  - Role of crystallisation in phase separation
  - Formation of PLA stereocomplex in copolymers
- Study design in discussions with the co-authors
  - Material selection and PLLA-PCL multiblock copolymer structure
  - PLLA-PCL / PDLA blends composition
  - Miscibility of components and phase separation
- Experimental work
  - Multiblock copolymer PLLA-PCL synthesis and PLLA-PCL / PDLA blends preparation
  - Characterisation of the synthesised PLLA-PCL molecular structure with NMR and GPC, investigation of the thermal properties of the PLLA-PCL / PDLA blends with DSC and DMTA
- Analysis and interpretation of the data
  - Interpretation of mutual dependency between molecular structure of PLLA-PCL and PDLA with thermal properties of their blends
  - Deduction of the phase structure of the PLLA-PCL / PDLA blends according to their thermal properties

- Analysis of the PLA and PCL domains distribution in the amorphous matrix
- Calculation of domain sizes with the correlation function

- Manuscript preparation
  - Manuscript outline in discussions with the co-authors
  - Writing the first draft of the manuscript
  - Manuscript revision and finalisation according to comments of the coauthors

Publication – Appendix I

Victor Izraylit, Oliver E.C. Gould, Karl Kratz, Andreas Lendlein, Investigating the phase-morphology of PLLA-PCL multiblock copolymer / PDLA blends cross-linked using stereocomplexation. *MRS Advances* **2019** *5* (14-15), 699-707

Chapter 5 – Strain recovery and stress relaxation behaviour of multiblock copolymer blends cross-linked with PLA stereocomplexation

Summary

In this publication, we evaluate whether PLA stereocomplexes can form stable physical cross-links in PLLA-PCL / PDLA blends. Through the investigation of the strain recovery in the step-cycle experiments and compliance of the stress relaxation behaviour with a three-component model for the deformation of semi-crystalline polymers, PLA stereocomplexes were found to possess sufficient stability in the true strain range $\varepsilon_H < 2.25$ to be described as firm physical netpoints at 70 °C in the studied blends with PLA stereocomplex content $\phi_{c\,SC} \geq 1.1$ wt%, when the PCL domains are melted. Limiting $\phi_{c\,SC} \leq 6$ wt% broadens the behaviour inherent to elastic cross-linked networks to the strain values up until breakage of the samples, while the increase of $\phi_{c\,SC}$ triggers plastic deformations typical for semi-crystalline polymers. Redistributing of internal stresses from the amorphous to crystalline domains at increase of ϕ_c, calculated with the adopted model, was identified as a reason of PLA stereocomplexes failure as stable physical network junctions at higher $\phi_{c\,SC}$. Within the experimentally determined strain and composition ranges, in which PLA stereocomplexes possess structural stability, they can form robust cross-links in a polymer network.

Contribution to the publication

- Literature review
  - Physical polymeric network junctions
  - Strain recovery and stress relaxation in polymeric networks
  - Molecular models for deformation of semi-crystalline polymers
  - Thermomechanical behaviour of PLA stereocomplex
- Study design in discussions with coauthors
  - Material selection
  - Selection of the three-component model
  - Developing the experimental procedure for strain recovery and stress relaxation experiments
  - Design of the ex-situ WAXS experiments
- Experimental work
  - Multiblock-copolymer PLLA-PCL synthesis and PLLA-PCL / PDLA blends preparation

- Creating a setup for the real-time video control of sample cross-section in mechanical experiments
- Conducting single elongation, step-cycle and stress relaxation experiments

- Analysis and interpretation of the data
  - Decomposition of deformation into subsequent strain ranges attributed to different deformation regimes of crystallites
  - Decomposition of the imposed stresses among viscoelastic, elastic and plastic contributions
  - Justification of characterizing PLLA-PCL / PDLA blends as physically cross-linked networks
  - Determination strain and composition limits for network-like and typical for semi-crystalline polymers behaviour
  - Experimental proof of PLA stereocomplexes fibrillation with WAXS indirectly observed in mechanical experiments

- Manuscript preparation
  - Manuscript outline in discussions with the co-authors
  - Writing the first draft of the manuscript
  - Manuscript revision and finalisation according to comments of the coauthors

Publication – Appendix II

Victor Izraylit, Matthias Heuchel, Oliver E.C. Gould, Karl Kratz, Andreas Lendlein, Strain recovery and stress relaxation behaviour of multiblock copolymer blends cross-linked with PLA stereocomplexation. *Polymer* **2020** *209*, 122984

Chapter 6 – Controlling actuation performance in physically cross-linked polylactone blends using polylactide stereocomplexation

Summary

The subject of this publication was PLLA–PCL multiblock-copolymer. By harnessing the stereocomplexation of copolymer chains with PDLA, we provide anchoring points for physical network formation and demonstrate how a blending process can be used to efficiently vary the mechanical properties of a shape-memory actuator. We investigate the effect of molecular structure on the actuation performance of the material in cyclic thermomechanical tests, with a maximum reversible shape change $\varepsilon'_{rev} = 13.4 \pm 1.5\%$ measured at 3.1 wt% of PLA stereocomplex content in the multiblock copolymer matrix. The thermophysical properties, crystalline structure, and phase morphology were analyzed with DSC, WAXS and AFM respectively, elucidating the structure-to-function relationship in physically cross-linked blended materials. The work demonstrates a one-step technique for manufacturing a polymeric actuator and tuning its performance in situ.

Contribution to the publication

- Literature review
  - Soft polymer actuators
  - Shape-memory actuation in physical polymeric networks
  - Multi-block copolymer synthesis
  - Thermomechanical behaviour of PLA stereocomplex
- Study design in discussions with the co-authors
  - Material selection and PLLA-PCL multiblock copolymer structure
  - Synthetic approach to PLLA-PCL
  - PLLA-PCL / PDLA blends composition and preparation technique
- Experimental work
  - Multiblock copolymer PLLA-PCL precursor and self-polycondensation catalyst synthesis
  - PLLA-PCL and PDLA synthesis, PLLA-PCL / PDLA blends preparation

  - Characterisation of the synthesised PLLA-PCL molecular structure with NMR and GPC, investigation of the thermal properties of the PLLA-PCL / PDLA blends with DSC and DMA
  - Conducting thermomechanical experiments (shape-memory actuation)
- Analysis and interpretation of the data
  - Identification of the averaged PLLA-PCL multiblock-copolymer molecular architecture
  - Identification of PLLA-PCL / PDLA blends crystalline structure
  - Analysis of critical parameters affecting shame-memory actuation capability
  - Identification of the blend composition as the key parameter for tuning the actuation performance
- Manuscript preparation
  - Manuscript outline in discussions with the co-authors
  - Writing the first draft of the manuscript
  - Manuscript revision and finalisation according to comments of the coauthors

Publication – Appendix III

Victor Izraylit, Tobias Rudolph, Oliver E.C. Gould, Karl Kratz, Andreas Lendlein, Controlling actuation performance in physically cross-linked polylactone blends using polylactide stereocomplexation. *Biomacromolecules* **2020** *21*, 338-348.

Chapter 7 – Discussion

In this chapter, the results presented in chapters 4-6 are collectively discussed in the context of the current state of the art. First, the advantages of the selected synthetic method of self-polycondensation of the designed diblock macromonomers in front of other techniques for multiblock copolymer synthesis are considered in respect to intended physical network functionality. These results and detailed design criteria are presented in chapter 6. Further, the synthesised PLLA-PCL / ODLA matrix is evaluated to consent the morphological criteria for shape-memory polymer actuators. Their properties are further compared to other types of polymer networks cross-linked with physical interactions. The findings discussed in this subsection are presented in chapters 4-6. Finally, shape-memory actuation in the PLLA-PCL / ODLA blends, its optimisation and opportunities for its non-synthetic tuning are weighted against other physically and chemically cross-linked shape-memory polymer actuators. The materials for these discussions are presented in chapters 6. The chemical structure and simplified morphology of PLLA-PCL / ODLA blends is presented in Figure 5.

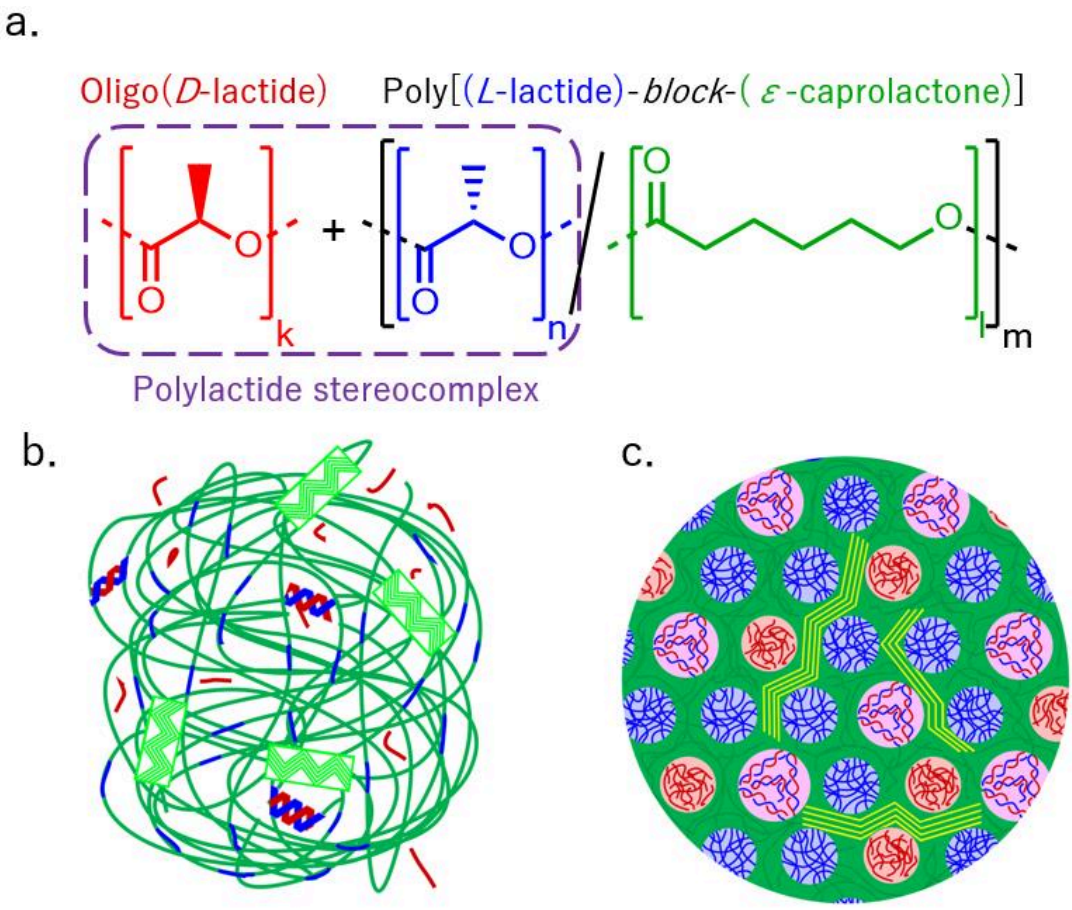

Figure 5. (a) Chemical structure of the PLLA-PCL / ODLA blend. The numbers of repeating units were varied as $3 \leq k \leq 350$; $12 \leq n \leq 15$; $20 \leq l \leq 80$ and m was corresponding to $M_n = 100 – 200$ kg·mol^{-1} **(b)** Schematic illustrating the morphology of the PLLA-PCL / ODLA blends. The matrix consists of amorphous (dark green) and crystalline (light green helices) PCL segments, amorphous PLLA segments (blue) and ODLA molecules (red). PLLA and ODLA form stereocomplexes, illustrated with red/blue helices. **(c)** Schematic illustrating the phase morphology of the PLLA-PCL / ODLA blends. A continuous PCL phase (green), containing amorphous domains and crystalline lamellae (light green), encases isolated domains of PLLA (red) and ODLA (blue), which can form semi-crystalline PLA stereocomplexes domains (red/blue). The size of PLA domains lies within range $d_0 = 12 – 19$ nm.

Preparation of PLLA-PCL / ODLA thermoplastic elastomer

The versatility of the copolymer chemistry has made them an attractive platform for the design of materials with desired structure and properties. To fulfill the strict morphological requirements for

shape-memory actuation a polymeric material has to possess three distinct structural units: two crystallisable domains and network junctions. The complexity of the thesis concept, to embed PCL crystallisable domains and PLLA anchoring points for PLA stereocomplexation into one multiblock copolymer molecule, demands a precise control over the sequence structure of the designed material, namely the repeating unit sequence length and tacticity of PLA repeating units. Sequential polymerisation of the monomers significantly increases the complexity of the reaction in synthesis of multiblock copolymers with larger amount of repeating segments. Longer ring-opening polymerisation reactions of lactones at elevated temperatures typically result in transesterification, which additionally harms the sequence structure.[129, 130] A broadly used approach of PEU synthesis is related to modification of the polymer backbone with urethane segments and diol initiator residues, which may cause unwanted hydrogen bonding between the multiblock copolymer molecules or hindering polyester segment crystallisation.[131] Highly attractive for many purposes click-chemistry reactions require presence of the end-groups not naturally inherent to polyesters and therefore chemical modification of macromonomers.[132, 133]

The selected synthetic approach, self-polycondensation of diblock macromonomers, allows for transferring an accurately designed sequence structure from the diblock macromonomers to the multiblock PLLA-PCL. The modularity of this method makes it possible to tune the structure of each constituent independently in a single process. In this way, the crystallinity of PLA and PCL, i.e. the structure of the functional units and density of the physically cross-linked network, can be designed at the synthesis step as a function of the PLLA-PCL sequence structure. The crystallinity can however be further altered and controlled for the application needs in the synthesised PLLA-PCL by in situ composition adjustments of the PLLA-PCL / ODLA blends and their thermal treatment. This approach is somehow similar to design of ionomeric networks, where the functional units are embedded into the polymer backbone and the role of cross-linking anchors is played by ionic side-groups.[134] The cross-linking agent there is an ion that is introduced into the matrix by e.g. mixing in a melt with salts or alkali treatment.[135, 136] Ionomers are typically manufactured via copolymerization of different monomers.[137, 138] A truly alternating sequence structure can be achieved in a similar manner by polycondensation.[137] Formation of hydrogen bonding between polymer molecules requires specific groups in the backbone or at the side chains.[139-141] Lacking necessity of a cross-linking agent on the one hand side eases the preparation of physical networks via cross-linking with hydrogen bonds. On the other hand side, this makes it

possible to tune the cross-linking density only at the synthetic step. This drawback makes hydrogen bonding a less alluring physical cross-linking method, than ionic interactions or the developed PLLA-PCL / ODLA stereocomplexation technique.

Evaluation structure-to-property relationship in PLLA-PCL / ODLA blends

The design of the PLLA-PCL / ODLA matrix implies that the PLA stereocomplexes bear the function of physical cross-links. To tackle with this role they have to fulfill three requirements, a morphological, thermal and mechanical, to be able to provide a network of cross-links that would remain stable during the thermomechanical treatment in shape-memory programming and cycles. PLA stereocomplexes have to be evenly distributed within the matrix, they have to remain intact in the temperature range of shape-memory actuation, and they have to maintain structural integrity during the mechanical treatment. Whereas the PLLA-PCL / ODLA blends have to fulfill additional morphological criteria inherent to all of the shape-memory polymer actuator matrices: possess two distinct crystallisable domains and remain flexible in their thermal transitions ranges for performing the actuation. The reduction of PLA stereocomplexes sizes in this perspective allows for increasing the content of the skeleton-forming and actuating domains, which favours higher generated actuating forces and therefore ε'_{rev}.

Morphology

PLA stereocomplexes are distributed stochastically in bulk. To ensure that no large domains without PLA stereocomplexes are formed, their amounts should be increased through the reduction of their sizes. The reduction of PLA stereocomplex sizes allows for achieving the same cross-linking density at a lower content of PLA, the cross-linking agent, increasing the content of the PCL domains.

A multiblock copolymer approach in the material design is a typical way to compatibilise immiscible polymers as PLA and PCL.[142, 143] Reduction of the average domain spacing to the nanometer scale leads to the miniaturisation of the PLA stereocomplex sizes and therefore their more even distribution in the PLL-PCL / ODLA matrix. Assuming that the domain average spacing is a function of the sequence lengths in PLLA-PCL, tuning the molecular structure and composition is the way to control the phase morphology. The PCL domains forming a continuous phase can form larger crystallites, which can be implemented as the actuating and skeleton-

forming units. The same principle for creating the phase morphology is used in all copolymer-based physical networks.[144-146] The crucial comparison point here is the content of the interacting moieties responsible for the physical cross-linking. Reduction of their sizes, i.e. mass, increases the content of the functional domains in the matrix. A hydrogen bond, as it requires no cross-linking agent, consists of the interaction itself and the interacting groups, which can be miniaturised to e.g. N-H···O=C lying in the backbone of a PEU.[147] To realise ionic interaction, the ionisable groups of an ionomer have to be neutralised with ions.[148] Unlikely the polymeric matrices cross-linked with hydrogen bonding, cross-linking with ionic interactions require more complicated moieties, which can even appear as oligomeric side-chains in e.g. sulfonated tetrafluoroethylene-based copolymer, and addition of ions, the content of which is however typically lower than 1 wt%.[135] Utilising polymeric crystals as physical netpoints requires their significantly higher presence of the cross-linking moieties in the material. It is necessary to have a certain length of a repeating unit sequence in a polymer to be able to form a crystal.[149] This value can even be higher in a copolymer due to interpenetration of the neighbouring polymer phase.[150, 151] Besides that, crystallites act as nucleation agents for further crystallisation involving additional molecules into one crystal.[152, 153] This significantly increases sizes of the physical cross-links comparing to hydrogen bonds or ionic interactions. PLLA-PCL / ODLA blends contain PLA stereocomplexes in volumes of d_0 = 12 – 19 nm strictly confined with PCL continuous phase, and they consist of short chains of 12 – 26 repeating units. This allows for reducing the content of PLA required for cross-linking down to 13 wt%, which is still incomparably more than content of side-chains and ions in ionomers, and interacting groups for hydrogen bonding. The reversible shape-memory actuation capability was shown to appear in PLLA-PCL / ODLA blends with only 1 wt% of ODLA, having maximum at 3 wt%. The PLLA content in PLLA-PCL was as high as 15 wt%, rendering its surplus unnecessary for PLA stereocomplexation. In light of that, a determined study can optimise the PLLA-PCL structure, decreasing the PLLA content in the copolymer and potentially reducing the total required PLA content in the blend down to 5 wt%.

The pure PLLA-PCL multiblock copolymers have demonstrated high compatibility of the components resulting in the formation of a mixed amorphous matrix. In the selected cases, only PCL crystallites were observed in the PLLA-PCL structure, demonstrating a successful suppression of PLLA isotactic crystallisation. At the same time, the domain sizes limited by microphase separated structure allow PLA stereocomplexes for being even distributed within the

matrix. The designed PLLA-PCL / ODLA structure and synthetic approach make it possible not only to create an isotropic physically cross-linked shape-memory matrix, but also to tailor the morphology and adapt it when the properties require change.

Thermal properties

Selection of PLA from the whole range of polymers capable of stereocomplexation was dictated by its outstanding thermal properties along with broad availability of optically pure dilactide monomers. High molar mass PLA melts at T_m = 185 – 190 °C,[91] while its stereocomplex T_m can go as high as 220 – 230 °C.[99] Other polyester stereocomplexes, such as poly(2-hydroxybutanoic acid) and poly(2-hydroxy-3-methylbutanoic acid), have lower T_m = 200 °C and 193 °C respectively, which would even decrease for low molar mass chains within a copolymer. Poly(*α*-methyl-*α*-ethyl-*β*-propiolactone) stereocomplex has comparable with PLA T_m = 215 °C.[154] Commercial unavailability and multi-step synthesis of its monomer make it a less attractive material. Several polycarbonates have been reported to form stereocomplex, e.g. poly(cyclohexane carbonate), CO_2/1,4-dihydronaphthalene oxide copolymer, etc.[155, 156] Although they can demonstrate significantly higher thermal stability T_m up to 370 °C than PLA, their degradation products are known to be acutely toxic.[157] Stereocomplexes of polyamides and polyketones were not considered due to synthetic reasons.

Non-overlapping melting peaks of PCL and PLA stereocomplex was imperative, thus, designed and realised already at the synthesis step. The multiblock structure of PLLA-PCL resulted in interpenetration of the phases typically occurring in copolymeric systems[158] or being a sign of compatibilisation in homopolymer blends.[159] This broadens melting peaks of PCL and PLA stereocomplex, even though the molecular weight distribution of the constituent molecules is narrow ($Đ_{PCL}$ = 1.11, $Đ_{ODLA}$ = 1.17). A broader temperature range of PCL melting facilitates its separation into the actuator and skeleton forming units with T_{high}. A similar effect broadening melting transitions has hydrogen bonding established between polymer molecules[160] and interactions in ionised ionomers.[161] A great advantage of the developed PLLA-PCL / ODLA blend is the reduced PLA stereocomplex melting point and high solubility in organic solvent unusual for PLA stereocomplex containing materials.[99] This broadens the melt processing window and opens opportunities for solution processing. PLLA-PCL / ODLA blend is an easily recyclable plastic, which combined with its full biodegradability and biological origin of the raw materials makes it

a highly sustainable polymer. Other physical polymeric networks cross-linked by hydrogen bonding and ionic interactions, especially industrially produced, have strictly limited end-of-life options.[136, 162, 163]

The discovered tunability of PLA stereocomplex thermal properties via adjustments of their morphology as physical cross-links in a polymer matrix opens a possibility of their combination with different copolymers in actuator materials. This also allows for adjusting processing and recycling conditions of physical networks cross-linked with PLA stereocomplexes.

Mechanical performance

Network properties of physical matrices can be evaluated by a number of approaches. The simplest one is the visual analysis of stress-strain curves, comparatively low Young's modulus and high elongation at break, or pronounced strengthening behaviour.[164, 165] However, the latter should be rather assigned to irreversible crystalline reorganisation processes and is a sign of plastic deformations in the material matrix.[166, 167] The lower boundary of PLA stereocomplex concentration required for formation of physical network can be determined with dynamic rheological measurements. Here, the change of the loss tangent tan(δ) (ω) from frequency-independent loss to extremal profile indicates the transition from viscoelastic to elastic behaviour of the material, i.e. network formation.[105, 106] On the other side, elastomeric behaviour can be differentiated from the plastic one in free recovery experiments determining the ratio between reversible and irreversible deformation. [168] However, all of these approaches have restraints, because they can only determine a limited number of material properties responsible for elastic network-like behaviour and do not explain reasons for failure of physical netpoints. The approach presented in this thesis, besides defining strain and composition limits for elastic behaviour of PLLA-PCL blends, assigns microscopic processes and quantifies distribution of stresses between amorphous and crystalline domains responsible for physical network failure.

The increase of covalent cross-linking density in an amorphous polymer first leads to formation of a chemical network and further to a thermoset. Low φ_c of PLA stereocomplexes in PLLA-PCL / ODLA blends grants it elastomeric properties, while further increase of PLA stereocomplexes φ_c would induce semi-crystalline behaviour.[169] From the mechanical point of view, the main difference between the covalent and physical cross-links is their activation energy. Where a dense covalent network demonstrates high mechanical strength, growing stresses stored in the

amorphous domains of a physical network are gradually redistributed to the network junctions causing their irreversible deformation. The transition between deformation regimes of crystallites discussed in the Introduction defines the strain limits of the PLLA-PCL / ODLA blends as physical networks. The structural failure of PLA stereocomplexes is the onset of fibrillation determined in the step-cycle test. In the fibrillation regime of deformation, the stresses stored in the entangled amorphous network are so high that disintegration of the crystallites require less energy than further stretching of the amorphous domains. Therefore, the increase is observed only in the plastic contribution to the deformation, while the elastic remains constant. Analogically to the transfer between plastic and elastic deformation observed in the step-cycle experiment, deviations from the expected viscoelastic behaviour in the relaxation experiment towards plastic reorganisation of the crystallites indicates their failure as physical cross-links.

The blending approach to formation of physical network in PLLA-PCL / ODLA blends allows for tuning the role of PLA stereocomplexes in the range from a cross-link to a structural element of the matrix. The minimal φ_c = 0.7%, i.e. network density, required for a network formation determined for PLLA-PCL / ODLA blends is significantly lower than 2.6 wt% or 5 wt% reported for other PLA stereocomplex based networks.[105, 106] This is explained by smaller PLA stereocomplex average sizes d_0 = 12 – 19 nm and their more even distribution in bulk than the micron scale crystallites reported in the literature.[105, 106] PLA stereocomplexes in PLLA-PCL / ODLA blends demonstrate stability in broad temperature and strain ranges as well as *in situ* tunability of their properties untypical for other types of physical interactions.

Shape-memory actuation

The achieved ε'_{rev} = 13.4 ± 1.5% was lower than 19-21% reported in the in classical works in the area,[30, 31] or 17% achieved in chemically cross-linked PCL.[44] A block copolymer approach was also employed for covalent shape-memory networks. For example, a diblock copolymer poly(ethylene-*block*-1-octene) can demonstrate ε'_{rev} up to 18% at the stress-free conditions.[58] Comparatively high ε'_{rev} = 25% has been achieved in chemically cross-linked blends of PCL and poly(ethylene-*co*-vinylacetate).[170] There, the components of the blend separately bear actuating and skeleton-forming functions. The actuation performance is a complex function of the morphological structure and thermomechanical treatment of the shape-memory actuator matrix. Design of specific polymeric materials and chemical cross-linking undisputedly can lead to higher

ε'_{rev}, however reprocessability and *in situ* tuning of ε'_{rev}, possible for the PLLA-PCL / ODLA blends, are a significant competitive feature. Comparing to other physical networks, ε'_{rev} is similar or even slightly higher than 10-11% reported for poly(3*S*-*iso*butylmorpholin-2,5-dione), [49] and assessed with formula (2) for poly(ethylene-*co*-methacrylic acid) or commercially available polyurethane composed of poly(1,4-butylene adipate) soft segments and 4,4′ methylenediphenyl diisocyanate, chain extended by 1,4-butanediol, as hard segments.[46, 56, 171]

Manifold structure of shape-memory polymeric actuators and complexity of the thermomechanical treatment provides a broad spectrum of variable parameters responsible for the magnitude of actuation, which can be approached by chemical modifications of the matrix or non-synthetic tuning of the shape-memory actuation procedure. Synthetic approaches to tuning Q_{eff} and ε'_{rev} are related to changes in the content of the actuating and skeleton-forming units or the cross-linking density of the matrix. Variations in the skeleton-to-actuator ratio or structural constraints on their maximal crystallinity alternate the forces generated with crystallisation and melting of the actuator and ability of the skeleton to resist the force generated by phase transitions of the neighbouring elements of the matrix. [172] Meanwhile, the modification of the cross-linking density changes the mobility of the matrix components and interactions between them.[48, 49] Common non-synthetic tools for tuning shape-memory actuation are adjusting thermomechanical parameters of the programming and actuation cycles. Here, programming conditions can be varied to achieve different degree of molecular orientation.[43, 46] However, higher elongations could lead to destruction of cross-links and disentangling of the amorphous network spoiling ε'_{rev}. With changing T_{low} and T_{high}, different portions of the actuating units can be melted and crystallised modifying ε_A and ε_B to tune ε'_{rev}.[56] In material systems, where one broad melting transition plays the role of both types of functional units, variation of T_{high} changes the ratio between them.

The key finding of the actuation study in this thesis was the development of a non-synthetic approach to control the physical cross-linking density. Changing the mass ratio between the components of the PLLA-PCL / ODLA blends we were able to tune PLA stereocomplex φ_c, i.e. the cross-linking density. The dependency $\varepsilon'_{rev}(\varphi_c)$ was found to have an extremal behaviour with the maximum at ε'_{rev} = 13.4 ± 1.5 % at φ_c = 3.1 wt%.

Lower strength of the physical cross-links negatively affects ε'_{rev} comparing to the covalent networks. Nevertheless, the developed PLLA-PCL / ODLA blends perform better than similar

physically cross-linked systems. The developed approach for *in situ* adjusting physical cross-linking density demonstrated that ε'_{rev} can be tuned without synthetic modification of the polymer architecture. Further, the reprocessability of the developed material removes the restrictions of a single post-processing geometry inherent to covalent networks.

Chapter 8 – Summary and outlook

A structure design and manufacturing approach for a two-component physical network of poly(*L*-lactide) and poly(*ε*-caprolactone) segments (PLLA-PCL) and poly(*D*-lactide) oligomer (ODLA) via PLA stereocomplexation have been developed. Modularity of its structure and synthesis procedures allows for modification of phase morphology and thermomechanical properties. *In situ* formation of the selected physical interactions and their reversibility grants the PLLA-PCL / ODLA matrix capability for fine tuning of the shape-memory actuation as well as its recyclability.

First, PLLA-PCL has been synthesised, where the PLLA segment was sufficiently long to form PLA stereocomplexes in the blends with ODLA, but not long enough to undergo isotactic crystallisation. The segment number average lengths of 12-15 *L*-lactic acid and approximately 60 hydroxyhexanoate repeating units have been experimentally determined for maximising the actuation performance ε'_{rev} among the selected series. The required precision of the segment structure has been achieved by employing self-polycondensation of diblock macromonomers as the synthetic route to the PLLA-PCL. Due to mild conditions (room temperature and DMAP catalytic system), this approach allowed for accurate translation of the diblock structure to the multiblock with negligibly low amount of transesterification reactions and change in PLLA segment tacticity. The achieved high molar mass $M_w \approx 500$ kg·mol^{-1} and narrow dispersity $Đ \approx 2$ positively affected the mechanical properties of the material by providing high amount of chain entanglements with the corresponding improvement in the strength and elasticity. Low $M_w = 4$ kg·mol^{-1} of ODLA and the multiblock structure made PLA stereocomplexes in the PLLA-PCL / ODLA blends soluble in chloroform allowing for (re)processing of these materials.

The structural components of the PLLA-PCL / ODLA blends have been evaluated to complement the requirements for realisation of shape-memory actuation. The multiblock structure of the macromolecules caused formation of a mixed amorphous phase of otherwise immiscible PLA and PCL with a single $T_g = -40 – 0$ °C depending on the material composition. The thermal transitions involved in the shape-memory actuation melting-crystallisation cycles onset in higher temperature ranges, making the PLLA-PCL / ODLA matrix elastic in the actuation temperature ranges. Partial phase dilution in PLLA-PCL, resulting in a broadening of PCL melting transition, made it possible to bisect its crystalline population into two domains, which were further assigned as more thermally stable skeleton-forming and less thermally stable actuating units.

The validity of PLA stereocomplex definition as physical netpoints has been evaluated with three criteria: morphological, thermal and mechanical. The even distribution of PLA stereocomplexes in the PLLA-PCL / ODLA matrix was derived from the microphase structure observed with TEM, SAXS and AFM. A structure of regular PLA domains surrounded by continuous PCL phase with average domain spacing d_0 = 12-19 nm suggested that the PLA stereocomplexes must have sizes comparable to d_0 allowing their even distribution in the material matrix. At the same time, the PCL continuous phase could contain larger crystallites favourable for shape-memory actuation. Due to lower M_w of the constituents and partial PLA/PCL phase dilution, PLA stereocomplex had comparatively lower melting temperature $T_m \approx 170$ °C. However, its melting onset at $T_{onset} \approx 100$ °C did not overlap with PCL melting transition ending at 70 °C proving that physical netpoints remain stable in the whole range of PCL thermal transitions.

For the evaluation of the mechanical integrity of PLA stereocomplexes in the thermomechanical ranges of shape-memory actuation, their deformation mechanisms at different temperatures and strains have been studied. The microscopic behaviour of the PLLA-PCL / ODLA blends at 70 °C for the samples with PLA stereocomplex $\varphi_c < 6\pm0.6$ wt% in the full range of strains ε was characterised as elastomeric with structurally stable physical netpoints. The increase in PLA stereocomplex φ_c to 6.8 wt% limited the strain range of elastomeric behaviour to ε = 1000% with further decrease to 850% at higher φ_c. High PCL φ_c at 0 °C grants PLLA-PCL and its ODLA blends a typical semi-crystalline behaviour. The effect of PCL on the mechanical properties at this temperature is so high that it was not possible to evaluate unambiguously PLA stereocomplexes mechanical stability. Decomposition of the applied stresses with an adopted three-component model for semi-crystalline polymers into viscoelastic, elastic and elastoplastic contributions demonstrated disproportionation between loads distributed in the amorphous and crystalline domains, causing stress concentration and further structural failure of the latter with an increase in crystallinity or applied deformation. Adjusting the morphology, molecular structure, and composition of the PLA stereocomplex physical cross-links, it was possible to tune their crystallinity and thermomechanical properties.

Suitable thermal parameters for shape-memory actuation were determined as T_{low} = 0 °C and T_{prog} = 70 °C as the boarders of the PCL melting transition. Further, T_{high} = 55 °C was determined in a shape-memory actuation experiment with variable T_{high}. Molecular orientation, sufficient for realisation of the shape-memory actuation could be achieved at ε_{prog} > 300%. The highest

ε'_{rev} = 13.4±1.5% has been achieved in the PLLA-PCL / ODLA blend with PLA stereocomplex φ_c = 3.1±0.3 wt%. The shape-memory actuation capability was found to be a function of PLA stereocomplex φ_c with maximal behaviour. The shape-memory actuation in the PLLA-PCL / ODLA blends can be tuned by adjusting ODLA content in range 1 – 10 wt%.

The modular structure of PLLA-PCL opens a broad perspective for combinations of various functional elements in the design of smart polymers. The obtained knowledge of deformation mechanisms in PLA stereocomplexes provide a theoretical basis for development of PLA stereocomplex based polymer systems that can be used as biodegradable commodity plastics. The developed method for evaluation of PLA stereocomplexes structural integrity can be further employed for assessment of thermoplastic elastomers cross-linked with stereocomplexes of other polylactones, PMMA or any polymeric crystallites. The advantage of non-synthetic tuning of the shape-memory actuation performance combined with reprocessability of the developed material makes it an attractive candidate for cost-effective manufacturing of reconfigurable devices in fine biomedical and mechatronic applications.

References

1. Mirvakili, S. M.; Hunter, I. W. Artificial Muscles: Mechanisms, Applications, and Challenges. *Adv Mater* **2018,** 30 (6), 1704407 DOI: 10.1002/adma.201704407.
2. Gaylord, R. H. Fluid actuated motor system and stroking device, US2844126A. July 22, 1958.
3. Zhao, Q.; Dunlop, J. W.; Qiu, X.; Huang, F.; Zhang, Z.; Heyda, J.; Dzubiella, J.; Antonietti, M.; Yuan, J. An instant multi-responsive porous polymer actuator driven by solvent molecule sorption. *Nat Commun* **2014,** 5, 4293 DOI: 10.1038/ncomms5293.
4. Mu, J.; Hou, C.; Zhu, B.; Wang, H.; Li, Y.; Zhang, Q. A multi-responsive water-driven actuator with instant and powerful performance for versatile applications. *Sci Rep* **2015,** 5, 9503 DOI: 10.1038/srep09503.
5. Ma, M.; Guo, L.; Anderson, D. G.; Langer, R. Bio-Inspired Polymer Composite Actuator and Generator Driven by Water Gradients. *Science* **2013,** 339, 186-189 DOI: 10.1126/science.1230262.
6. Arazoe, H.; Miyajima, D.; Akaike, K.; Araoka, F.; Sato, E.; Hikima, T.; Kawamoto, M.; Aida, T. An autonomous actuator driven by fluctuations in ambient humidity. *Nat Mater* **2016,** 15 (10), 1084-9 DOI: 10.1038/nmat4693.
7. Greiner, R.; Allerdissen, M.; Voigt, A.; Richter, A. Fluidic microchemomechanical integrated circuits processing chemical information. *Lab Chip* **2012,** 12 (23), 5034-44 DOI: 10.1039/c2lc40617a.
8. Xia, L. W.; Xie, R.; Ju, X. J.; Wang, W.; Chen, Q.; Chu, L. Y. Nano-structured smart hydrogels with rapid response and high elasticity. *Nat Commun* **2013,** 4, 2226 DOI: 10.1038/ncomms3226.
9. Baughman, R. H. Conducting polymer artificial muscles. *Synthetic Metals* **1996,** 78 (3), 339-353 DOI: 10.1016/0379-6779(96)80158-5.
10. Otero, T. F.; Martinez, J. G.; Arias-Pardilla, J. Biomimetic electrochemistry from conducting polymers. A review. *Electrochimica Acta* **2012,** 84, 112-128 DOI: 10.1016/j.electacta.2012.03.097.
11. Nemat-Nasser, S. Micromechanics of actuation of ionic polymer-metal composites. *Journal of Applied Physics* **2002,** 92 (5), 2899-2915 DOI: 10.1063/1.1495888.
12. Jo, C.; Pugal, D.; Oh, I.-K.; Kim, K. J.; Asaka, K. Recent advances in ionic polymer–metal composite actuators and their modeling and applications. *Progress in Polymer Science* **2013,** 38 (7), 1037-1066 DOI: 10.1016/j.progpolymsci.2013.04.003.
13. Kong, L.; Chen, W. Carbon nanotube and graphene-based bioinspired electrochemical actuators. *Adv Mater* **2014,** 26 (7), 1025-43 DOI: 10.1002/adma.201303432.
14. Jang, S. J.; Uchino, K.; Nomura, S.; Cross, L. E. Electrostrictive Behavior of Lead Magnesium Niobate Based Ceramic Dielectrics. *Ferroelectrics* **1980,** 27 (1-4), 31-34 DOI: Doi 10.1080/00150198008226059.
15. Casalini, R.; Roland, C. M. Highly electrostrictive poly(vinylidene fluoride–trifluoroethylene) networks. *Applied Physics Letters* **2001,** 79 (16), 2627-2629 DOI: 10.1063/1.1409595.
16. Liu, J.; Jiang, C.; Xu, H. Giant magnetostrictive materials. *Science China Technological Sciences* **2012,** 55 (5), 1319-1326 DOI: 10.1007/s11431-012-4810-0.

17. Duenas, T. A.; Carman, G. P. Large magnetostrictive response of Terfenol-D resin composites. *Journal of Applied Physics* **2000,** 87 (9), 4696-4701 DOI: 10.1063/1.373133.
18. Uchino, K. New applications of photostrictive ferroics. *Mater Res Innov* **1997,** 1 (3), 163-168 DOI: DOI 10.1007/s100190050036.
19. Kundys, B. Photostrictive materials. *Applied Physics Reviews* **2015,** 2 (1), 011301 DOI: 10.1063/1.4905505.
20. Hugel, T.; Holland, N. B.; Cattani, A.; Moroder, L.; Seitz, M.; Gaub, H. E. Single-molecule optomechanical cycle. *Science* **2002,** 296 (5570), 1103-6 DOI: 10.1126/science.1069856.
21. Lu, X.; Guo, S.; Tong, X.; Xia, H.; Zhao, Y. Tunable Photocontrolled Motions Using Stored Strain Energy in Malleable Azobenzene Liquid Crystalline Polymer Actuators. *Advanced Materials* **2017,** 29 (28), 1606467 DOI: 10.1002/adma.201606467.
22. Wang, Z. L.; Song, J. Piezoelectric nanogenerators based on zinc oxide nanowire arrays. *Science* **2006,** 312 (5771), 242-6 DOI: 10.1126/science.1124005.
23. Xu, S.; Hansen, B. J.; Wang, Z. L. Piezoelectric-nanowire-enabled power source for driving wireless microelectronics. *Nat Commun* **2010,** 1, 93 DOI: 10.1038/ncomms1098.
24. Copic, D.; Hart, A. J. Corrugated paraffin nanocomposite films as large stroke thermal actuators and self-activating thermal interfaces. *ACS Appl Mater Interfaces* **2015,** 7 (15), 8218-24 DOI: 10.1021/acsami.5b01141.
25. Lima, M. D.; Li, N.; Jung de Andrade, M.; Fang, S.; Oh, J.; Spinks, G. M.; Kozlov, M. E.; Haines, C. S.; Suh, D.; Foroughi, J.; Kim, S. J.; Chen, Y.; Ware, T.; Shin, M. K.; Machado, L. D.; Fonseca, A. F.; Madden, J. D.; Voit, W. E.; Galvao, D. S.; Baughman, R. H. Electrically, chemically, and photonically powered torsional and tensile actuation of hybrid carbon nanotube yarn muscles. *Science* **2012,** 338 (6109), 928-32 DOI: 10.1126/science.1226762.
26. Lee, J. A.; Li, N.; Haines, C. S.; Kim, K. J.; Lepro, X.; Ovalle-Robles, R.; Kim, S. J.; Baughman, R. H. Electrochemically Powered, Energy-Conserving Carbon Nanotube Artificial Muscles. *Adv Mater* **2017,** 29 (31), 1700870 DOI: 10.1002/adma.201700870.
27. Lendlein, A.; Kelch, S. Shape-Memory Polymers. *Angewandte Chemie International Edition* **2002,** 41, 2034 DOI: 10.1002/1521-3773(20020617)41:12<2034::AID-ANIE2034>3.0.CO;2-M.
28. Behl, M.; Lendlein, A. Actively moving polymers. *Soft Matter* **2006,** 3 (1), 58-67 DOI: 10.1039/b610611k.
29. Lendlein, A.; Gould, O. E. C. Reprogrammable recovery and actuation behaviour of shape-memory polymers. *Nat Rev Mater* **2019,** 4 (2), 116-133 DOI: 10.1038/s41578-018-0078-8.
30. Behl, M.; Kratz, K.; Zotzmann, J.; Nochel, U.; Lendlein, A. Reversible bidirectional shape-memory polymers. *Adv Mater* **2013,** 25 (32), 4466-9 DOI: 10.1002/adma.201300880.
31. Behl, M.; Kratz, K.; Noechel, U.; Sauter, T.; Lendlein, A. Temperature-memory polymer actuators. *Proceedings of the National Academy of Sciences of the United States of America* **2013,** 110, 12555-9 DOI: 10.1073/pnas.1301895110.
32. Kolesov, I.; Dolynchuk, O.; Borreck, S.; Radusch, H.-J. Morphology-controlled multiple one- and two-way shape-memory behavior of cross-linked polyethylene/poly(ε-caprolactone) blends. *Polymers for Advanced Technologies* **2014,** 25 (11), 1315-1322 DOI: 10.1002/pat.3338.
33. Chan, B. Q.; Low, Z. W.; Heng, S. J.; Chan, S. Y.; Owh, C.; Loh, X. J. Recent Advances in Shape Memory Soft Materials for Biomedical Applications. *ACS Appl Mater Interfaces* **2016,** 8 (16), 10070-87 DOI: 10.1021/acsami.6b01295.

34. Pilate, F.; Toncheva, A.; Dubois, P.; Raquez, J.-M. Shape-memory polymers for multiple applications in the materials world. *European Polymer Journal* **2016,** 80, 268-294 DOI: 10.1016/j.eurpolymj.2016.05.004.
35. Teoh, J. E. M.; Zhao, Y.; An, J.; Chua, C. K.; Liu, Y. Multi-stage responsive 4D printed smart structure through varying geometric thickness of shape memory polymer. *Smart Materials and Structures* **2017,** 26 (12), 125001 DOI: 10.1088/1361-665X/aa908a.
36. Razzaq, M. Y.; Behl, M.; Nöchel, U.; Lendlein, A. Magnetically controlled shape-memory effects of hybrid nanocomposites from oligo(ω-pentadecalactone) and covalently integrated magnetite nanoparticles. *Polymer (United Kingdom)* **2014,** 55, 5953-5960 DOI: 10.1016/j.polymer.2014.07.025.
37. Wang, L.; Razzaq, M. Y.; Rudolph, T.; Heuchel, M.; Nöchel, U.; Mansfeld, U.; Jiang, Y.; Gould, O. E. C. C.; Behl, M.; Kratz, K.; Lendlein, A. Reprogrammable, magnetically controlled polymeric nanocomposite actuators. *Materials Horizons* **2018,** 5, 861-867 DOI: 10.1039/C8MH00266E.
38. Yu, L.; Yu, H. Light-powered tumbler movement of graphene oxide/polymer nanocomposites. *ACS Appl Mater Interfaces* **2015,** 7 (6), 3834-9 DOI: 10.1021/am508970k.
39. Lowenberg, C.; Balk, M.; Wischke, C.; Behl, M.; Lendlein, A. Shape-Memory Hydrogels: Evolution of Structural Principles To Enable Shape Switching of Hydrophilic Polymer Networks. *Acc Chem Res* **2017,** 50 (4), 723-732 DOI: 10.1021/acs.accounts.6b00584.
40. Olabis, O., *Polymer-Polymer Miscibility*. Elsevier: 2012; p 382.
41. Kolesov, I.; Dolynchuk, O.; Radusch, H. J. Shape-memory behavior of cross-linked semi-crystalline polymers and their blends. *Express Polymer Letters* **2015,** 9, 255-276 DOI: 10.3144/expresspolymlett.2015.24.
42. Abetz, V.; Simon, P. F. W. Phase behaviour and morphologies of block copolymers. *Adv Polym Sci* **2005,** 189, 125-212 DOI: 10.1007/12_004.
43. Huang, M.; Dong, X.; Wang, L.; Zhao, J.; Liu, G.; Wang, D. Two-way shape memory property and its structural origin of cross-linked poly(ε-caprolactone). *RSC Adv.* **2014,** 4 (98), 55483-55494 DOI: 10.1039/c4ra09385b.
44. Saatchi, M.; Behl, M.; Nöchel, U.; Lendlein, A. Copolymer networks from oligo (ε -caprolactone) and n -butyl acrylate enable a reversible bidirectional shape-memory effect at human body temperature. *Macromolecular Rapid Communications* **2015,** 36, 880-884 DOI: 10.1002/marc.201400729.
45. Dolynchuk, O.; Kolesov, I.; Jehnichen, D.; Reuter, U.; Radusch, H.-J.; Sommer, J.-U. Reversible Shape-Memory Effect in Cross-Linked Linear Poly(ε-caprolactone) under Stress and Stress-Free Conditions. *Macromolecules* **2017,** 50 (10), 3841-3854 DOI: 10.1021/acs.macromol.7b00481.
46. Yan, W.; Rudolph, T.; Noechel, U.; Gould, O.; Behl, M.; Kratz, K.; Lendlein, A. Reversible Actuation of Thermoplastic Multiblock Copolymers with Overlapping Thermal Transitions of Crystalline and Glassy Domains. *Macromolecules* **2018,** 51 (12), 4624-4632 DOI: 10.1021/acs.macromol.8b00322.
47. Beyer, M. K.; Clausen-Schaumann, H. Mechanochemistry: The mechanical activation of covalent bonds. *Chemical Reviews* **2005,** 105, 2921-2948 DOI: 10.1021/cr030697h.
48. Pandini, S.; Baldi, F.; Paderni, K.; Messori, M.; Toselli, M.; Pilati, F.; Gianoncelli, A.; Brisotto, M.; Bontempi, E.; Riccò, T. One-way and two-way shape memory behaviour of semi-crystalline networks based on sol-gel cross-linked poly(ε-caprolactone). *Polymer* **2013,** 54, 4253-4265 DOI: 10.1016/j.polymer.2013.06.016.

49. Zhou, J.; Turner, S. A.; Brosnan, S. M.; Li, Q.; Carrillo, J. M. Y.; Nykypanchuk, D.; Gang, O.; Ashby, V. S.; Dobrynin, A. V.; Sheiko, S. S. Shapeshifting: Reversible shape memory in semicrystalline elastomers. *Macromolecules* **2014,** 47, 1768-1776 DOI: 10.1021/ma4023185.
50. Bowman, C. N.; Kloxin, C. J. Covalent adaptable networks: reversible bond structures incorporated in polymer networks. *Angew Chem Int Ed Engl* **2012,** 51 (18), 4272-4 DOI: 10.1002/anie.201200708.
51. Tanaka, F.; Edwards, S. F. Viscoelastic Properties of Physically Cross-Linked Networks. Transient Network Theory. *Macromolecules* **1992,** 25, 1516-1523 DOI: 10.1021/ma00031a024.
52. Coleman, M. M.; Lee, K. H.; Skrovanek, D. J.; Painter, P. C. Hydrogen bonding in polymers. 4. Infrared temperature studies of a simple polyurethane. *Macromolecules* **1986,** 19 (8), 2149-2157 DOI: 10.1021/ma00162a008.
53. Lange, R. F. M.; Van Gurp, M.; Meijer, E. W. Hydrogen-bonded supramolecular polymer networks. *Journal of Polymer Science Part A: Polymer Chemistry* **1999,** 37 (19), 3657-3670 DOI: 10.1002/(sici)1099-0518(19991001)37:19<3657::aid-pola1>3.0.co;2-6.
54. Hu, X.; Vatankhah-Varnoosfaderani, M.; Zhou, J.; Li, Q.; Sheiko, S. S. Weak Hydrogen Bonding Enables Hard, Strong, Tough, and Elastic Hydrogels. *Adv Mater* **2015,** 27 (43), 6899-905 DOI: 10.1002/adma.201503724.
55. Xie, H.-Q.; Xu, J.; Zhou, S. Polymer blends with two kinds of elastomeric ionomers. *Polymer* **1991,** 32 (1), 95-102 DOI: 10.1016/0032-3861(91)90568-4.
56. Lu, L.; Li, G. One-Way Multishape-Memory Effect and Tunable Two-Way Shape Memory Effect of Ionomer Poly(ethylene-co-methacrylic acid). *ACS Applied Materials and Interfaces* **2016,** 8, 14812-14823 DOI: 10.1021/acsami.6b04105.
57. Dolog, R.; Weiss, R. A. Shape memory behavior of a polyethylene-based carboxylate ionomer. *Macromolecules* **2013,** 46, 7845-7852 DOI: 10.1021/ma401631j.
58. Gao, Y.; Liu, W.; Zhu, S. Polyolefin Thermoplastics for Multiple Shape and Reversible Shape Memory. *ACS Applied Materials and Interfaces* **2017,** 9, 4882-4889 DOI: 10.1021/acsami.6b14728.
59. Bensason, S.; Minick, J.; Moet, A.; Chum, S.; Hiltner, A.; Baer, E. Classification of homogeneous ethylene-octene copolymers based on comonomer content. *Journal of Polymer Science Part B: Polymer Physics* **1996,** 34 (7), 1301-1315 DOI: 10.1002/(sici)1099-0488(199605)34:7<1301::aid-polb12>3.0.co;2-e.
60. Bandelli, D.; Alex, J.; Weber, C.; Schubert, U. S. Polyester Stereocomplexes Beyond PLA: Could Synthetic Opportunities Revolutionize Established Material Blending? *Macromol Rapid Commun* **2020,** 41 (1), 1900560 DOI: 10.1002/marc.201900560.
61. Liu, Y.; Ren, W.-M.; Wang, M.; Liu, C.; Lu, X.-B. Crystalline Stereocomplexed Polycarbonates: Hydrogen-Bond-Driven Interlocked Orderly Assembly of the Opposite Enantiomers. *Angewandte Chemie* **2015,** 127 (7), 2269-2272 DOI: 10.1002/ange.201410692.
62. Leiras, S.; Freire, F.; Quinoa, E.; Riguera, R. Reversible assembly of enantiomeric helical polymers: from fibers to gels. *Chem Sci* **2015,** 6 (1), 246-253 DOI: 10.1039/c4sc02401j.
63. Brizzolara, D.; Cantow, H. J.; Diederichs, K.; Keller, E.; Domb, A. J. Mechanism of the stereocomplex formation between enantiomeric poly(lactide)s. *Macromolecules* **1996,** 29, 191-197 DOI: 10.1021/ma951144e.
64. Azzam, T.; Eliyahu, H.; Shapira, L.; Linial, M.; Barenholz, Y.; Domb, A. J. Polysaccharide-oligoamine based conjugates for gene delivery. *J Med Chem* **2002,** 45 (9), 1817-24 DOI: 10.1021/jm0105528.

65. Zhang, J.; Sato, H.; Tsuji, H.; Noda, I.; Ozaki, Y. Infrared Spectroscopic Study of CH3···OC Interaction during Poly(l-lactide)/Poly(d-lactide) Stereocomplex Formation. *Macromolecules* **2005,** 38 (5), 1822-1828 DOI: 10.1021/ma047872w.
66. Sarasua, J. R.; Rodriguez, N. L.; Arraiza, A. L.; Meaurio, E. Stereoselective crystallization and specific interactions in polylactides. *Macromolecules* **2005,** 38, 8362-8371 DOI: 10.1021/ma051266z.
67. Pan, P.; Yang, J.; Shan, G.; Bao, Y.; Weng, Z.; Cao, A.; Yazawa, K.; Inoue, Y. Temperature-Variable FTIR and Solid-State 13C NMR Investigations on Crystalline Structure and Molecular Dynamics of Polymorphic Poly(l-lactide) and Poly(l-lactide)/Poly(d-lactide) Stereocomplex. *Macromolecules* **2011,** 45 (1), 189-197 DOI: 10.1021/ma201906a.
68. Tsuji, H.; Hyon, S. H.; Ikada, Y. Stereocomplex Formation between Enantiomeric Poly(lactic acid)s. 4. Differential Scanning Calorimetric Studies on Precipitates from Mixed Solutions of Poly(D-lactic acid) and Poly(L-lactic acid). *Macromolecules* **1991,** 24, 5657-5662 DOI: 10.1021/ma00020a027.
69. Xie, Q.; Yu, C.; Pan, P., Stereocomplex Crystallization of Polymers With Complementary Configurations. In *Crystallization in Multiphase Polymer Systems*, 1st ed.; Elsevier: 2018; pp 535-573.
70. Andersson, S. R.; Hakkarainen, M.; Inkinen, S.; Sodergard, A.; Albertsson, A. C. Polylactide stereocomplexation leads to higher hydrolytic stability but more acidic hydrolysis product pattern. *Biomacromolecules* **2010,** 11 (4), 1067-73 DOI: 10.1021/bm100029t.
71. Tsuji, H.; Okumura, A. Crystallization and hydrolytic/thermal degradation of a novel stereocomplexationable blend of poly(L-2-hydroxybutyrate) and poly(D-2-hydroxybutyrate). *Polymer Journal* **2010,** 43 (3), 317-324 DOI: 10.1038/pj.2010.133.
72. Mao, H.; Shan, G.; Bao, Y.; Wu, Z. L.; Pan, P. Thermoresponsive physical hydrogels of poly(lactic acid)/poly(ethylene glycol) stereoblock copolymers tuned by stereostructure and hydrophobic block sequence. *Soft Matter* **2016,** 12 (20), 4628-37 DOI: 10.1039/c6sm00517a.
73. Mao, H.; Pan, P.; Shan, G.; Bao, Y. In Situ Formation and Gelation Mechanism of Thermoresponsive Stereocomplexed Hydrogels upon Mixing Diblock and Triblock Poly(Lactic Acid)/Poly(Ethylene Glycol) Copolymers. *The Journal of Physical Chemistry B* **2015,** 119, 6471-6480 DOI: 10.1021/acs.jpcb.5b03610.
74. Yang, D.-d.; Liu, W.; Zhu, H.-m.; Wu, G.; Chen, S.-c.; Wang, X.-l.; Wang, Y.-z. Toward Super-Tough Poly (L - lactide) via Constructing Pseudo-Cross- link Network in Toughening Phase Anchored by Stereocomplex Crystallites at the Interface. *ACS Applied Materials & Interfaces* **2018,** 10, 26594-26603 DOI: 10.1021/acsami.8b06343.
75. Lavallee, C.; Prud'homme, R. E. Stereocomplexation of isotactic polyesters of opposite configurations. *Macromolecules* **1989,** 22 (5), 2438-2446 DOI: 10.1021/ma00195a074.
76. Tsuji, H.; Okumura, A. Stereocomplex Formation between Enantiomeric Substituted Poly(lactide)s: Blends of Poly[(S)-2-hydroxybutyrate] and Poly[(R)-2-hydroxybutyrate]. *Macromolecules* **2009,** 42 (19), 7263-7266 DOI: 10.1021/ma9015483.
77. Longo, J. M.; DiCiccio, A. M.; Coates, G. W. Poly(propylene succinate): a new polymer stereocomplex. *J Am Chem Soc* **2014,** 136 (45), 15897-900 DOI: 10.1021/ja509440g.
78. Auriemma, F.; De Rosa, C.; Di Caprio, M. R.; Di Girolamo, R.; Ellis, W. C.; Coates, G. W. Stereocomplexed poly(limonene carbonate): a unique example of the cocrystallization of amorphous enantiomeric polymers. *Angew Chem Int Ed Engl* **2015,** 54 (4), 1215-8 DOI: 10.1002/anie.201410211.

79. Yoshikawa, M.; Tsujita, Y.; Uematsu, I.; Uematsu, Y. Transition of Mixture of Poly(γ-benzyl L-glutamate) and Poly(γ-benzyl D-glutamate). *Polymer Journal* **1975,** 7 (1), 96-100 DOI: 10.1295/polymj.7.96.
80. Marín, R.; Alla, A.; Muñoz-Guerra, S. Stereocomplex Formation from Enantiomeric Polyamides Derived from Tartaric Acid. *Macromolecular Rapid Communications* **2006,** 27 (22), 1955-1961 DOI: 10.1002/marc.200600410.
81. Jiang, Z.; Boyer, M. T.; Sen, A. Chiral and Steric Recognition in Optically Active, Isotactic, Alternating .alpha.-Olefin-Carbon Monoxide Copolymers. Effect on Physical Properties and Chemical Reactivity. *Journal of the American Chemical Society* **1995,** 117 (26), 7037-7038 DOI: 10.1021/ja00131a041.
82. Meyer, A.; Weidner, S. M.; Kricheldorf, H. R. Stereocomplexation of cyclic polylactides with each other and with linear poly(l-lactide)s. *Polymer Chemistry* **2019,** 10 (45), 6191-6199 DOI: 10.1039/c9py01236b.
83. Shin, E. J.; Jones, A. E.; Waymouth, R. M. Stereocomplexation in Cyclic and Linear Polylactide Blends. *Macromolecules* **2011,** 45 (1), 595-598 DOI: 10.1021/ma202184j.
84. Xu, H.; Teng, C.; Yu, M. Improvements of thermal property and crystallization behavior of PLLA based multiblock copolymer by forming stereocomplex with PDLA oligomer. *Polymer* **2006,** 47 (11), 3922-3928 DOI: 10.1016/j.polymer.2006.03.090.
85. Han, L.; Xie, Q.; Bao, J.; Shan, G.; Bao, Y.; Pan, P. Click chemistry synthesis, stereocomplex formation, and enhanced thermal properties of well-defined poly(l-lactic acid)-b-poly(d-lactic acid) stereo diblock copolymers. *Polymer Chemistry* **2017,** 8 (6), 1006-1016 DOI: 10.1039/c6py01989g.
86. Slager, J.; Domb, A. J. Heterostereocomplexes prepared from d-poly(lactide) and leuprolide. I. Characterization. *Biomacromolecules* **2003,** 4 (5), 1308-15 DOI: 10.1021/bm030023g.
87. Tsuji, H.; Hosokawa, M.; Sakamoto, Y. Ternary Stereocomplex Formation of One l-Configured and Two d-Configured Optically Active Polyesters, Poly(l-2-hydroxybutanoic acid), Poly(d-2-hydroxybutanoic acid), and Poly(d-lactic acid). *ACS Macro Letters* **2012,** 1 (6), 687-691 DOI: 10.1021/mz300155f.
88. Fox, T. G.; Garrett, B. S.; Goode, W. E.; Gratch, S.; Kincaid, J. F.; Spell, A.; Stroupe, J. D. Crystalline Polymers of Methyl Methacrylate. *Journal of the American Chemical Society* **1958,** 80 (7), 1768-1769 DOI: 10.1021/ja01540a068.
89. Serizawa, T.; Hamada, K.-i.; Kitayama, T.; Fujimoto, N.; Hatada, K.; Akashi, M. Stepwise Stereocomplex Assembly of Stereoregular Poly(methyl methacrylate)s on a Substrate. *Journal of the American Chemical Society* **2000,** 122 (9), 1891-1899 DOI: 10.1021/ja9913535.
90. Tsuji, H.; Sobue, T. Stereocomplex crystallization and homo-crystallization of enantiomeric substituted poly(lactic acid)s, poly(2-hydroxy-3-methylbutanoic acid)s. *Polymer* **2015,** 69, 186-192 DOI: 10.1016/j.polymer.2015.05.056.
91. Garlotta, D. A literature review of poly(lactic acid). *Journal of Polymers and the Environment* **2001,** 9 (2), 63-84 DOI: Unsp 1566-2543/01/0400-0063/0
Doi 10.1023/A:1020200822435.
92. Tsuji, H. Poly(lactic acid) stereocomplexes: A decade of progress. *Advanced Drug Delivery Reviews* **2016,** 107, 97-135 DOI: 10.1016/j.addr.2016.04.017.
93. Tsuji, H.; Matsuoka, H. Stereoselective Interaction between Isotactic and Optically Active Poly(lactic acid) and Phenyl-Substituted Poly(lactic acid). *Macromolecular Rapid Communications* **2008,** 29 (16), 1372-1377 DOI: 10.1002/marc.200800278.

94. Andersson, S. R.; Hakkarainen, M.; Albertsson, A. C. Stereocomplexation between PLA-like substituted oligomers and the influence on the hydrolytic degradation. *Polymer (United Kingdom)* **2013,** 54, 4105-4111 DOI: 10.1016/j.polymer.2013.06.008.
95. Buchard, A.; Carbery, D. R.; Davidson, M. G.; Ivanova, P. K.; Jeffery, B. J.; Kociok-Köhn, G. I.; Lowe, J. P. Preparation of Stereoregular Isotactic Poly(mandelic acid) through Organocatalytic Ring-Opening Polymerization of a CyclicO-Carboxyanhydride. *Angewandte Chemie* **2014,** 126 (50), 14078-14081 DOI: 10.1002/ange.201407525.
96. Wasanasuk, K.; Tashiro, K.; Hanesaka, M.; Ohhara, T.; Kurihara, K.; Kuroki, R.; Tamada, T.; Ozeki, T.; Kanamoto, T. Crystal Structure Analysis of Poly(l-lactic Acid) α Form On the basis of the 2-Dimensional Wide-Angle Synchrotron X-ray and Neutron Diffraction Measurements. *Macromolecules* **2011,** 44 (16), 6441-6452 DOI: 10.1021/ma2006624.
97. Tashiro, K.; Kouno, N.; Wang, H.; Tsuji, H. Crystal Structure of Poly(lactic acid) Stereocomplex: Random Packing Model of PDLA and PLLA Chains As Studied by X-ray Diffraction Analysis. *Macromolecules* **2017,** 50, 8048-8065 DOI: 10.1021/acs.macromol.7b01468.
98. de Jong, S. J.; van Dijk-Wolthuis, W. N. E.; Kettenes-van den Bosch, J. J.; Schuyl, P. J. W.; Hennink, W. E. Monodisperse Enantiomeric Lactic Acid Oligomers: Preparation, Characterization, and Stereocomplex Formation. *Macromolecules* **1998,** 31, 6397-6402 DOI: 10.1021/ma980553i.
99. Tsuji, H. Poly(lactide) stereocomplexes: Formation, structure, properties, degradation, and applications. *Macromolecular Bioscience* **2005,** 5, 569-597 DOI: 10.1002/mabi.200500062.
100. de Jong, S. J.; De Smedt, S. C.; Wahls, M. W. C.; Demeester, J.; Kettenes-van den Bosch, J. J.; Hennink, W. E. Novel Self-assembled Hydrogels by Stereocomplex Formation in Aqueous Solution of Enantiomeric Lactic Acid Oligomers Grafted To Dextran. *Macromolecules* **2000,** 33 (10), 3680-3686 DOI: 10.1021/ma992067g.
101. Li, S.; Vert, M. Synthesis, Characterization, and Stereocomplex-Induced Gelation of Block Copolymers Prepared by Ring-Opening Polymerization of L(D)-Lactide in the Presence of Poly(ethylene glycol). *Macromolecules* **2003,** 36, 8008-8014 DOI: 10.1021/ma034734i.
102. Hsu, Y.-I.; Masutani, K.; Yamaoka, T.; Kimura, Y. Strengthening of hydrogels made from enantiomeric block copolymers of polylactide (PLA) and poly(ethylene glycol) (PEG) by the chain extending Diels–Alder reaction at the hydrophilic PEG terminals. *Polymer* **2015,** 67, 157-166 DOI: 10.1016/j.polymer.2015.04.026.
103. Saeidlou, S.; Huneault, M. A.; Li, H.; Sammut, P.; Park, C. B. Evidence of a dual network/spherulitic crystalline morphology in PLA stereocomplexes. *Polymer* **2012,** 53 (25), 5816-5824 DOI: 10.1016/j.polymer.2012.10.030.
104. Ma, P.; Shen, T.; Xu, P.; Dong, W.; Lemstra, P. J.; Chen, M. Superior Performance of Fully Biobased Poly(lactide) via Stereocomplexation-Induced Phase Separation: Structure versus Property. *ACS Sustainable Chemistry & Engineering* **2015,** 3 (7), 1470-1478 DOI: 10.1021/acssuschemeng.5b00208.
105. Wei, X. F.; Bao, R. Y.; Cao, Z. Q.; Yang, W.; Xie, B. H.; Yang, M. B. Stereocomplex crystallite network in asymmetric PLLA/PDLA blends: Formation, structure, and confining effect on the crystallization rate of homocrystallites. *Macromolecules* **2014,** 47, 1439-1448 DOI: 10.1021/ma402653a.
106. Li, Y.; Xin, S. Y.; Bian, Y. J.; Dong, Q. L.; Han, C. Y.; Xu, K.; Dong, L. S. Stereocomplex crystallite network in poly(D,L-lactide): formation, structure and the effect on shape memory

behaviors and enzymatic hydrolysis of poly(D,L-lactide). *Rsc Adv* **2015,** 5 (31), 24352-24362 DOI: 10.1039/c5ra01624j.
107. Wanamaker, C. L.; Bluemle, M. J.; Pitet, L. M.; O'Leary, L. E.; Tolman, W. B.; Hillmyer, M. A. Consequences of polylactide stereochemistry on the properties of polylactide-polymenthide-polylactide thermoplastic elastomers. *Biomacromolecules* **2009,** 10 (10), 2904-11 DOI: 10.1021/bm900721p.
108. Huang, Y.; Chang, R.; Han, L.; Shan, G.; Bao, Y.; Pan, P. ABA-Type Thermoplastic Elastomers Composed of Poly(ε-caprolactone-co-δ-valerolactone) Soft Midblock and Polymorphic Poly(lactic acid) Hard End blocks. *ACS Sustainable Chemistry and Engineering* **2016,** 4, 121-128 DOI: 10.1021/acssuschemeng.5b00855.
109. Nakayama, Y.; Aihara, K.; Yamanishi, H.; Fukuoka, H.; Tanaka, R.; Cai, Z.; Shiono, T. Synthesis of biodegradable thermoplastic elastomers fromε-caprolactone and lactide. *Journal of Polymer Science Part A: Polymer Chemistry* **2015,** 53 (3), 489-495 DOI: 10.1002/pola.27463.
110. Cohn, D.; Salomon, A. H. Designing biodegradable multiblock PCL/PLA thermoplastic elastomers. *Biomaterials* **2005,** 26 (15), 2297-305 DOI: 10.1016/j.biomaterials.2004.07.052.
111. Peterlin, A. Molecular model of drawing polyethylene and polypropylene. *Journal of Materials Science* **1971,** 6, 490-508 DOI: 10.1007/BF00550305.
112. Lin, L.; Argon, A. S. Structure and plastic deformation of polyethylene. *Journal of Materials Science* **1994,** 29, 294-323 DOI: 10.1007/BF01162485.
113. Men, Y.; Strobl, G. Critical strains determining the yield behavior of s-PP. *Journal of Macromolecular Science - Physics* **2001,** 40 B, 775-796 DOI: 10.1081/MB-100107561.
114. Séguéla, R. On the natural draw ratio of semi-crystalline polymers: Review of the mechanical, physical and molecular aspects. *Macromolecular Materials and Engineering* **2007,** 292, 235-244 DOI: 10.1002/mame.200600389.
115. Spathis, G.; Kontou, E. Experimental and theoretical description of the plastic behaviour of semicrystalline polymers. *Polymer* **1998,** 39, 135-142 DOI: 10.1016/S0032-3861(97)00221-8.
116. Jabbari-Farouji, S.; Rottler, J.; Lame, O.; Makke, A.; Perez, M.; Barrat, J.-L. Plastic Deformation Mechanisms of Semicrystalline and Amorphous Polymers. *ACS Macro Letters* **2015,** 4, 147-150 DOI: 10.1021/mz500754b.
117. Bartczak, Z.; Vozniak, A. WAXS/SAXS study of plastic deformation instabilities and lamellae fragmentation in polyethylene. *Polymer* **2019,** 177, 160-177 DOI: 10.1016/j.polymer.2019.05.076.
118. Nikolov, S.; Lebensohn, R.; Raabe, D. Self-consistent modeling of large plastic deformation, texture and morphology evolution in semi-crystalline polymers. *Journal of the Mechanics and Physics of Solids* **2006,** 54, 1350-1375 DOI: 10.1016/j.jmps.2006.01.008.
119. Hiss, R.; Hobeika, S.; Lynn, C.; Strobl, G. Network Stretching, Slip Processes, and Fragmentation of Crystallites during Uniaxial Drawing of Polyethylene and Related Copolymers. A Comparative Study. *Macromolecules* **1999,** 32, 4390-4403 DOI: 10.1021/ma981776b.
120. Sperling, L. H., *Introduction to Physical Polymer Science*. 4th ed.; John Wiley & Sons, Inc.: 2005; p 880.
121. Zener, C. M.; Siegel, S. Elasticity and Anelasticity of Metals. *The Journal of Physical and Colloid Chemistry* **1949,** 53 (9), 1468-1468 DOI: 10.1021/j150474a017.
122. Heuchel, M.; Cui, J.; Kratz, K.; Kosmella, H.; Lendlein, A. Relaxation based modeling of tunable shape recovery kinetics observed under isothermal conditions for amorphous shape-memory polymers. *Polymer* **2010,** 51, 6212-6218 DOI: 10.1016/j.polymer.2010.10.051.

123. Haward, R. N.; Thackray, G. The use of a mathematical model to describe isothermal stress-strain curves in glassy thermoplastics. *Proc. R. Soc. London, Ser. A* **1968,** 302 (1471), 453-472 DOI: 10.1098/rspa.1968.0029.
124. Nguyen, T.; Jerryqi, H.; Castro, F.; Long, K. A thermoviscoelastic model for amorphous shape memory polymers: Incorporating structural and stress relaxation. *Journal of the Mechanics and Physics of Solids* **2008,** 56 (9), 2792-2814 DOI: 10.1016/j.jmps.2008.04.007.
125. Halsey, G.; White, H. J.; Eyring, H. Mechanical Properties of Textiles, I. *Textile Research* **1945,** 15 (9), 295-311 DOI: 10.1177/004051754501500901.
126. Buckley, C. Glass-rubber constitutive model for amorphous polymers near the glass transition. *Polymer* **1995,** 36 (17), 3301-3312 DOI: 10.1016/0032-3861(95)99429-x.
127. Hong, K.; Rastogi, A.; Strobl, G. A model treating tensile deformation of semicrystalline polymers: Quasi-static stress-strain relationship and viscous stress determined for a sample of polyethylene. *Macromolecules* **2004,** 37 (26), 10165-10173 DOI: 10.1021/ma049174h.
128. Hong, K.; Rastogi, A.; Strobl, G. Model treatment of tensile deformation of semicrystalline polymers: Static elastic moduli and creep parameters derived for a sample of polyethylene. *Macromolecules* **2004,** 37, 10174-10179 DOI: 10.1021/ma049172x.
129. Duda, A.; Biela, T.; Libiszowski, J.; Penczek, S.; Dubois, P.; Mecerreyes, D.; Jérome, R. Block and random copolymers of ε-caprolactone. *Polymer Degradation and Stability* **1998,** 59 (1-3), 215-222 DOI: 10.1016/s0141-3910(97)00167-5.
130. Stridsberg, K. M.; Ryner, M.; Albertsson, A.-C., Controlled Ring-Opening Polymerization: Polymers with designed Macromolecular Architecture. In *Degradable Aliphatic Polyesters*, Springer Berlin Heidelberg: Berlin, Heidelberg, 2002; pp 41-65.
131. Han, J.; Cao, R. W.; Chen, B.; Ye, L.; Zhang, A. Y.; Zhang, J.; Feng, Z. G. Electrospinning and biocompatibility evaluation of biodegradable polyurethanes based on L-lysine diisocyanate and L-lysine chain extender. *J Biomed Mater Res A* **2011,** 96 (4), 705-14 DOI: 10.1002/jbm.a.33023.
132. Kolb, H. C.; Finn, M. G.; Sharpless, K. B. Click Chemistry: Diverse Chemical Function from a Few Good Reactions. *Angewandte Chemie - International Edition* **2001,** 40, 2004-2021 DOI: 10.1002/1521-3773(20010601)40:11<2004::AID-ANIE2004>3.0.CO;2-5.
133. Riva, R.; Schmeits, S.; Stoffelbach, F.; Jerome, C.; Jerome, R.; Lecomte, P. Combination of ring-opening polymerization and "click" chemistry towards functionalization of aliphatic polyesters. *Chem Commun (Camb)* **2005,** (42), 5334-6 DOI: 10.1039/b510282k.
134. Zhang, H.; Shen, P. K. Recent development of polymer electrolyte membranes for fuel cells. *Chemical Reviews* **2012,** 112 (5), 2780-832 DOI: 10.1021/cr200035s.
135. Gao, Y.; Choudhury, N. R.; Dutta, N. K. Effects of neutralization on the structure and properties of an ionomer. *Journal of Applied Polymer Science* **2012,** 124 (4), 2908-2918 DOI: 10.1002/app.35310.
136. Zhan, S.; Wang, X.; Sun, J. Rediscovering Surlyn: A Supramolecular Thermoset Capable of Healing and Recycling. *Macromol Rapid Commun* **2020,** 41 (24), 2000097 DOI: 10.1002/marc.202000097.
137. Tanaka, M.; Fukasawa, K.; Nishino, E.; Yamaguchi, S.; Yamada, K.; Tanaka, H.; Bae, B.; Miyatake, K.; Watanabe, M. Anion conductive block poly(arylene ether)s: synthesis, properties, and application in alkaline fuel cells. *J Am Chem Soc* **2011,** 133 (27), 10646-54 DOI: 10.1021/ja204166e.

138. Li, N.; Leng, Y.; Hickner, M. A.; Wang, C. Y. Highly stable, anion conductive, comb-shaped copolymers for alkaline fuel cells. *J Am Chem Soc* **2013,** 135 (27), 10124-33 DOI: 10.1021/ja403671u.
139. Yen, F.-S.; Lin, L.-L.; Hong, J.-L. Hydrogen-Bond Interactions between Urethane−Urethane and Urethane−Ester Linkages in a Liquid Crystalline Poly(ester−urethane). *Macromolecules* **1999,** 32 (9), 3068-3079 DOI: 10.1021/ma9804186.
140. Wittenberg, E.; Meyer, A.; Eggers, S.; Abetz, V. Hydrogen bonding and thermoplastic elastomers - a nice couple with temperature-adjustable mechanical properties. *Soft Matter* **2018,** 14 (14), 2701-2711 DOI: 10.1039/C8SM00296G.
141. Tee, H. T.; Koynov, K.; Reichel, T.; Wurm, F. R. Noncovalent Hydrogen Bonds Tune the Mechanical Properties of Phosphoester Polyethylene Mimics. *ACS Omega* **2019,** 4 (5), 9324-9332 DOI: 10.1021/acsomega.9b01040.
142. Lohse, D. J.; Hadjichristidis, N. Microphase separation in block copolymers. *Current Opinion in Colloid & Interface Science* **1997,** 2 (2), 171-176 DOI: 10.1016/s1359-0294(97)80023-4.
143. Jeong, S. I.; Kim, B. S.; Lee, Y. M.; Ihn, K. J.; Kim, S. H.; Kim, Y. H. Morphology of elastic poly(L-lactide-co-epsilon-caprolactone) copolymers and in vitro and in vivo degradation behavior of their scaffolds. *Biomacromolecules* **2004,** 5 (4), 1303-9 DOI: 10.1021/bm049921i.
144. Koning, C.; Van Duin, M.; Pagnoulle, C.; Jerome, R. Strategies for compatibilization of polymer blends. *Progress in Polymer Science (Oxford)* **1998,** 23, 707-757 DOI: 10.1016/S0079-6700(97)00054-3.
145. Jiang, L.; Wolcott, M. P.; Zhang, J. Study of biodegradable polylactide/poly(butylene adipate-co-terephthalate) blends. *Biomacromolecules* **2006,** 7, 199-207 DOI: 10.1021/bm050581q.
146. Liu, H.; Song, W.; Chen, F.; Guo, L.; Zhang, J. Interaction of Microstructure and Interfacial Adhesion on Impact Performance of Polylactide (PLA) Ternary Blends. *Macromolecules* **2011,** 44 (6), 1513-1522 DOI: 10.1021/ma1026934.
147. Coleman, M. M.; Skrovanek, D. J.; Hu, J.; Painter, P. C. Hydrogen bonding in polymer blends. 1. FTIR studies of urethane-ether blends. *Macromolecules* **1988,** 21 (1), 59-65 DOI: 10.1021/ma00179a014.
148. Tant, M. R.; Mauritz, K. A.; Wilkes, G. L., *Ionomers*. Springer Netherlands: 1997; p 514.
149. Kimata, S.; Sakurai, T.; Nozue, Y.; Kasahara, T.; Yamaguchi, N.; Karino, T.; Shibayama, M.; Kornfield, J. A. Molecular basis of the shish-kebab morphology in polymer crystallization. *Science* **2007,** 316 (5827), 1014-7 DOI: 10.1126/science.1140132.
150. Loo, Y. L.; Register, R. A.; Ryan, A. J. Polymer crystallization in 25-nm spheres. *Physical Review Letters* **2000,** 84 (18), 4120-3 DOI: 10.1103/PhysRevLett.84.4120.
151. Huang, P.; Zhu, L.; Cheng, S. Z. D.; Ge, Q.; Quirk, R. P.; Thomas, E. L.; Lotz, B.; Hsiao, B. S.; Liu, L.; Yeh, F. Crystal Orientation Changes in Two-Dimensionally Confined Nanocylinders in a Poly(ethylene oxide)-b-polystyrene/Polystyrene Blend. *Macromolecules* **2001,** 34 (19), 6649-6657 DOI: 10.1021/ma010671x.
152. Mercier, J. P. Nucleation in polymer crystallization: A physical or a chemical mechanism? *Polym Eng Sci* **1990,** 30 (5), 270-278 DOI: 10.1002/pen.760300504.
153. Sangroniz, L.; Cavallo, D.; Müller, A. J. Self-Nucleation Effects on Polymer Crystallization. *Macromolecules* **2020,** 53 (12), 4581-4604 DOI: 10.1021/acs.macromol.0c00223.

154. Fraschini, C.; Pennors, A.; Prud'homme, R. E. Stereocomplex formation between enantiomeric poly(α-methyl-α-ethyl-β-propiolactones): Effect of molecular weight. *Journal of Polymer Science Part B: Polymer Physics* **2007,** 45 (17), 2380-2389 DOI: 10.1002/polb.21240.
155. Wu, G.-p.; Jiang, S.-d.; Lu, X.-b.; Ren, W.-m.; Yan, S.-k. Stereoregular poly(cyclohexene carbonate)s: Unique crystallization behavior. *Chinese Journal of Polymer Science* **2012,** 30 (4), 487-492 DOI: 10.1007/s10118-012-1171-x.
156. Liu, Y.; Wang, M.; Ren, W. M.; Xu, Y. C.; Lu, X. B. Crystalline hetero-stereocomplexed polycarbonates produced from amorphous opposite enantiomers having different chemical structures. *Angewandte Chemie* **2015,** 54 (24), 7042-6 DOI: 10.1002/anie.201501417.
157. Howdeshell, K. L.; Peterman, P. H.; Judy, B. M.; Taylor, J. A.; Orazio, C. E.; Ruhlen, R. L.; Vom Saal, F. S.; Welshons, W. V. Bisphenol A is released from used polycarbonate animal cages into water at room temperature. *Environ Health Perspect* **2003,** 111 (9), 1180-7 DOI: 10.1289/ehp.5993.
158. Niemczyk, A.; Piegat, A.; Sonseca Olalla, Á.; El Fray, M. New approach to evaluate microphase separation in segmented polyurethanes containing carbonate macrodiol. *European Polymer Journal* **2017,** 93, 182-191 DOI: 10.1016/j.eurpolymj.2017.05.046.
159. Ponnamma, D.; George, J.; Thomas, M. G.; Chan, C. H.; Valić, S.; Mozetič, M.; Cvelbar, U.; Thomas, S. Investigation on the thermal and crystallization behavior of high density polyethylene/acrylonitrile butadiene rubber blends and their composites. *Polymer Engineering & Science* **2015,** 55 (5), 1203-1210 DOI: 10.1002/pen.23992.
160. Yilgör, E.; Yurtsever, E.; Yilgör, I. Hydrogen bonding and polyurethane morphology. II. Spectroscopic, thermal and crystallization behavior of polyether blends with 1,3-dimethylurea and a model urethane compound. *Polymer* **2002,** 43 (24), 6561-6568 DOI: 10.1016/s0032-3861(02)00566-9.
161. Marx, C. L.; Cooper, S. L. The crystallinity of ionomers. *Journal of Macromolecular Science, Part B* **2006,** 9 (1), 19-33 DOI: 10.1080/00222347408204538.
162. Papaspyrides, C. D.; Poulakis, J. G.; Arvanitopoulos, C. D. Recycling of glass fiber reinforced thermo-plastic composites. I. Ionomer and low density polyethylene based composites. *Resources, Conservation and Recycling* **1995,** 14 (2), 91-101 DOI: 10.1016/s0921-3449(95)80003-4.
163. Nishida, H. Development of materials and technologies for control of polymer recycling. *Polymer Journal* **2011,** 43 (5), 435-447 DOI: 10.1038/pj.2011.16.
164. Fernandez, J.; Etxeberria, A.; Sarasua, J. R. Synthesis, structure and properties of poly(L-lactide-co-epsilon-caprolactone) statistical copolymers. *J Mech Behav Biomed Mater* **2012,** 9, 100-12 DOI: 10.1016/j.jmbbm.2012.01.003.
165. Watts, A.; Kurokawa, N.; Hillmyer, M. A. Strong, Resilient, and Sustainable Aliphatic Polyester Thermoplastic Elastomers. *Biomacromolecules* **2017,** 18 (6), 1845-1854 DOI: 10.1021/acs.biomac.7b00283.
166. Haward, R. N. Strain hardening of thermoplastics. *Macromolecules* **1993,** 26, 5860-5869 DOI: 10.1021/ma00074a006.
167. Schrauwen, B. A. G.; Janssen, R. P. M.; Govaert, L. E.; Meijer, H. E. H. Intrinsic deformation behavior of semicrystalline polymers. *Macromolecules* **2004,** 37, 6069-6078 DOI: 10.1021/ma035279t.
168. Wang, W.; Ping, P.; Yu, H.; Chen, X.; Jing, X. Synthesis and characterization of a novel biodegradable, thermoplastic polyurethane elastomer. *Journal of Polymer Science Part A: Polymer Chemistry* **2006,** 44 (19), 5505-5512 DOI: 10.1002/pola.21643.

169. Daniel, W. F. M.; Xie, G.; Vatankhah Varnoosfaderani, M.; Burdyńska, J.; Li, Q.; Nykypanchuk, D.; Gang, O.; Matyjaszewski, K.; Sheiko, S. S. Bottlebrush-Guided Polymer Crystallization Resulting in Supersoft and Reversibly Moldable Physical Networks. *Macromolecules* **2017,** 50 (5), 2103-2111 DOI: 10.1021/acs.macromol.7b00030.
170. Farhan, M.; Rudolph, T.; Nöchel, U.; Yan, W.; Kratz, K.; Lendlein, A. Noncontinuously responding polymeric actuators. *ACS Applied Materials and Interfaces* **2017,** 9, 33559-33564 DOI: 10.1021/acsami.7b11316.
171. Bothe, M.; Pretsch, T. Bidirectional actuation of a thermoplastic polyurethane elastomer. *Journal of Materials Chemistry A* **2013,** 1, 14491-14497 DOI: 10.1039/c3ta13414h.
172. Wang, K.; Jia, Y. G.; Zhu, X. X. Two-Way Reversible Shape Memory Polymers Made of Cross-Linked Cocrystallizable Random Copolymers with Tunable Actuation Temperatures. *Macromolecules* **2017,** 50, 8570-8579 DOI: 10.1021/acs.macromol.7b01815.

MRS Advances © 2019 Materials Research Society
DOI: 10.1557/adv.2019.465

Appendix I:

Investigating the Phase-Morphology of PLLA-PCL Multiblock Copolymer / PDLA Blends Cross-linked Using Stereocomplexation

Victor Izraylit[1,2], Oliver E. C. Gould[1], Karl Kratz[1], Andreas Lendlein[1,2*]

[1] *Institute of Biomaterial Science and Berlin-Brandenburg Centre for Regenerative Therapies, Helmholtz-Zentrum Geesthacht, Kantstrasse 55, 14513 Teltow, Germany*
[2] *Institute of Chemistry, University of Potsdam, Karl-Liebknecht-Str. 24/25, 14476 Potsdam, Germany*

ABSTRACT

The macroscale function of multicomponent polymeric materials is dependent on their phase-morphology. Here, we investigate the morphological structure of a multiblock copolymer consisting of poly(L-lactide) and poly(ε-caprolactone) segments (PLLA-PCL), physically cross-linked by stereocomplexation with a low molecular weight poly(D-lactide) oligomer (PDLA). The effects of blend composition and PLLA-PCL molecular structure on the morphology are elucidated by AFM, TEM and SAXS. We identify the formation of a lattice pattern, composed of PLA domains within a PCL matrix, with an average domain spacing d0 = 12 – 19 nm. The size of the PLA domains were found to be proportional to the block length of the PCL segment of the copolymer and inversely proportional to the PDLA content of the blend. Changing the PLLA-PCL / PDLA ratio caused a shift in the melt transition Tm attributed to the PLA stereocomplex crystallites, indicating partial amorphous phase dilution of the PLA and PCL components within the semicrystalline material. By elucidating the phase structure and thermal character of multifunctional PLLA-PCL / PDLA blends, we illustrate how composition affects the internal structure and thermal properties of multicomponent polymeric materials. This study should facilitate the more effective incorporation of a variety of polymeric structural units capable of stimuli responsive phase transitions, where an understanding the phase-morphology of each component will enable the production of multifunctional soft-actuators with enhanced performance.

INTRODUCTION

Biodegradable polymers such as polylactones [1] and their blends are highly desirable for the creation of degradable implants [2, 3], drug delivery systems [4, 5] and sustainable packaging solutions [6]. The synthetic alteration of lactide-based copolyesters and their combination with other polymeric segments has led to the

determination of a structure-property relationship and enabled tailoring of their bulk properties [7, 8], with the realization of emergent behavior unseen in homopolymer materials [9-11]. However, the combination of multiple chemically distinct entities (e.g. segments in block copolymers or blend components) must overcome issues with their compatibility to control the resulting matrix architecture and subsequent function [12, 13]. It is essential to understand the distribution of each polymeric component within the material.

Polylactide (PLA) is a bioresorbable thermoplastic material, whose potential applications have been limited by its high stiffness and inherent brittleness (E = 1.5 – 4 GPa, ε_{break} < 100% in ambient conditions) [14]. Poly(ε-caprolactone) (PCL) is a highly elastic biodegradable polymer, with significantly higher mechanical stability (E = 0.2 – 0.4 GPa, ε_{break} up to 1000% in ambient conditions) [15]. The combination of these two polymers gives a semicrystalline material with two thermally distinct crystalline domains, from PCL ($T_g \approx$ –60 °C and $T_m \approx$ 60 °C) [14] and PLA ($T_g \approx$ 60 °C and $T_m \approx$ 170 °C)[15], and greatly enhanced mechanical properties.

Blending approaches provide a low-cost and efficient means to combine the two polymers, where the blend ratio can be used to tune the thermal and mechanical properties of the materials [16]. However, due to their immiscibility [17], phase separation leads to inhomogeneity within the material [18]. The blending of PLA and PCL homopolymers has been demonstrated to result in the formation of micrometer-scale droplets of the minority component with sizes dependent on the blend ratio [19]. Altering the PCL-to-PLA ratio within the blend also resulted in an approx. 10 °C change in the measured melting temperature of PCL, caused by a variation in the interpenetration of PCL and PLA amorphous phases within the semicrystalline material.

The synthetic realization of copolymers with both PCL and PLA segments has enabled the creation of materials with higher phase interpenetration than their homopolymer blend equivalents. Bi-continuous lamellar or cylindrical morphologies are formed dependant on the ratio of two segments within the material [20]. Within the semicrystalline material the separated amorphous domains of the PLA and PCL copolymer segments can partially interpenetrate, resulting in a composition-dependent shift of the maximum in the PLA melting transition of up to 15 °C [21, 22].

Crystallization plays an important role in determining the morphological structure of the material. Upon cooling, the crystallization of PLA and PCL domains drives further phase separation, observed by SAXS, before an increase in miscibility is observed upon melting [20]. The introduction of PLA stereocomplexation has recently received interest for the creation of tuneable physical netpoints within pseudo-cross-linked matrices [23]. The corresponding increase in PLA crystallization rate, caused by the energetic favourability of stereocomplex crystallites [24], has been shown to promote phase separation in PLA-based copolymer blends [25, 26]. Further clarification of the roles of these different compositional elements, specifically their spatial distribution and structure, should enhance our control over the thermal and mechanical characteristics of multicomponent polymeric materials.

In this work we investigate the phase-morphology of a blend material, consisting of a multiblock copolymer with poly(*L*-lactide) and poly(ε-caprolactone) segments (PLLA-PCL) and a poly(*D*-lactide) oligomer (PDLA). Within this material, PDLA molecules and PLLA segments form a physically crosslinked network via PLA stereocomplexation. Through investigation with SAXS, AFM, TEM and DSC we elucidate the phase-morphology of PLLA-PCL / PDLA blends and its influence on the thermal properties of the material.

EXPERIMENTAL SECTION

Material preparation

The multiblock copolymer containing poly(*L*-lactide) and poly(ε-caprolactone) segments was synthesized as reported elsewhere [27, 28].

Three batches of PLLA-PCL were synthesized in this work: PLLA12-PCL58, PLLA15-PCL64 and PLLA12-PCL20, where numbers stand for number average lengths of the respective segments as determined with ^{1}H NMR. The weight average molecular weight M_w of all of the PLLA-PCL batches were similar around 500 kg · mol^{-1} determined by a multidetector GPC setup. The difference in molecular characteristics between the two batches (PLLA12-PCL58 and PLLA15-PCL64) were found to be insignificant within margin of error of the used techniques (12% and 10% of the measured value for ^{1}H NMR and GPC respectively).

Poly(*D*-lactide) (PDLA) was synthesized via the ring-opening polymerization of *D,D*-dilactide (99.5%, Corbion, Amsterdam, Netherlands), using tin(II)-*2*-hexanoate ($Sn(Oct)_2$) (96%, Alfa Aesar, Ward Hill, USA) as the catalyst and 1-hexanol (99%, Acros Organics, Geel, Belgium) as the initiator. The number average molecular weight of PDLA was determined with ^{1}H NMR as M_n = 1.9 kg · mol^{-1}.

Films were prepared via solution casting. The polymers were dissolved at a predetermined ratio in chloroform (99.9%, Carl Roth, Karlsruhe, Germany). The solution was stirred for 3 hours until the polymers were dissolved, before pouring into a polytetrafluoroethylene (PTFE) Petri dish, covering with aluminium foil and left to evaporate in ambient conditions for 2 days. The produced blends were named as PLLA12-PCL58-SCX, were X stays for the weight content of PDLA in the blends.

Nuclear magnetic resonance spectroscopy (NMR)

^{1}H NMR spectra were recorded using a DRX Avance 500 MHz spectrometer (Bruker, Rheinstetten, Germany) at room temperature in deuterated chloroform. Chemical shifts (δ) are reported in parts per million (ppm) relative to residual chloroform at δ 7.26 ppm. Samples were dissolved in $CDCl_3$ at concentration of 15 mg·mL^{-1}. The spectra were evaluated according to the position and intensity of signals as reporter elsewhere.[29]

X-ray crystallographic analysis

Weight average molecular weights of starting materials and products were determined by gel permeation chromatography (GPC), using a Tosoh EcoSEC HLC-8320 Gel Permeation Chromatograph equipped with a refractive index detector (Tosoh Bioscience, Stuttgart, Germany) combined with a PSS Universal Data Center (PSS, Mainz, Germany), a viscometer ETA2010 (PSS, Mainz, Germany), an EcoSEC UV detector 8320 (Tosoh Bioscience), a light scattering detector SLD7100 (PSS, Mainz, Germany) and two HT-GPC columns type PSS SDV analytical linear M 5 µm (PSS, Mainz, Germany) connected in series. For the measurements, by universal calibration, tetrahydrofuran (THF) was used as an eluent (35 °C, 1.0 mL·min^{-1}) with 0.05 weight content 3,5-di-*tert*-butyl-4-hydroxytoluene as an internal standard. Molecular weight calculations were performed using WINGPC 6.2 (PSS) SEC software (Polymer Standard Service, Mainz, Germany).

Differential scanning calorimetry (DSC)

DSC experiments were conducted on a Netzsch DSC 204 Phoenix (Selb, Germany) at heating and cooling rates of 10 °C·min^{-1} in pierced aluminum pans. For determining the thermal properties of the polymers and blends, the materials were scanned in the temperature range -100 – 200 °C. The crystallinity of all components was calculated according to the equation:

$$\chi_c = \frac{\Delta H_m}{\Delta H_m^{100}} \cdot \frac{1}{W} \cdot 100$$

Where ΔH_m is the experimental melting enthalpy of a fraction, determined as the area under the melting peak. ΔH_m^{100} is the specific melting enthalpy of 100% crystalline polymer, which is 135 J·g^{-1} for PCL [30] and 142 J·g^{-1} for PLA stereocomplex [31]. *W* is the weight content of the fraction in the copolymer of the blend. The PLA stereocomplex fraction was calculated as the maximal amount of coupling *L*- and *D*-lactide units. The data was registered at the first cooling and the second heating run.

X-ray crystallographic analysis

Wide angle X-ray scattering (WAXS) measurements were performed with a D8 Discover spectrometer with a 2D-detector from (Bruker AXS, Karlsruhe, Germany) in the temperature range 25 – 70 °C. The samples of dimensions 2 x 0.5 cm and width 150 µm were fixed at both ends during characterization.

Small angle X-ray scattering (SAXS) experiments were performed on a Bruker Nanostar diffractometer (Bruker AXS, Karlsruhe, Germany), using a 400 µm beam with a wavelength of 0.15418 nm (CuKα) and a Vantec-2000 detector (2048*2048 pixel, 68 µm pixel size) to record scattered intensities at a distance of 1050 mm from the samples.

Transition electron microscopy (TEM)

TEM investigations were performed on a Talos F200A (FEI, Eindhoven, The Netherlands) with high-brightness electron source (X-FEG) and an information limit of 0.12 nm. The prepared samples were all analyzed at 200 kV using a CompuStage Single-Tilt holder (FEI, Eindhoven, The Netherlands). The images were obtained with a CMOS technology based camera model Ceta 16M (FEI, Eindhoven, The Netherlands) with a resolution of 4000×4000 pixels. The samples were prepared by cutting with a diamond knife. The cuts were deposited at Lacey-carbon film on 400 mesh copper grid with 42 µm mesh size. The surface area morphology was evaluated using ImageJ software.

Atomic force microscopy (AFM)

AFM measurements were performed by AFM Multimode with NanoScope V Controller with Veeco thermal application controller (Veeco Instrument Inc., New York, USA). The samples were prepared by cutting with a diamond knife. Samples with an approximate thickness of 100 nm were then placed on a silica grid, before scanning at ambient temperature (25 °C). Imaging was performed in a tapping mode with a scan rate of 0.8–1.0 Hz. An RTESPA-150 probe (Bruker, Karlsruhe, Germany) with a typical driving frequency of 150 kHz (individual difference ranged from 90 to 210 kHz) and a typical spring constant of 5 N·m^{-1} (individual difference ranged from 1.5 to 10 N·m^{-1}) was used. The tip radius and height were 10 – 15 nm and 10 ± 2 µm respectively. The tip

was of rectangular shape with a front angle of 15 ±2 °, a side angle of 17.5 ±2 ° and a back angle of 25 ± 2°. Scans sizes of 1 ×1 μm were chosen to visualize the morphology of the material.

Dynamic mechanical thermal analysis (DMTA)

DMTA measurements were performed using an Eplexor 25 N (Gabo, Ahlden, Germany) equipped with a 25 N load cell using a standard test specimen type (DIN EN ISO 527-2/1BB). The applied oscillation frequency was 1 Hz. The measurement was performed in the temperature sweep mode from −100 to 100 °C with a constant heating rate of 1 °C·min−1. The glass transition (T_g) was determined at the peak maximum of loss modulus (E'') vs temperature curve.

RESULTS AND DISCUSSION

Thermal properties

The thermal characteristics of the samples, obtained from differential scanning calorimetry (DSC) analysis, are shown in Table I. Glass transition T_g was not visible in DSC. Mixed glass transition T_g = – 40 ± 3 °C was determined for all studied samples as maximum of loss modulus E'' in dynamic mechanical thermo-analysis (DMTA). A mixed glass transition indicates interpenetration of PLA and PCL amorphous phases [32]. A thermal transition of PLLA12-PCL58 attributed to the melting of PCL domains within the material was observed with a peak maximum at T_m = 52 ± 1 °C with a melting enthalpy ΔH corresponding to a relative crystallinity χ_c = 36 ± 4%. PLA homopolymer is incapable of crystallization at block lengths of lower than 7 repeating units [33]. PLA stereocomplex, being an energetically preferable structure, can be formed with only 5 repeating units. However, the additional loss of flexibility of the chain as a result of its incorporation in a multiblock copolymer structure, renders several end monomer units of each block unavailable for crystallization. The minimal block length required for crystallization and stereocomplexation of PLLA segments within a multiblock copolymer is slightly higher. 12 – 15 repeating units were experimentally determined for the polymer samples presented here to be sufficient for PLA stereocomplex formation, but still too short for the formation of pure PLLA crystallites. This is supported by the absence of a PLLA melting transition in DSC. The observed melt transition of PCL T_m remains similar with the addition of up to 10 wt.% PDLA into the blend. PCL crystallinity was observed to increase to χ_c = 48 ± 5% in PLLA12-PCL58-SC2 and further decrease to χ_c = 38 ± 4% with the increase of PDLA content to 10 wt.%. Block copolymer segments generally hinder the crystallization of each other, however, segments of close compositions have been reported to support crystallization of neighboring units [34, 35]. The cross-link density, i.e. the PLA stereocomplex content, did not appear to disturb the crystallinity of the PCL matrix, while the introduction of cross-links formed from covalent chemical bonding generally disrupt the ability of a material to crystallize [36]. DSC traces of all of the blend samples possess a broad PLA stereocomplex melting transition with a maximum in the region of T_m = 171 – 181 °C. The observed lower melt transition T_m, when compared to that reported in the literature T_m > 200 °C, is the result of the low M_w of the PLLA segment [24] and dilution of the amorphous phases of PLA and PCL [19, 21, 22]. The increase in T_m of PLA stereocomplex and absence of any effect on T_m of PCL with the increase of PDLA content in the matrix suggests that although PLLA and PCL amorphous phases of the

pure PLLA-PCL are partially interpenetrated, PDLA has higher affinity to the PLLA part of the matrix and does not dilute the PCL amorphous phase. A decrease in the crystallinity of the PLA stereocomplex from χ_c = 57 ± 6% to 35 ± 4% was observed, with higher values in the blends with higher PDLA content.

Table I. Thermal properties of PLLA-PCL and its PDLA blends obtained from DSC

Sample[a]	**PCL***			**PLA stereocomplex***		
	ΔH ($J \cdot g^{-1}$)[b]	T_m (°C)[b]	χ_c (%)[c]	ΔH ($J \cdot g^{-1}$)[b]	T_m (°C)[b]	χ_c (%)[c]
PLLA12-PCL58	42±4	52±1	36±4	-	-	-
PLLA12-PCL58-SC1	42±4	54±1	42±5	1.6±0.2	177±1	57±6
PLLA12-PCL58-SC2	43±5	54±1	44±5	2.3±0.2	181±1	41±4
PLLA12-PCL58-SC5	42±4	54±1	46±5	5±0.5	180±1	35±4
PLLA12-PCL58-SC10	34±3	42±1	38±4	10±1	171±1	37±4

* Attributed to the respective crystalline domains according to literature data. [a] Sample name PLLAX-PCLY-SCZ where X and Y stay for number average block length of PLLA and PCL respectively in PLLA-PCL multiblock copolymer respectively, determined with ^{1}H NMR, Z stays for PLLA-PCL / PDLA wt. ratio of the blend. [b] Intrinsic melting enthalpy, as the peak area, and melting temperature, as the peak maximum position. [c] Degree of crystallinity, as the ratio between ΔH and ΔH_m^{100} of 100% crystalline polymers. T_g was not visible in DSC measurements and was determined as T_g = –40 ± 3 °C for all samples with DMTA. DSC error was considered according to technical specification of the equipment.

Crystalline structure

The crystalline structure of the materials was studied by WAXS at room temperature. A representative WAXS profile is presented in Figure 1. The PCL crystalline reflections (110) and (200) in the positions 2θ = 21.5° and 2θ = 24° respectively overlap with PLA stereocomplex (300) and (030) signals at 2θ = 20.5° an (220) at 2θ = 24°. A singular 2θ = 12° signal originates from the scattering of the (110) PLA stereocomplex plane. The absence of a significant signal in 2θ = 16° region further confirms the incapability of PLLA segments or PDLA molecules to crystallize outside of stereocomplexation. The presence of PCL crystallites in the pure multiblock copolymer samples PLLA12-PCL58 and PLLA12-PCL20 was observed. Both PCL crystalline domains and PLA stereocomplexes crystallites were observed in the structure of the blends PLLA12-PCL58-SC10 and PLLA12-PCL20-SC20.

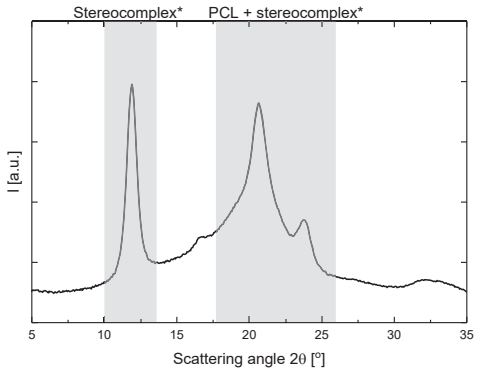

Figure 1. WAXS spectra of PLLA12-PCL20-SC20 showing the presence of stereocomplex crystallites and PCL crystalline domains (indicated in grey). * Attributed to the respective crystalline domains according to the literature data.

Phase-morphology

To understand the phase-morphology of the material depending on its composition and the distribution of PCL and PLA domains, AFM, TEM and SAXS were used to characterize the samples.

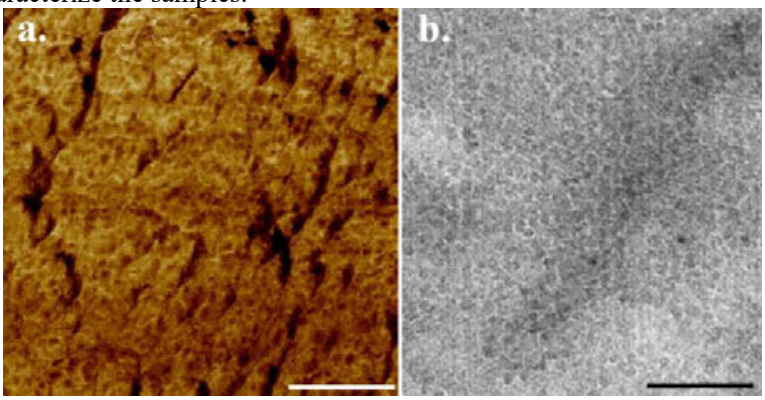

Figure 2. (a) AFM phase image and (b) TEM image of PLLA15-PCL64-SC1. Scale bar 200 nm.

AFM phase imaging at 25 °C (Figure 2a) shows distinct separation between harder and softer domains. Softer regions with a diameter of d = 18 – 25 nm are surrounded by harder regions with width h = 4 – 8 nm. As imaging was performed at a temperature higher than the T_g of PLA, as measured by DMTA, we attribute the softer areas to the PLA domains that exist in an amorphous state in this sample (Table I). The higher crystallinity of the PCL within the material should cause higher local mechanical stiffness, resulting in a contrast difference between the two components by AFM phase imaging. We therefore attribute the harder regions to crystalline PCL.

TEM images taken at 25 °C, as shown in Figure 2b, reveal a similar microphase separated lattice morphology. The average domain spacing d = 10 – 20 nm is in agreement with the AFM findings. The displayed images are representative of all of the studied blend samples and a similar morphology was also observed for the pure PLLA-PCL sample. The form of the domains did not change with the variation of PLLA-PCL block structure, PLLA-PCL / PDLA blend ratio and crystallinity of the components of the matrix. The similarity in the morphology observed by TEM, where differences in electron density provide contrast, and AFM phase imaging, where differences in mechanical stiffness provide contrast, indicates that the observed domains are chemically and mechanically distinct. Based on the observed difference in electron density and local mechanical stiffness of the islands and the spaces between them, we believe that the islands are formed of predominantly amorphous PLA and contain the PLA stereocomplex crystallites, while the spacing is formed of predominantly crystalline PCL. Additional PCL crystalline lamellae can also be seen in the TEM images.

The observed change in the maximum of the melt transition attributed to the PLA stereocomplex, as measured by DSC, provides evidence of PLA/PCL amorphous phase dilution. As the PLA content of the material is increased the relative disruption of PLA crystallization by amorphous PCL segments is reduced, leading to an increase in melting temperature. Despite the partial interpenetration of the amorphous phase of both polymer segments, they remain phase separated.

SAXS analysis was performed to further characterize the observed morphological features. The average domain spacing was calculated as a maximum of

the $I(d)\cdot q^2$ function (Figure 3a). The results further support the AFM and TEM data, with a strong maximum measured corresponding to d_0 = 15 – 20 nm, which we attribute to the morphological domain observed by TEM and AFM. The observed second maximum in the $2q_0$ region for all of the curves implies presence of ordered structures. A linear dependency of d_0 on the matrix composition was observed for the PLLA15-PCL64-SCX blends in the studied region (Figure 3b). However, the pure multiblock copolymer PLLA15-PCL64 did not follow this trend, indicating that stereocomplexation affects the microphase separation. An increase in the PDLA content of the material, and subsequently the PLA stereocomplex content reduces d_0 as a result of the denser packing of PLA domains with the increase in crystallization. The shorter PCL average segment length of PLLA12-PCL20, results in a lower value of d_0 = 15.8 nm, which further decreases to a value of 12.1 nm in the PLLA12-PCL20-SC20 blend.

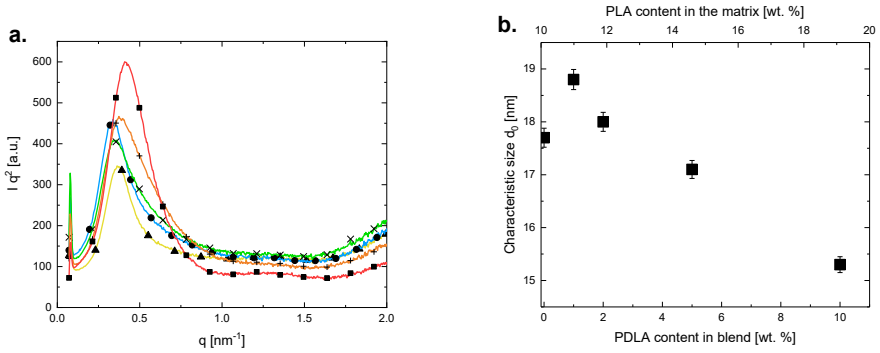

Figure 3. (a) SAXS spectra of PLLA15-SC64 – yellow (triangles), PLLA15-SC64-SC1 – blue (circles), PLLA15-SC64-SC2 – green (cross symbol), PLLA15-SC64-SC5 – orange (plus symbol) and PLLA15-SC64-SC10 – red (squares). (b) Effect of PDLA content in PLLA15-SC64 blends on the average domain spacing studied by SAXS.

CONCLUSION

In this work we investigate the morphology of blends composed of a multiblock copolymer (PLLA-PCL) containing poly(*L*-lactide) and poly(ε-caprolactone) segments and a poly(*D*-lactide) oligomer (PDLA). Different PLLA-PCL block structures (20 and 64 average monomer repeating units of ε-caprolactone) and different blend compositions (1 wt.%, 2 wt.%, 5 wt.%, 10 wt.% and 20 wt.% of PDLA content) were studied. AFM and TEM analysis revealed a lattice pattern of PLA islands within a PCL matrix, caused by the phase separation of PLA and PCL domains. The average domain spacing d_0 = 12 – 19 nm, determined from SAXS data, was observed to vary with the PDLA and PCL content of the material. A reduction in the PCL average segment length from 64 to 20 repeating units caused the value of d_0 to decrease from 17.7 nm to 15.8 nm. Further, a 5 °C increase in the maximum of the PLA stereocomplex melt transition was observed with a 5 wt.% increase of PDLA content of the matrix, indicating the partial dilution of PCL and PLA amorphous phases within the semicrystalline material. The insight into the phase-separated structure of PCL and PLA containing materials provided here should further facilitate their use in actuator materials whose requirements in terms of thermal and morphological structure closely match those reported here.

Acknowledgments

This work was financially supported by the Helmholtz-Association of German Research Centers (through program-oriented funding, and through the Helmholtz Graduate School of Macromolecular Bioscience [MacroBio], grant no. VH-GS-503). The authors thank Ms. Susanne Schwanz for the XRD and DSC measurements, Ms. Yvonne Pieper for the TEM scans and Dr. Liudmila Lysyakova for the AFM experiments.

References

1. M.A. Hillmyer and W.B. Tolman, *Acc. Chem. Res.* **47**, 2390 (2014).
2. A.-C. Albertsson and I.K. Varma, *Biomacromolecules* **4**, 1466 (2003).
3. S. Farah, D.G. Anderson and R. Langer, *Adv. Drug Del. Rev.* **107**, 367 (2016).
4. T.M. Allen and P.R. Cullis, *Science* **303**, 1818 (2004).
5. P. Saini, M. Arora and M.N.V.R. Kumar, *Adv. Drug Del. Rev.* **107**, 47 (2016).
6. R. Auras, B. Harte and S. Selke, *Macromol. Biosci.* **4**, 835 (2004).
7. M. Hiljanen-Vainio, P. Varpomaa, J. Seppälä and P. Törmälä, *Macromol. Chem. Phys.* **197**, 1503 (1996).
8. H. Liu and J. Zhang, *J. Polym. Sci., Part B: Polym. Phys.* **49**, 1051 (2011).
9. M.J. Fasolka and A.M. Mayes, *Annu. Rev. Mater. Res.* **31**, 323 (2001).
10. J.K. Kim, S.Y. Yang, Y. Lee and Y. Kim, *Progress in Polymer Science (Oxford)* **35**, 1325 (2010).
11. A. Lendlein and O.E.C. Gould, *Nat. Rev. Mater.* **4**, 116 (2019).
12. C. Koning, M. Van Duin, C. Pagnoulle and R. Jerome, *Progress in Polymer Science (Oxford)* **23**, 707 (1998).
13. L. Jiang, M.P. Wolcott and J. Zhang, *Biomacromolecules* **7**, 199 (2006).
14. D. Garlotta, *J. Polym. Environ.* **9**, 63 (2001).
15. M. Labet and W. Thielemans, *Chem. Soc. Rev.* **38**, 3484 (2009).
16. J.-m. Yang, H.-l. Chen, J.-w. You and J.C. Hwang, **29**, 657 (1997).
17. R. Dell'Erba, G. Groeninckx, G. Maglio, M. Malinconico and A. Migliozzi, *Polymer* **42**, 7831 (2001).
18. O.J. Botlhoko, J. Ramontja and S.S. Ray, *Polym. Degrad. Stab.* **154**, 84 (2018).
19. D. Newman, E. Laredo, A. Bello, A. Grillo, J.L. Feijoo and A.J. Muller, *Macromolecules* **42**, 5219 (2009).
20. A.M. Mannion, F.S. Bates and C.W. MacOsko, *Macromolecules* **49**, 4587 (2016).
21. E. Laredo, N. Prutsky, A. Bello, M. Grimau, R.V. Castillo, A.J. Müller and P. Dubois, *European Physical Journal E* **23**, 295 (2007).
22. W. Han, X. Liao, Q. Yang, G. Li, B. He, W. Zhu and Z. Hao, *RSC Advances* **7**, 22515 (2017).
23. D.-d. Yang, W. Liu, H.-m. Zhu, G. Wu, S.-c. Chen, X.-l. Wang and Y.-z. Wang, *ACS Appl. Mater. Interfaces* **10**, 26594 (2018).
24. H. Tsuji, *Adv. Drug Del. Rev.* **107**, 97 (2016).
25. C.L. Wanamaker, W.B. Tolman and M.A. Hillmyer, *Macromolecular Symposia* **283-284**, 130 (2009).
26. Z. Xiong, X. Zhang, R.R. Wang, S. De Vos, R.R. Wang, C.A.P. Joziasse and D. Wang, *Polymer* **76**, 98 (2015).
27. M. Jikei, Y. Takeyama, Y. Yamadoi, N. Shinbo, K. Matsumoto, M. Motokawa, K. Ishibashi and F. Yamamoto, *Polym. J.* **47**, 657 (2015).
28. V. Izraylit, *Private Communication*.
29. G. Perego, T. Vercellio and G. Balbontin, *Die Makromolekulare Chemie* **194**, 2463 (1993).
30. V. Crescenzi, G. Manzini, G. Calzolari and C. Borri, *Eur. Polym. J.* **8**, 449 (1972).
31. H. Tsuji, *Macromol. Biosci.* **5**, 569 (2005).
32. A. Lendlein and S. Kelch, *Angew. Chem. Int. Ed.* **41**, 2034 (2002).
33. S.J. de Jong, W.N.E.E. van Dijk-Wolthuis, J.J. Kettenes-Van Den Bosch, P.J.W.W. Schuyl and W.E. Hennink, *Macromolecules* **31**, 6397 (1998).
34. S. Pensec, M. Leroy, H. Akkouche and N. Spassky, *Polym. Bull.* **45**, 373 (2000).
35. O.V. Stoyanov, R.M. Khuzakhanov, L.F. Stoyanova, V.K. Gerasimov, A.E. Chalykh, A.D. Aliev and M.V. Vokal', *Polymer Science Series D* **4**, 118 (2011).
36. K. Sen, B. Mukherjee, A.S. Bhattacharyya, L.K. Sanghi, K. Bhowmick and R.T. Centre, **157**, 45 (1990).

Polymer 209 (2020) 122984

Contents lists available at ScienceDirect

Polymer

journal homepage: http://www.elsevier.com/locate/polymer

Appendix II:

Strain recovery and stress relaxation behaviour of multiblock copolymer blends physically cross-linked with PLA stereocomplexation

Victor Izraylit [a,b], Matthias Heuchel [a], Oliver E.C. Gould [a], Karl Kratz [a], Andreas Lendlein [a,b,*]

[a] Institute of Biomaterial Science and Berlin-Brandenburg Centre for Regenerative Therapies, Helmholtz-Zentrum Geesthacht, Kantstr. 55, 14513 Teltow, Germany
[b] Institute of Chemistry, University of Potsdam, Karl-Liebknecht-Str. 24/25, 14476 Potsdam, Germany

ARTICLE INFO

Keywords:
Thermoplastic elastomers
Physical cross-links
Polylactide stereocomplexation

ABSTRACT

Polylactide (PLA) stereocomplexes have attracted attention due to their ability to improve the thermal stability of bioplastics. Here, we evaluate whether PLA stereocomplexes can form stable physical cross-links in blends of a multiblock copolymer with poly(*L*-lactide) and poly(ε-caprolactone) segments (PLLA-PCL) and a poly(*D*-lactide) oligomer (PDLA). Through the investigation of the strain recovery in step-cycle experiments and compliance of stress relaxation behaviour with a three-component model for the deformation of semi-crystalline polymers, PLA stereocomplexes were found to possess sufficient stability in the true strain range $\varepsilon_H < 2.25$ to be described as firm physical netpoints at 70 °C in the studied blends with PLA stereocomplex content $\phi_{c,SC} \geq 1.1$ wt%, when the PCL domains are melted. Limiting $\phi_{c,SC} \leq 6$ wt% broadens the behaviour inherent to elastic cross-linked networks to the strain values up until breakage of the samples, while the increase of $\phi_{c,SC}$ triggers plastic deformations typical for semi-crystalline polymers. Redistributing of internal stresses from the amorphous to crystalline domains at increase of ϕ_c calculated with the adopted model was identified as reason of PLA stereocomplexes failure as stable physical network junctions at higher $\phi_{c,SC}$. Within the experimentally determined strain and composition ranges, in which PLA stereocomplexes possess structural stability, they can form robust cross-links in a polymer network. The knowledge gained here provides valuable design criteria for multifunctional thermoplastic elastomers.

1. Introduction

Biobased polymers are sustainable materials synthesized from renewable resources characterized by neutral carbon footprint [1]. Among others, polylactide (PLA), its copolymers and blends find versatile applications in medicine, packaging production and agriculture due to facile tunability of their physical properties [2–6]. Similarly to other polyesters with a stereocentre in the backbone [7], PLA tends to form thermally and mechanically stable stereocomplexes between two opposite stereoisomers [8]. This feature allows their use as an alternative for covalent cross-links in traditional polymeric networks [9–12], combining thermomechanical stability of the latter with reprocessability of the physical intermolecular interactions. Higher elasticity and resistance to creep [13–15], inherent to thermoplastic elastomers cross-linked with PLA stereocomplexation, facilitates implementation of smart functionalities as shape-memory effect [16–18].

Although often referred as physical netpoints, PLA stereocomplexes are crystallites, which are less strong than covalent bonds and upon deformation should undergo a multi-step process of elasto-plastic structural reorganization typical for all crystals [19]. This raises the question, whether PLA stereocomplexes can be fully perceived as cross-links and what the limitations of this functionality are. A significant part of the reported material systems cross-linked with PLA stereocomplexes contain an additional semi-crystalline component [20]. This suggests the additional questions how the PLA stereocomplex netpoints interact with the second crystalline component and how its content affects the deformation behaviour of the whole system.

In this work we attempt to classify PLA stereocomplexes as physical netpoints in a multiblock copolymer with poly(*L*-lactide) and poly(ε-caprolactone) segments (PLLA-PCL), where a network of physical cross-links is introduced through PLA stereocomplexation in blends with poly(*D*-lactide) oligomer (PDLA). The number-average block length for PLLA and PCL was fixed to 15 and 64 repeating units, respectively, and the number-average molar mass of PLLA-PCL was $M_n = 238$ kg mol^{-1},

* Corresponding author. Institute of Biomaterial Science and Berlin-Brandenburg Centre for Regenerative Therapies, Helmholtz-Zentrum Geesthacht, Kantstr. 55, 14513 Teltow, Germany.
E-mail address: andreas.lendlein@hzg.de (A. Lendlein).

https://doi.org/10.1016/j.polymer.2020.122984
Received 22 June 2020; Received in revised form 19 August 2020; Accepted 23 August 2020
Available online 29 August 2020
0032-3861/© 2020 Helmholtz-Zentrum Geesthacht. Published by Elsevier Ltd. This is an open access article under the CC BY license (http://creativecommons.org/licenses/by/4.0/).

while the PDLA oligomeric compound had $M_n = 3.5$ kg mol^{-1}. Detailed material design considerations and a study of its crystalline structure and phase morphology were presented in the previous work [18,21]. In short, PLLA number-average segment length of 15 repeating units was found to be capable of PLA stereocomplexation, but not of isotactic crystallization, preventing formation of an additional crystallinity in the material, leaving PCL as the only crystalline domain in the pure PLLA-PCL. PCL number-average segment length of 64 repeating units was sufficient to form large crystalline population with content $\phi_{c\ PCL}$ up to 34 wt% and maintain high amount of PLLA segments for physical cross-linking. The morphological changes during PLA stereocomplex formation in the studied materials are schematically illustrated in Fig. 1a. Briefly, the short number-average length of the PLLA segments (15 repeating units) and PDLA molecules (26 repeating units) leads to smaller sizes of PLA stereocomplex crystallites and their even distribution in the matrix. The cross-linking density, i.e. PLA stereocomplex content $\phi_{c\ SC}$, can be tuned by adjusting the PLLA-PCL/PDLA ratio in the blend. Miscibility of the blend components provided by multiblock structure of the PLLA-PCL and

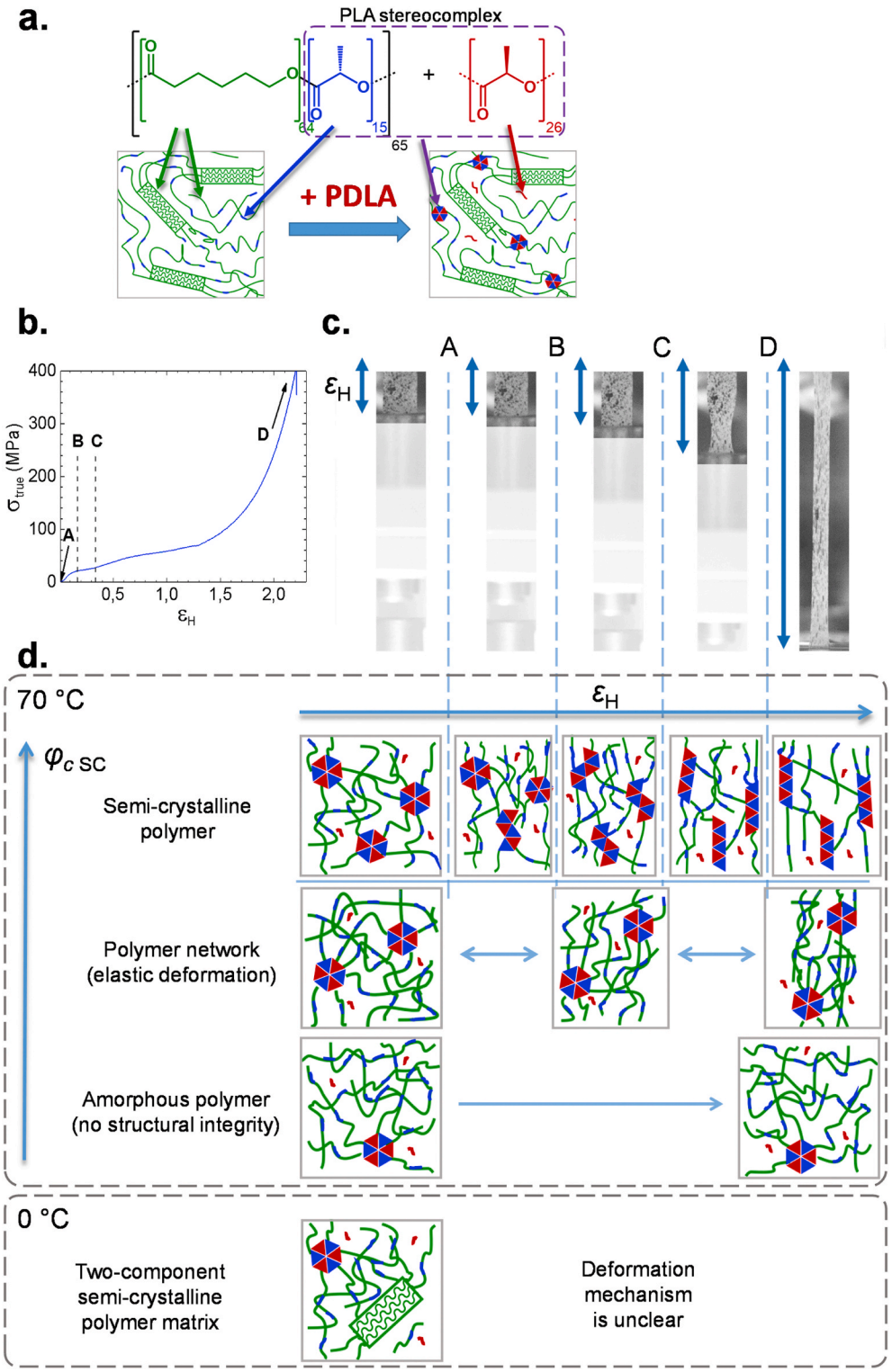

Fig. 1. (a) Schematic illustrating PLLA–PCL/PDLA blend structural change upon addition of PDLA homopolymer component. PDLA homopolymer (red) and PLLA segments (blue) form PLA stereocomplex crystallites, which act as physical netpoints within the semi-crystalline PCL matrix (green). **(b)** Exemplary stress-strain curve for PLLA-PCL-SC10 at 0 °C with estimated positions of the critical points ***A***, ***B***, ***C*** and ***D***. **(c)** Exemplary images of a PLLA–PCL/PDLA blend sample passing through thresholds of deformation: ***A*** – true elastic limit, ***B*** – elastic limit; ***C*** – fibrillation onset; ***D*** – disentangling onset. **(d)** Schematic illustrating the anticipated differences in structural changes in PLLA–PCL/PDLA blends during deformation ε at 70 °C with different PLA stereocomplex content $\phi_{c\ SC}$, as if they behave as semi-crystalline polymers passing through subsequent deformation regimes: truly elastic, elastic, crystallite sliding, fibrillation and network disentangling; as elastic cross-linked polymer networks, where the network junctions remain undeformed; or amorphous polymer. The microscopic deformation mechanisms of a two-component semi-crystalline matrix at 0 °C having PCL crystals and PLA stereocomplexes is unclear. (For interpretation of the references to colour in this figure legend, the reader is referred to the Web version of this article.)

high mobility of the PDLA elaborates formation of mixed amorphous phase with a mixed glass transition $T_g \approx -40$ °C providing the materials with elasticity in the application temperature range. A transition between one- and two-component semi-crystalline systems can be done by melting the PCL domain at 70 °C and reaching its highest degree of crystallinity χ_c at 0 °C.

In order to find out how PLA stereocomplex in the PLLA-PCL/PDLA blend should be classified, the precise differences between the mechanical behaviour of the networks and the semi-crystalline polymers should be defined. Mechanistically, the deformation of covalent networks generally implicates that any microscopic transformations occur in the amorphous phase [22]. Here, the models are built around entropic elasticity of the polymer chains [23,24], confinements applied to the junctions fluctuations [25,26] and restrictions of the chain movements provided by entanglements [27–29], while the netpoints internal structure is postulated to be stable. The model for behaviour of a semi-crystalline polymer matrix was initially proposed by Peterlin [19]. Within semi-crystalline polymeric materials, crystalline domains, dispersed between amorphous polymer, are organized into ordered lamellae within larger spherulites [30]. The classical understanding of plastic deformation of a semi-crystalline polymeric material involves compartmentalization into a series of deformation regimes [19]. At low strain, before the onset of necking, the lamellae are sterically reorganized via shear, slip and rotation before spherulites are stretched into fibrils [31]. This process is accompanied by a partial loss of crystallinity [32,33]. Finally, the interaction of neighbouring fibrils stretches interfibrillar ties and leads to unfolding [34]. Subsequently, the density of the material increases due to strain-induced crystallization and strain hardening is observed [35,36].

A schematic representation of the anticipated structural reorganizations in PLA stereocomplex cross-linked PLLA-PCL/PDLA blends is illustrated in Fig. 1c and d. Here, if the density of the physical cross-links is too low, it would be insufficient to provide mechanical stability and the material would flow as a melted polymer. On the other hand, if the cross-link density is too high, the deformation would be transferred from the amorphous network to the PLA stereocomplex netpoints at lower strains causing elasto-plastic deformation of the latter. In this case the material would behave as a typical semi-crystalline polymer. The intermediate cross-link density should be sufficient to provide mechanical stability and the spacing between the netpoints should be high enough to grant the material an elastic behaviour typical for a polymer network. Unclear, however, remains the deformation mechanism of a matrix containing both PCL crystallites and PLA stereocomplexes.

To identify, whether the PLLA-PCL/PDLA blends behave as a semi-crystalline polymer or a network and at which $\phi_{c\ SC}$ the transition between these behaviours happens, their deformation behaviour was described with a model for semi-crystalline polymers initially proposed by Strobl's group [37,38]. The deviations observed in the behaviour of the studied blends from the elements of the adopted model were interpreted in the context of the behaviour anticipated for polymer networks. The model postulates that the deformation consists of a reversible elastic and irreversible plastic contribution. Changes in their ratio indicate critical strain values, namely at points *A*, *B*, *C* and *D*, where the deformation mechanisms subsequently substitute one another. Fig. 1c and d demonstrate a schematic representation of the morphological changes at these points and Fig. 1b shows their approximate positions on the stress-strain curve. Above point *A*, the true elastic limit, the deformation is no longer purely elastic. Isolated crystal sliding events provide an irreversible plastic contribution to the overall elongation. The crystal motion becomes a collective phenomenon at the elastic limit, point *B*. It can be characterized as the point with the maximal curvature at the yield point on the stress-strain diagram. At point *C* the stress reaches its critical value, at which crystallites are no longer stable, and fibril formation begins. Finally, at point *D* the strain reaches a value which initiates the disentangling of the amorphous network. The strain values at *A*, *B* and *C* have been reported to be invariant strain values, showing no variation with crystallinity or temperature [37,39–41]. However, the stress values at these points directly depend on χ_c. The strain at point *D* can vary, depending on the conditions of the experiment, e.g. temperature.

At the same time, the stresses are distributed within a semi-crystalline matrix among three constituents: viscous forces, elastic response of the amorphous network and the deformation forces of the crystalline domains. The principle schematics of the Hong-Strobl model is depicted in Fig. 2. The three branches describe three principle processes happening during the stretching of a semi-crystalline polymeric material to ε_H with stress σ. The first branch is responsible for the viscoelastic behaviour of the material. The relaxing stress component σ_r is distributed to this branch of the model. This process can be described with an elastic modulus E_r and the viscous parameters of the Eyring law of viscosities: the reference stress σ_0 and the reference strain rate $\dot{\varepsilon_0}$. The second branch describes the purely elastic behaviour of the entangled amorphous network. As related to the amorphous network stress $(1 - \phi_c)\sigma_n(\varepsilon_H)$, dependent on the crystallite content in the material ϕ_c and the extension of the sample ε_H stored in this branch. The third branch deals with the stresses affecting the crystalline blocks and the elasto-plastic deformations $\varepsilon_e(\varepsilon_H)$ and $\varepsilon_p(\varepsilon_H)$. The crystalline contribution of the stress $\phi_c\ \sigma_c(\varepsilon_H)$ is distributed to this element. For the stress relaxation kinetics the Hong-Strobl model gives the following equation [37,38]:

$$\Delta\sigma\left(t\right) = \sigma_r(0) - 2\sigma_0 \mathrm{atanh}\left[\tanh\left(\frac{\sigma_r(0)}{2\sigma_0}\right)\exp\left(-\frac{t}{\tau_r}\right)\right] \quad (1)$$

where $\Delta\sigma(t) = \sigma_r(t{=}0) - \sigma_r(t)$ is the stress decay in a relaxation process, σ_0 is the above mentioned reference stress and τ_r is the relaxation characteristic time. Three fitting parameters are involved in this equation: $\sigma_r(0)$ – the stress that will relax in infinite time, σ_0 is the characteristic stress representing the slope of the stress relaxation curve in $\Delta\sigma_r(\ln t)$ coordinates and the characteristic time of the process τ_r.

The effect of PLA stereocomplex content in PLLA-PCL/PDLA blends on the deformation behaviour of the material was investigated to establish compliance with the Hong-Strobl model. The mechanical properties were studied in single elongation experiments at $T = 0$ °C and 70 °C. The strain ranges, at which the material gives a purely elastic response, and undergoes lamellar reordering and fibrillation were defined via decomposition of the tensile deformation into plastic and elastic component in the step-cycle experiment. Further, the distribution of stresses between viscoelastic, elastic and elasto-plastic contributions was investigated to understand which domain of the material experiences the applied tensile loads. The stress relaxation behaviour was analyzed and fitted with the Hong-Strobl model Eq. (1) to determine the σ_r viscous forces. The $(1\text{-}\phi_c)\sigma_n(\varepsilon_H)$ amorphous network stresses were estimated in the ideal rubber approximation [42]. Finally, the dependency of the stress constituents on the PLA stereocomplex content in

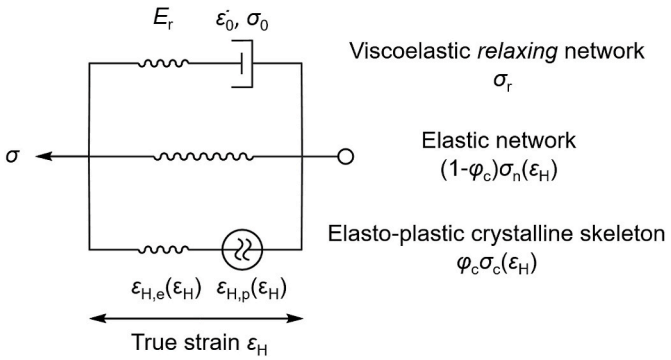

Fig. 2. Stress distribution according to Hong-Strobl model threating deformation of semi-crystalline polymeric materials [37,38]. Adapted with permission from Ref. [37]. Copyright 2004 American Chemical Society.

the PLLA-PCL/PDLA blend was investigated. Out of these detailed thermo-mechanical investigations the strain and elongation ranges, at which PLA stereocomplexes provide sufficiently stable cross-links to preserve the integrity of the physical network, were derived.

2. Experimental

2.1. Materials

The synthesis of PLLA-PCL, PDLA oligomer and film preparation as well as a detailed study of the crystalline structure and phase morphology was reported elsewhere [18,21]. PLLA-PCL studied in this work had number-average molecular weight of $M_n = 238$ kg mol^{-1} and a polydispersity index of $Đ = 2.01$. The number-average block structure has been reported as 15 repeating units for the PLLA segment and 64 repeating units for the PCL segment. PDLA used for PLA stereocomplexes formation possessed $M_n = 3.5$ kg mol^{-1} and $Đ = 1.17$. A series of samples was studied in the work: the pure PLLA-PCL and its blends with 0.5, 1, 2, 5, 6, 7, 8, 9 and 10 wt% of PDLA, where 10 wt% corresponds to its equimolar ratio with PLLA. The content of each crystalline fraction is shown in Table S1. The sample codes are PLLA-PCL-SCX, where X stands for the weight content of PDLA in a blend. A blend PLLA-PCL/PLLA10 with 10 wt% of PLLA of $M_n = 1.4$ kg mol^{-1} was prepared as a control sample.

2.2. Mechanical tests

All mechanical tests were performed with a thermomechanical tensile tester Zwick Z1.0 (Ulm, Germany) equipped with a thermochamber and a temperature controller. The clamping distance was 10 mm in all of the experiments.

Hencky measure of strain was used in the experimental data representation $\varepsilon_H = \ln\lambda$, where λ is the extension ratio. The change of sample cross-section was monitored in real time with a Optronis CR600x2 high-speed camera (Kehl, Germany) with Zeiss Planar T* 1,4/50 zf.2 optics (Oberkochen, Germany). The videos were achieved at a frame rate of 500 fps in 1280 × 1024 resolution. The true sample width was calculated with digital image correlation (DIC). The frame rate was reduced to 2 fps and the series of images were processed in GOM Correlate software (Braunschweig, Germany). Exemplary sample images are presented in Fig. 1c and an exemplary dependency of a sample width on its elongation is presented in Fig. S1. The true stress σ_{true} was calculated by dividing load by the true cross-section area. The width of samples was measured with 5% error.

Stress-strain curves were achieved by stretching the samples at defined temperatures and a constant deformation rate of 5 mm min^{-1} until breakage occurred. Elongation ε_{break} and stress σ_{break} at break were recorded. Young's modulus E was calculated as the slope of the initial linear segment of $\sigma_{true}(\varepsilon)$ curves. The values were calculated as average of three measurements.

A step-cycle test was performed as it is described in the literature [39,40]. In short, a sample was stretched to a certain ε_H with a constant extension rate of 5 mm min^{-1}. Then, the stress was removed to 0 at the same contraction rate. At each following step the sample was elongated to a higher strain than at the previous one. The cycles were continued until sample breakage.

For stress relaxation experiments a sample was stretched to a certain strain, which was defined according to the deformation step at the stress-strain diagram, at constant temperature, which was defined according to the state of the material as reported with DSC-thermograms [18], at a strain rate of 5 mm min^{-1} . The sample was left at constant temperature and strain for several hours. The stress relaxation in time was registered.

2.3. Differential scanning calorimetry (DSC)

DSC experiments were conducted on a Netzsch DSC 204 Phoenix (Nezsch, Selb, Germany) at heating and cooling rates of 10 K min^{-1}. Samples were weighed directly into pierced aluminium pans. For the determination of the thermal properties of the polymers and blends, measurements were taken during the first cooling and second heating run in the temperature range from −100 to 200 °C. The crystallite content ϕ_c of all components was calculated from the obtained melting enthalpies ΔH_m according to the equation:

$$\phi_c = \frac{\Delta H_m}{\Delta H_m^{100}} \cdot 100\% \quad (2)$$

where ΔH_m is the experimental melting enthalpy of a fraction, determined as the area under the melting peak. ΔH_m^{100} is the specific melting enthalpy of 100% crystalline polymer, which is 135 J g^{-1} for PCL [43] and 142 J g^{-1} for PLA stereocomplex [44]. A statistical error of 10% for the measured enthalpy and 1 °C for the peak position provided by the manufacturer was considered for the measurements.

2.4. X-ray crystallographic analysis

Wide angle X-ray scattering (WAXS) measurements were performed with a D8 Discover spectrometer with a 2D-detector from Bruker AXS (Karlsruhe, Germany). The samples were stretched in a tensile machine at 70 °C to a predetermined strain at a constant deformation rate of 5 mm min^{-1} and fixed in a WAXS sample holder. The samples were transferred into the spectrometer and the *ex-situ* measurements were done at 70 °C. The sample dimensions during the measurements were approximately 20 × 1 × 0.15 mm^3. Peak position was determined with $\Delta\theta = 0.1°$ error originating from variations in sample thickness and position in the sample holder.

3. Results and discussion

3.1. Mechanical properties

3.1.1. Deformation behaviour

Stress-strain curves, as shown in Fig. 1b and Fig. S2a, show the typical stretching behaviour of PLLA-PCL and its PDLA blends at 0 °C. A pronounced necking is followed by significant strain hardening. The stress-strain curves for all of the studied samples at 0 °C show little variation. However, the increase of total ϕ_c of both crystalline fractions in the samples with higher PDLA content results in the higher E. This indicates that the mechanical properties of the materials at this temperature are influenced complimentarily by PCL crystallites and PLA stereocomplexes, while PCL crystallinity has an overwhelming effect due to its comparatively higher $\phi_{c\ PCL}$. At 70 °C, when the PCL domains are in amorphous state, the mechanical properties of the specimens strongly depend on the PLA stereocomplex content (Fig. S2b and Table S2). No necking is observed and the profile of the curves is typical for elastomers [45]. The sample PLLA-PCL-SC05 having $\phi_{c\ SC} = 0.7 \pm 0.1$ wt% exhibited no form stability at 70 °C. This suggests that the physical network formed by PLA stereocomplexes in low $\phi_{c\ SC} < 1.1$ wt% is not continuous within the volume of the sample, leaving unconnected cross-linked domains, which cannot contribute to macroscopic structural function. Although possessing some PLA stereocomplexes, the macroscopic behaviour of PLLA-PCL-SC05 is inherent to amorphous polymers. PLLA-PCL/PLLA10 having no PLA stereocomplexes possessed very low σ_{break} at 70 °C comparing to the other samples demonstrating that the mechanical strength at this temperature is provided by PLA stereocomplexation between PLLA-PCL and PDLA.

To determine the strain ranges, where the macroscopic deformation of PLLA-PCL and its PDLA blends proceeds via different deformation mechanisms, a series of step-cycle experiments at $T = 0$ °C and 70 °C

were performed. At 0 °C the PCL domains have the highest crystallinity [18] and their effect on the strain recovery behaviour is maximized. At 70 °C, the PCL crystalline domains are melted and only the impact of PLA stereocomplex on the mechanical properties is observed. The decomposition of the total strain into an elastic and plastic part allows determination of the four critical points: true elastic limit *A*, elastic limit *B*, onset of fibrillation *C* and amorphous network disentanglement initiation *D* [39]. Strain values at these points define the elongation ranges, where PLA stereocomplex junctions remain intact and the deformation of the PLLA-PCL/PDLA blends is characterized by the behaviour attributed to elastic polymeric networks. Approximate positions of the deformation critical points on the stress-strain curve is shown in Fig. 1b.The effect of PDLA content, i.e. PLA stereocomplex crystallinity, and temperature on critical ε_H was studied.

Overlaying the step-cycle experimental data and a continuous stress-strain curve (Fig. 3a) demonstrates that the deformation behaviour is not affected by cyclic strain-recovery. The decomposition of the strain into plastic and elastic contribution was performed as follows: The recovered strain was subtracted from the peak strain value in the current cycle. The values of the elastic ε_e and plastic ε_p contributions to the deformation were determined as recovered and non-recovered elongation respectively (Fig. 3b).

The critical points can be determined in two ways: from the profile of $\varepsilon_H(\sigma_{true})$ or $\varepsilon_{e,p}(\varepsilon_H)$ plots. The critical point *A* limits the region where the total ε_H and ε_e overlap, and where $\varepsilon_p(\sigma_{true})$ intersects the σ_{true} axis or $\varepsilon_p(\varepsilon_H)$ intersects the ε_H axis. The point *B* is defined as the point of gradient increase in the $\varepsilon_p(\sigma_{true})$ curve. The point *C* is assigned to the onset of the plateau of $\varepsilon_e(\sigma_{true})$ or $\varepsilon_e(\varepsilon_H)$. *D* is assigned to the point where the ε_e plot starts decreasing in $\varepsilon_H(\sigma_{true})$ and $\varepsilon_{e,p}(\varepsilon_H)$ representations [39,40]. The decomposition curves are depicted in Fig. 4 and S3 for the experiments at 0 °C and in Fig. 6 and S5 for the experiments at 70 °C. The effect of $\phi_{c\ SC}$ on the ε_H values at critical points is shown in Fig. 5.

Strain values at the critical points at 0 °C were determined from the decomposition $\varepsilon_H(\sigma_{true})$ of the stress-strain curves (Fig. 4 and S3). The deformation decomposition $\varepsilon_{p,e}(\varepsilon_H)$ of all samples at 0 °C overlap and show no dependency on $\phi_{c\ SC}$ (exemplary curves can be found in Fig. S4). This indicates that the PCL crystalline domains have an overwhelming effect on the mechanical properties at this temperature. The determined positions of the critical points are presented in Fig. 5.

Point ***A*** was determined for all tested samples at 0 °C as $\varepsilon_H = 0.01$. The true elastic limit remained invariant for all of the tested specimens. Purely elastic deformation of the amorphous matrix was observed at the same low value of $\varepsilon_H < 0.01$ in all of the studied blends. At point ***B*** in the step-cycle experiment at 0 °C, the elastic limit was determined in the range $\varepsilon_H = 0.07$–0.11 (Fig. 5). The elastic limit should not depend on the crystallinity of the material [40,41]. Here, $\phi_{c\ PCL}$ is similar in all of the samples [18]. The obtained result indicates that the density of PLA stereocomplex junctions and their interaction with PCL crystalline domains affect the deformation regimes compartmentalization of the latter. However, this could imply that the initial assumption that the critical stresses determined at 0 °C should be assigned exclusively to the PCL crystallites was not correct. The variation in ε_H at point ***B*** stems from simultaneous transfer between the deformation regimes of the both crystalline domains. The onset of fibrillation, point ***C***, was determined at 0 °C in the range of $\varepsilon_H = 0.31$–0.33 for the pure PLLA-PCL and the blend samples with lower PDLA content (PLLA-PCL-SC1 and PLLA-PCL-SC2) and as $\varepsilon_H = 0.23$ for PLLA-PCL-SC5 and PLLA-PCL-SC10. This can be a consequence of the higher number of crystalline domains. The corresponding decrease of the amorphous spacing between them results in the reduced mobility of polymer chains. Therefore, the stresses required for disintegration of the crystallites through fibrillation are reached at lower deformations of the matrix. This leads to a shift of point ***C*** towards lower ε_H. Point ***D*** was not observed in any of the tested samples. We assume that the amorphous network does not disentangle before the breakage of the specimens.

The ranges of the ε_H values at the critical points ***A***, ***B*** and ***C*** correspond to the PCL values previously reported in the literature [46]. Due to high $\phi_{c\ PCL}$ at 0 °C and its respectively high effect on the mechanical properties of the materials, the effect of $\phi_{c\ SC}$ is not clear. Neither definite is the stability and role of PLA stereocomplexes in the matrix at this temperature. The characteristic behaviour of the PLLA-PCL/PDLA blends at 0 °C is overwhelmed by deformation of PCL crystallites. No deviations from the adopted model were observed and the studied materials at 0 °C should be perceived as a semi-crystalline polymer matrix.

The decomposed $\varepsilon_{p,e}(\varepsilon_H)$ curves at 70 °C are presented in Fig. 6 and S5. At this temperature PLLA-PCL lost all mechanical integrity and could not be analyzed. Due to low PLA stereocomplex ϕ_c, the studied effects are not so pronounced as in the experiments at 0 °C and the definition of points ***A*** and ***B*** was challenging. The position of point ***A*** $\varepsilon_H = 0.04$ could be determined only from the PLLA-PCL-SC1 $\varepsilon_{p,e}(\varepsilon_H)$ curves (Fig. S6). Higher ε_H value in the true elastic limit stem from higher spacing between PLA stereocomplex crystallites and respectively higher elongations required before they undergo any plastic deformations. Point ***B*** for PLLA-PCL-SC1 was determined as $\varepsilon_H = 0.12$. The defined elastic limit is close to the values obtained at 0 °C.

Interestingly, the $\varepsilon_{p,e}(\varepsilon_H)$ decomposition curves at 70 °C demonstrated a behaviour attributed to fibrillation only for the samples with $\phi_{c\ SC} \geq 6.8$ wt%. $\varepsilon_e(\varepsilon_H)$ reaches a plateau indicating the fibril formation mode of deformation at $\varepsilon_C = 2.2$–2.5 [39]. Similarly to the experiments at 0 °C, ε_H at point ***C*** decreases with the increase of $\phi_{c\ SC}$. Point ***D*** could be determined only for the samples with the $\phi_{c\ SC} \geq 7.4$ wt% as 2.7–2.8. For the samples with $\phi_{c\ SC} \leq 6$ wt%, $\varepsilon_{p,e}(\varepsilon_H)$ curves rise evenly until the sample breakage. This profile of the curves deviates from the observations in other experiments in this study and previously reported in the literature [39,41,47–49]. Comparing to the literature examples, such high deformations should result in fibrillation of PLA stereocomplexes

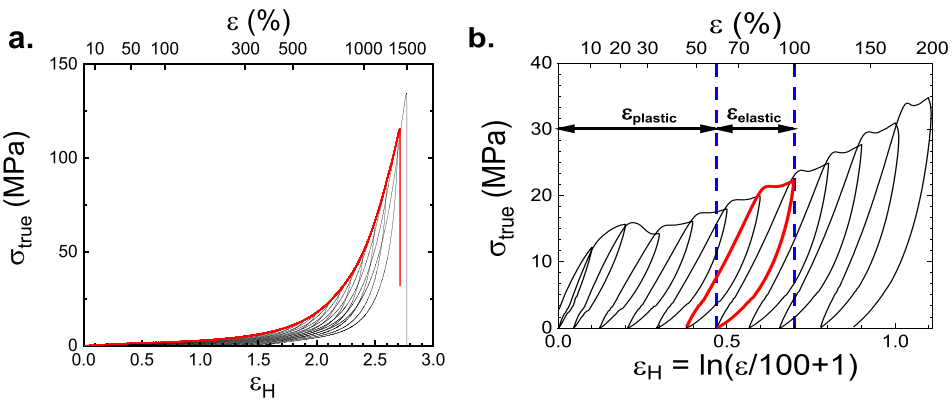

Fig. 3. **(a)** Step-cycle experiment curve (black) and stress-strain curve (red) of PLLA-PCL-SC5 at $T = 70$ °C. **(b)** Decomposition of strain into plastic ε_p and elastic ε_e components of PLLA-PCL-SC5 at $T = 0$ °C. (For interpretation of the references to colour in this figure legend, the reader is referred to the Web version of this article.)

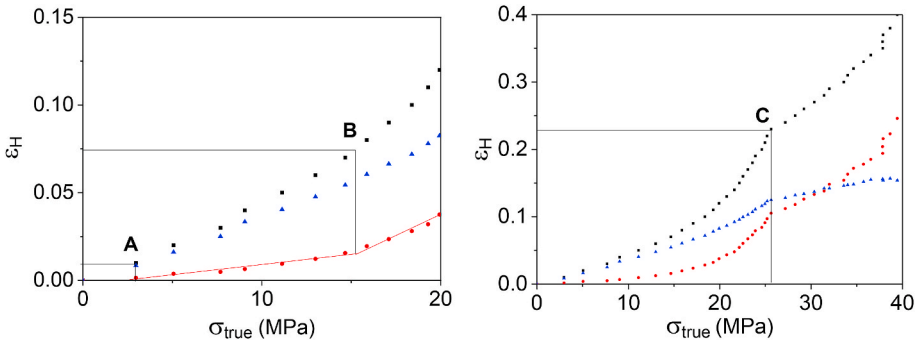

Fig. 4. Determination of critical points *A*, *B* and *C* for PLLA-PCL-SC5 at 0 °C from decomposition $\varepsilon_H(\sigma_{true})$ in the step-cycle experiment. Red – plastic contribution, blue – elastic contribution, black – total deformation. Deformation decomposition of other samples is presented in Fig. S3. (For interpretation of the references to colour in this figure legend, the reader is referred to the Web version of this article.)

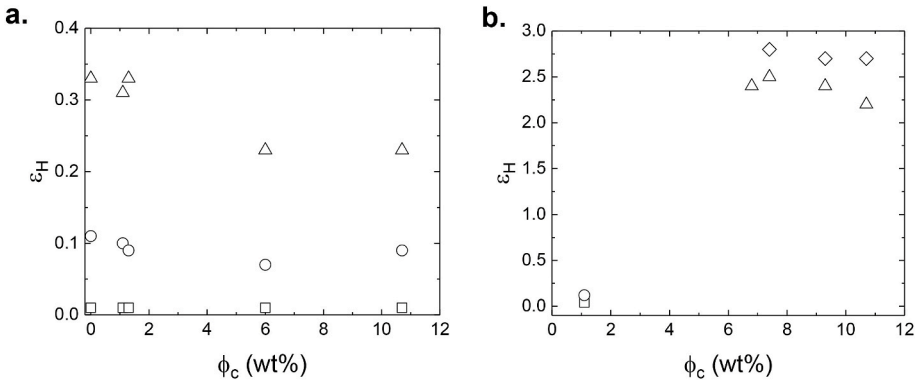

Fig. 5. ε_H values at critical points determined in the step-cycle tests: square – point ***A***; circle – point ***B***; triangle – point ***C***; rhombus – point ***D***. **(a)** – at 0 °C and **(b)** – at 70 °C. Missing data points were not observable in the step-cycle tests.

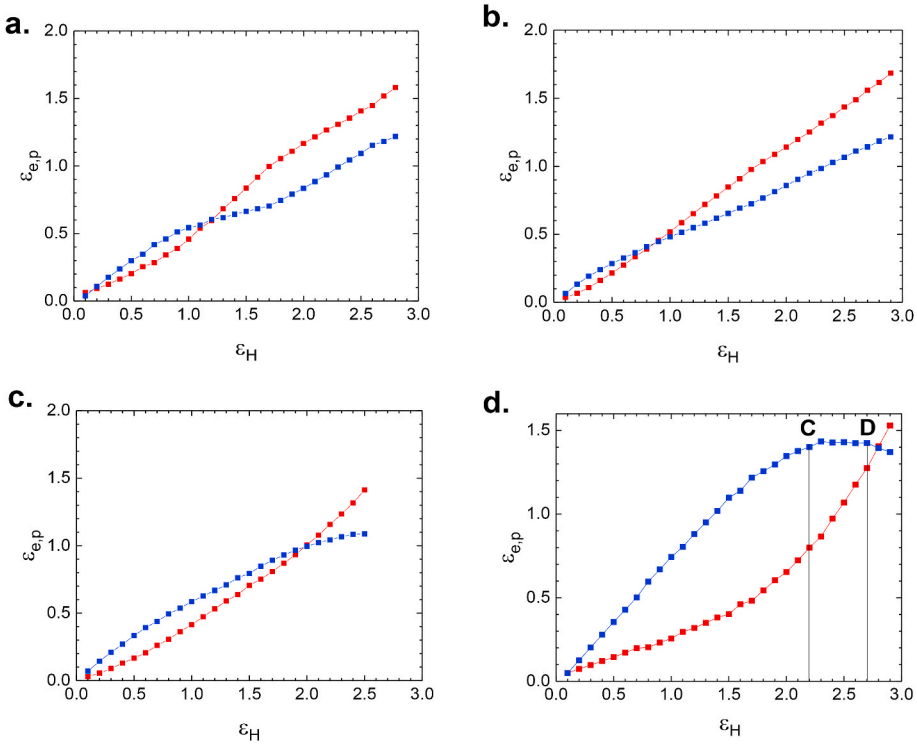

Fig. 6. Strain decomposition $\varepsilon_{p,e}(\varepsilon_H)$ in step-cycle experiments at 70 °C for (a) PLLA-PCL-SC1, (b) PLLA-PCL-SC6, (c) PLLA-PCL-SC7 and (d) PLLA-PCL-SC10. Deformation decomposition of other samples is presented in Fig. S5.

and, as it is seen in the samples with $\phi_{c\ SC} \geq 7.4$ wt%, disentangling of the amorphous network. However, these effects were not observed in the samples with $\phi_{c\ SC} \leq 6$ wt%.

The fibrillation of PLA stereocomplexes was observed with WAXS. The deformation of PLLA-PCL blends happens in two steps. Initially, a strong equatorial maximum draws intensity from 300 isotropic reflection of PLA stereocomplexes with the increase of ε_H. Further, additional reflections occur, suggesting appearance of a new component, which can be attributed to PLA stereocomplex fibrils. Simultaneously, the free-standing 110 isotropic reflection starts developing into an equatorial maximum. The critical ε_H at which the onset of the fibrillation is observed in the WAXS experiments correlates with ε_C determined with the step-cycle tests. Exemplary 2D WAXS diagrams and orientational distribution function evolution are presented in Fig. 7.

At lower PLA stereocomplex contents (≤6 wt% as in PLLA-PCL-SC6) due to higher spacing between crystallites the deformation of the amorphous matrix is not transferred to them. PLA stereocomplexes do not undergo fibrillation and remain intact as physical netpoints in the full ε_H range until breakage of the samples. Structural integrity of PLA stereocomplexes allows to interpret the observed elastic behaviour of the PLLA-PCL/PDLA blends with lower $\phi_{c\ SC} \leq 6$ wt% at 70 °C as a physically cross-linked network.

3.1.2. Stress relaxation

Stress relaxation experiments were performed to evaluate, if a model [37,38] treating deformation of semi-crystalline polymers is suitable for explanation of physical processes in PLLA-PCL/PDLA blends. Further, we extract the viscoelastic stress constituent $\sigma_r(0)$ (Fig. 2) to treat the deformation of the studied materials with the adopted Hong-Strobl model.

The stress relaxation of the samples was investigated at two temperatures: at 70 °C to isolate PLA stereocomplex from semi-crystalline PCL and at 0 °C to ensure the crystallinity of both components. The effect of the variation of PLA stereocomplex crystallinity was studied in experiments with PLLA-PCL/PDLA blend variation. Stress relaxation curves were set at a fixed $\varepsilon_0 = 1.8$ to determine the influence of temperature and blend composition. The variation of the initial deformation ε_0 in range 0.18–2.4 was performed to observe how stress relaxation processes in PLLA-PCL-SC10 change in different deformation regions ε_H, which were determined in the previous section (Fig. 5).

To simplify data analysis with the model Eq. (1), the stress relaxation curves are plotted in $\Delta\sigma_r(\ln t)$ coordinates. Two exemplary curves of the stress relaxation of PLLA-PCL-SC10 with $\varepsilon_0 = 1.8$ at $T = 0$ °C and 70 °C are presented in Fig. 8a and b respectively.

The stress relaxation curves at 70 °C (exemplary curve in Fig. 8b) conform with the previously described systems [37]. The curves can be fitted with Eq. (1) with high precision, with the error of the fitting parameters calculation lower than 5% and their mutual dependency lower than 0.2. This implies that the model is applicable to PLLA-PCL/PDLA blends cross-linked with PLA stereocomplexation.

With the incorporation of PCL crystallites to the network at 0 °C, the interaction of the semi-crystalline matrices of PCL and PLA stereocomplex changes the stress relaxation behaviour of the materials (exemplary curve in Fig. 8a). The central part of experimental curve $\Delta\sigma(\ln t)$ can no longer be approximated with a line with a slope of σ_0, as for the curve at 70 °C. This implies that the viscoelastic behaviour can no longer be described by the Hong-Strobl model. This profile of this relaxation curve is closely related to the high overall crystallinity of a material. Similar curves were reported by the authors of the model for samples of higher crystallinities [50].

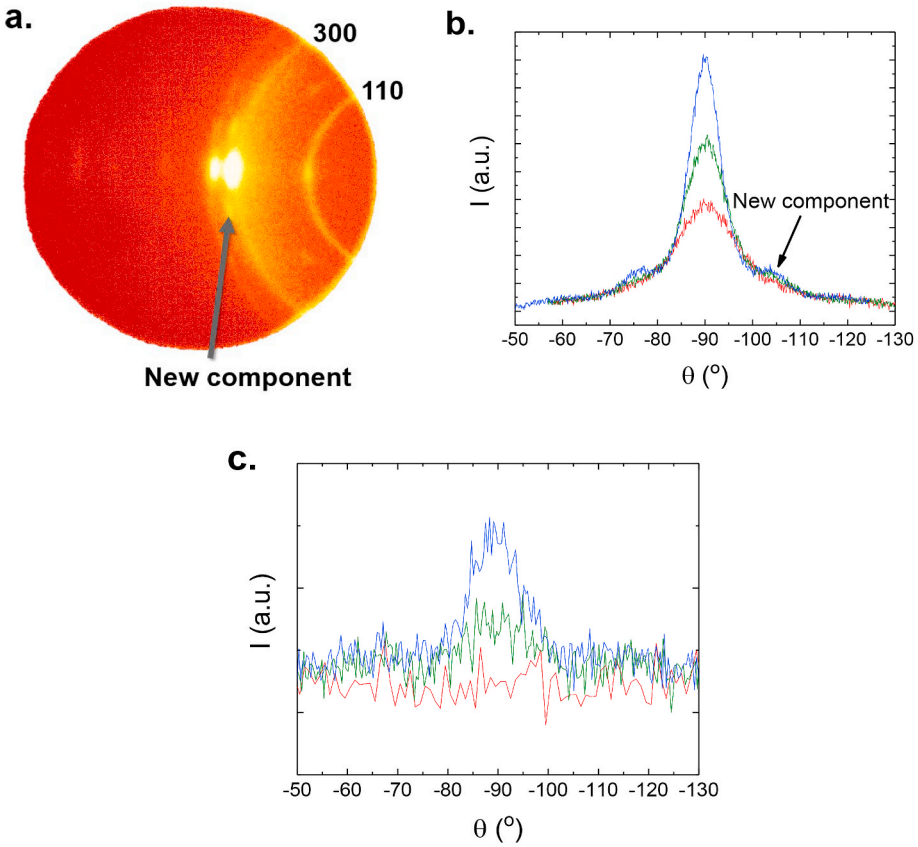

Fig. 7. (a) 2D WAXS diagram of PLLA-PCL-SC10 stretched to $\varepsilon_H = 2.6$ in vertical direction. Orientational distribution function evolution of 300 **(b)** and 110 **(c)** reflections. Red – $\varepsilon_H = 2$, green – $\varepsilon_H = 2.4$ and blue – $\varepsilon_H = 2.6$. θ – angle between the lattice plane normal and the tensile axis. (For interpretation of the references to colour in this figure legend, the reader is referred to the Web version of this article.)

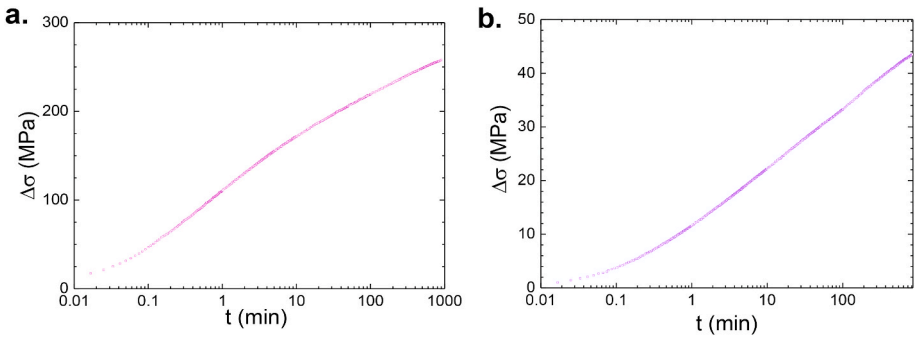

Fig. 8. Stress relaxation curves of PLLA-PCL-SC10 with $\varepsilon_0 = 1.8$ at 0 °C **(a)** and at 70 °C **(b)**.

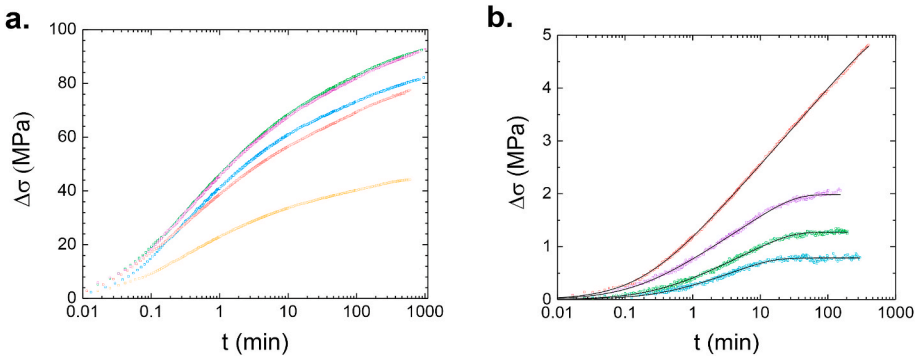

Fig. 9. Stress relaxation curves of PLLA-PCL – yellow, PLLA-PCL-SC1 – blue, PLLA-PCL-SC2 – green, PLLA-PCL-SC5 – purple, and PLLA-PCL-SC10 – red. Black – fitting curves achieved with Hong-Strobl model [37] with $\varepsilon_0 = 1.8$ at (**a**) $T = 0$ °C and (**b**) $T = 70$ °C. (For interpretation of the references to colour in this figure legend, the reader is referred to the Web version of this article.)

The stress relaxation curves illustrating the effect of matrix content on the stress relaxation behaviour are depicted in Fig. 9. At $T = 70$ °C the PLLA-PCL sample was observed to possess no mechanical strength. Further, $\Delta\sigma(t)$ of the relaxation processes in the PLLA-PCL-SCX series align according to $\phi_{c\ SC}$ in the matrix (Fig. 9b). Although the relaxation times τ_r were reported not to be dependent on the crystallinity of the matrix components, for PLLA-PCL-SCX blends they are proportional to the content of PLA stereocomplex in the matrix. Stress relaxation process in PLLA-PCL-SC10 demonstrate an increase in relaxation characteristic times from $\tau_r = 6.9$ min in PLLA-PCL-SC1 to 300 min (Table 1). Very low overall crystalline content in the blend samples PLLA-PCL-SC1, PLLA-PCL-SC2 and PLLA-PCL-SC5 led to high matrix elasticity at 70 °C, where PCL is amorphous. Due to the higher mobility of the polymer chains in the amorphous network in blends with a lower $\phi_{c\ SC}$, the viscoelastic rearrangement of the amorphous matrix required less time. The increase of the relaxed stress $\sigma_r(0)$ and characteristic stress σ_0 is explained with higher values of σ_{true} in the beginning of relaxation process due to higher $\phi_{c\ SC}$. Viscoelastic stress relaxation at 70 °C in all of the studied blends follows the Hong-Strobl model. This indicates that there is no significant amount of microscopic reorganizational processes in the PLA stereocomplex junctions parallel to viscoelastic flow in the amorphous domains, which could affect the stress distribution among amorphous and crystalline domains. In other words, PLA stereocomplex stay stable in all of the studied blends during stress relaxation at 70 °C demonstrating their suitability as netpoints in a physical matrix. The extracted $\sigma_r(0)$ were used in the following section to distribute stresses between the branches of the Hong-Strobl model (Fig. 2).

All stress relaxation curves at 0 °C (Fig. 9a) demonstrate an unexpected behaviour, which cannot be fitted with the Hong-Strobl model Eq. (1). No dependency on PLA stereocomplex content in the PLLA-PCL-SCX blend samples is observed. However, the pure PLLA-PCL follows a similar relaxation pathway as the blends, although it possesses only PCL crystallinity. This implies that unusual relaxation behaviour comes not from interaction of PLA stereocomplex and PCL crystallinity, but solely from high $\phi_{c\ PCL}$. Assuming that PCL domains are able to form larger crystallites than PLA stereocomplex, due to bigger number-average sizes of the constituent molecules (64 repeating units per segment for PCL versus 15 repeating units per segment for PLLA), PCL has higher crystalline presence in the matrix and smaller potential spacing between its crystallites. This may result in greater microscopic rearrangements in PCL crystalline domains when compared to PLA stereocomplex at lower macroscopic deformations of the matrix. Crystalline sliding and fibrillation attributed to PCL in the previous sections happen at comparatively low strains: $\varepsilon_B = 0.09$ and $\varepsilon_C = 0.27$. At deformation $\varepsilon_H = 1.8$ in

Table 1
Stress relaxation fitting parameters as achieved treating the stress relaxation of PLLA-PCL/PDLA blends at 70 °C with the Hong-Strobl model [37].

Sample ID[a]	ε_0[b]	$\sigma_r(0)$, MPa[c]	σ_0, MPa[c]	τ_r, min[c]
PLLA-PCL	1.8	–	–	–
PLLA-PCL-SC1	1.8	0.78	0.23	6.9
PLLA-PCL-SC2	1.8	1.3	0.29	13
PLLA-PCL-SC5	1.8	2	0.37	14.7
PLLA-PCL-SC10	0.18	0.08	0.02	4.9
	0.4	0.31	0.06	5.7
	0.9	1.2	0.21	40
	1.8	5.1	0.63	300
	2.4	64	4.8	10,000

The error of determination is lower than 5% of the values. The mutual parameter dependency is lower than 0.2.

[a] Sample code in format PLLA-PCL-SCX, where X stands for the weight ratio of PDLA in a blend.

[b] Initial strain in stress relaxation experiments.

[c] Hong-Strobl model fitting parameters.

parallel to the viscoelastic relaxation of the amorphous domains, the PCL crystallites experience continuous process of breakage and restructuring [51]. The effect of this process on the macroscopic mechanical behaviour is so pronounced that it is impossible to define by the implemented experimental techniques what happens to the PLA stereocomplex network junctions.

The relaxation curves in the experiments with a variation of ε_0 are presented in $\Delta\sigma_r(\ln t)$ coordinates in Fig. S7.

At 0 °C the stress relaxation curves at $\varepsilon_0 = 0.18$ behave differently when compared to the experiments at other initial deformations, which possess similar profiles. Here, $\varepsilon_0 = 0.18$ lies in the strain range characterized with the crystallite sliding deformation mechanism, while at the higher strains $\varepsilon_H = 0.4 - 2.4$ the crystallites in the sample were observed to undergo fibrillation. (Fig. 5). This alters the distribution of internal stresses among the branches of the Hong-Strobl model (Fig. 2). The contribution of the elasto-plastic branch is significantly lower in comparison to the viscoelastic and elastic branches in the case of $\varepsilon_H = 0.18$. Interestingly, high $\phi_{c\ PCL}$ at 0 °C makes it impossible to apply relaxation equation to the Hong-Strobl model **(1)** even at low deformations $\varepsilon_0 = 0.18$, further indicating that PLLA-PCL/PDLA blends cannot be studied as a physical network at this temperature and any strains.

The profile of stress relaxation curves at 70 °C analogously depends on the deformation mechanism at a particular ε_0 (Fig. S7). A dependency of the calculated relaxation time τ_r on ε_0 was observed, increasing from 5 min at $\varepsilon_0 = 0.18$ to 10,000 min at $\varepsilon_0 = 2.4$. Reports in the literature indicate that no changes in the characteristic relaxation time is expected with the variation of ε_0 [37]. In the studied materials such a large increase can be explained by the collective effect of the variation in ε_0, different matrix structure and low $\phi_{c\ SC} = 10.7$ wt%. The high molecular weight $M_n = 238$ kg mol^{-1} of PLLA-PCL and low length of crystallizable segments, number-average 15 repeating units, lead to a high dispersity of PLA stereocomplexes in the matrix and high elasticity of the material. As a result, the viscoelastic flow of PLLA-PCL at 70 °C differs from behaviour of the semi-crystalline PEVA initially reported for the model [37]. Further, consent with the model equation indicates that PLA stereocomplex junctions undergo no or little irreversible restructuring as breakage and recrystallization. This demonstrates that PLA stereocomplexes possess sufficient thermomechanical stability at 70 °C to act as firm cross-links in a broad range of deformations.

3.2. Model considerations of the deformation of PLLA-PCL/PDLA

The stress constituents σ_r, $(1 - \phi_c)\sigma_n(\varepsilon_H)$ and $\phi_c\ \sigma_c(\varepsilon_H)$ in a quasi-static stress-strain dependence were extracted from the stress relaxation and deformation data in the previous sections. Here, the viscoelastic forces σ_r were determined as the relaxed stresses at infinite time (Table 1). The amorphous network elastic contribution $(1 - \phi_c)\sigma_n(\varepsilon_H)$ can be determined from the stress-strain curves in an ideal rubber approximation [42]. Plotting $\sigma_{true}(\lambda^2 - \lambda^{-1})$ and approximating its strain hardening region with a straight line, the shear modulus G of a Gaussian network can be calculated:

$$(1 - \phi_c)\sigma_n = (1 - \phi_c)G(\lambda^2 - \lambda^{-1}) \quad (3)$$

Exemplary plots can be found in Fig. S8. The contribution of crystalline domains $\phi_c\ \sigma_c(\varepsilon_H)$ can be calculated simply by subtraction of the elastic and viscoelastic constituents from the total stress. An exemplary stress decomposition of the stress-strain curve of PLLA-PCL-SC10 at 70 °C is depicted in Fig. S9.

The decomposition of the stress-strain curves at 0 °C would incur significant errors, because the stress relaxation model Eq. (1) cannot reliably extract σ_r from the relaxation curves. The experiments at 70 °C were treated with the Hong-Strobl model. The effect of PLA stereocomplex content on the fraction of each stress component for different PLA stereocomplex content ϕ_c in PLLA-PCL/PDLA blends at $\varepsilon_H = 1.8$ is shown in Fig. 10.

The absolute value of all three stress fractions increases with the increase of PLA stereocomplex ϕ_c. The fraction of the elastic forces in the total stress was observed to be independent from the PLA stereocomplex content. The fraction of elasto-plastic forces increases followed, by the decrease of the viscoelastic constituent. The stresses are redistributed from the amorphous domains to the crystalline network junctions with the increase of cross-linking density causing their plastic deformation. This result supports findings made in the strain recovery section, where at 70 °C only the sample with the highest PLA stereocomplex ϕ_c showed the behaviour typical for semi-crystalline polymers.

4. Conclusion

The performance of PLA stereocomplexes as physical netpoints in blends of a multiblock copolymer with poly(L-lactide) and poly(ε-caprolactone) (PLLA-PCL) segments with poly(D-lactide) oligomer (PDLA) was investigated. Structural stability of PLA stereocomplexes at 70 °C in PLLA-PCL/PDLA blends with PLA stereocomplex content $\phi_{c\ SC} \leq 6$ wt% in a strain range of $\varepsilon_H < 3$ observed in step-cycle experiments indicates that the mechanical stability of the physical cross-links in the studied materials is sufficient to provide the latter with an elastic network-like behaviour. The increase of $\phi_{c\ SC}$ over 6.8 wt% restricts the behaviour inherent to elastic cross-linked network to the strain range of $\varepsilon_H \leq 2.4$, with further decrease to $\varepsilon_H = 2.2$ at $\phi_{c\ SC} = 10.7$ wt%. Above these $\phi_{c\ SC}$ and ε_H ranges PLLA-PCL/PDLA blends deformation behaviour can be attributed to plastic deformation of semi-crystalline polymers. $\phi_{c\ SC} = 0.7 \pm 0.1$ wt% is too low to provide a consistent physically cross-linked network, which is required for realization of the targeted macroscopic structural function. Compliance of stress relaxation at 70 °C in PLLA-PCL/PDLA blends with $\phi_{c\ SC}$ up to 10.7 wt% with the Hong-Strobl model for mechanical behaviour of a semi-crystalline polymer demonstrates that no crystalline reorganization occurs, at least not in a significant amount, in parallel to the relaxation processes. PLA stereocomplexes remain intact and can serve as firm physical network junctions in a strain range of $\varepsilon_H \leq 2.25$. The decomposition of the

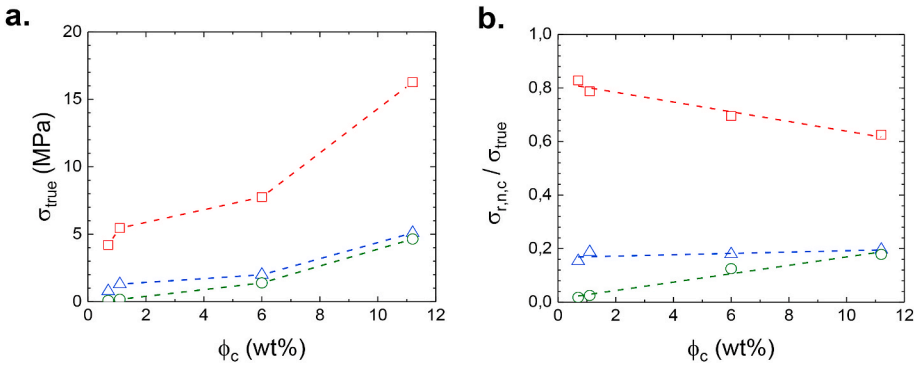

Fig. 10. Contribution to σ of viscoelastic (red squares), elastic (blue triangles) and elasto-plastic (green circles) forces for PLA stereocomplex content ϕ_c variation in PLLA-PCL/PDLA blends at $\varepsilon_H = 1.8$ and $T = 70$ °C in absolute values **(a)** and their fractions of σ_{true} **(b)**. The error considered in the calculations stems from systematic error of the single elongation and stress relaxation experiments, fitting error of the Hong-Strobl model and error in the ideal rubber approximation. It was calculated as 13% of the σ_{true} value. (For interpretation of the references to colour in this figure legend, the reader is referred to the Web version of this article.)

elongation curves at 70 °C into viscoelastic, elastic and elasto-plastic contributions illustrates that with the increase of $\phi_{c\ SC}$ the internal stresses are redistributed from the viscoelastic constituent of the amorphous phase to the elasto-plastic deformations of the PLA stereocomplex domains causing their irreversible restructuring and further failure as network junctions. At the lower $T = 0$ °C, the effect of PCL crystalline domains on the mechanical behaviour of the studied blends was too prominent to unambiguously identify the influence of PLA stereocomplexes and their suitability as physical cross-links. The presented results define the strain and composition limitations where PLA stereocomplexes can generate mechanically stable physical netpoints. The applied methods for basic investigation of semi-crystalline polymer deformation can provide a solid platform for assessment of structural stability of physical cross-links in polymer networks. This knowledge is relevant for the design of multifunctional thermoplastic elastomers or hydrogels, which can exhibit functions, such as degradability or a shape-memory behaviour.

Declaration of competing interest

The authors declare that they have no known competing financial interests or personal relationships that could have appeared to influence the work reported in this paper.

Acknowledgments

The authors thank Ms. Susanne Schwanz for WAXS measurements. This work was financially supported by the Helmholtz Association of German Research Centers through programme-oriented funding and through the Helmholtz Graduate School of Macromolecular Bioscience [MacroBio], grant no. VH-GS-503.

Appendix A. Supplementary data

Supplementary data to this article can be found online at https://doi.org/10.1016/j.polymer.2020.122984.

References

[1] T. Iwata, Biodegradable and bio-based polymers: future prospects of eco-friendly plastics, Angew Chem. Int. Ed. Engl. 54 (11) (2015) 3210–3215.
[2] R. Auras, B. Harte, S. Selke, An overview of polylactides as packaging materials, Macromol. Biosci. 4 (2004) 835–864.
[3] K. Madhavan Nampoothiri, N.R. Nair, R.P. John, An overview of the recent developments in polylactide (PLA) research, Bioresour. Technol. 101 (22) (2010) 8493–8501.
[4] S. Farah, D.G. Anderson, R. Langer, Physical and mechanical properties of PLA, and their functions in widespread applications — a comprehensive review, Adv. Drug Deliv. Rev. 107 (2016) 367–392.
[5] P. Saini, M. Arora, M.N.V.R. Kumar, Poly(lactic acid) blends in biomedical applications, Adv. Drug Deliv. Rev. 107 (2016) 47–59.
[6] Y. Ramot, M. Haim-Zada, A.J. Domb, A. Nyska, Biocompatibility and safety of PLA and its copolymers, Adv. Drug Deliv. Rev. 107 (2016) 153–162.
[7] D. Bandelli, J. Alex, C. Weber, U.S. Schubert, Polyester stereocomplexes beyond PLA: could synthetic opportunities revolutionize established material blending? Macromol. Rapid Commun. 41 (1) (2020), e1900560.
[8] Y. Ikada, K. Jamshidi, H. Tsuji, S.H. Hyon, Stereocomplex formation between enantiomeric poly(lactides), Macromolecules 20 (1987) 904–906.
[9] S. Saeidlou, M.A. Huneault, H. Li, P. Sammut, C.B. Park, Evidence of a dual network/spherulitic crystalline morphology in PLA stereocomplexes, Polymer 53 (25) (2012) 5816–5824.
[10] X.F. Wei, R.Y. Bao, Z.Q. Cao, W. Yang, B.H. Xie, M.B. Yang, Stereocomplex crystallite network in asymmetric PLLA/PDLA blends: formation, structure, and confining effect on the crystallization rate of homocrystallites, Macromolecules 47 (2014) 1439–1448.
[11] J. Wang, R. Lv, B. Wang, B. Na, H. Liu, Direct observation of a stereocomplex crystallite network in the asymmetric polylactide enantiomeric blends, Polymer 143 (2018) 52–57.
[12] D.-d. Yang, W. Liu, H.-m. Zhu, G. Wu, S.-c. Chen, X.-l. Wang, Y.-z. Wang, Toward super-tough poly (L - lactide) via constructing pseudo-cross- link network in toughening phase Anchored by stereocomplex crystallites at the interface, ACS Appl. Mater. Interfaces 10 (2018) 26594–26603.
[13] Z. Zhang, D.W. Grijpma, J. Feijen, Creep-resistant porous structures based on stereo-complex forming triblock copolymers of 1,3-trimethylene carbonate and lactides, J. Mater. Sci. Mater. Med. 15 (4) (2004) 381–385.
[14] P. Ma, T. Shen, P. Xu, W. Dong, P.J. Lemstra, M. Chen, Superior performance of fully biobased poly(lactide) via stereocomplexation-induced phase separation: structure versus property, ACS Sustain. Chem. Eng. 3 (7) (2015) 1470–1478.
[15] Y. Nakayama, K. Aihara, H. Yamanishi, H. Fukuoka, R. Tanaka, Z. Cai, T. Shiono, Synthesis of biodegradable thermoplastic elastomers from ε-caprolactone and lactide, J. Polym. Sci., Part A: Polym. Chem. 53 (3) (2015) 489–495.
[16] Y. Li, S. Xin, Y. Bian, Q. Dong, C. Han, K. Xu, L. Dong, Stereocomplex crystallite network in poly(D,L-lactide): formation, structure and the effect on shape memory behaviors and enzymatic hydrolysis of poly(D,L-lactide), RSC Adv. 5 (2015) 24352–24362.
[17] M. Balk, M. Behl, C. Wischke, J. Zotzmann, A. Lendlein, Recent advances in degradable lactide-based shape-memory polymers, Adv. Drug Deliv. Rev. 107 (2016) 136–152.
[18] V. Izraylit, O.E.C. Gould, T. Rudolph, K. Kratz, A. Lendlein, Controlling actuation performance in physically cross-linked polylactone blends using polylactide stereocomplexation, Biomacromolecules 21 (2) (2020) 338–348.
[19] A. Peterlin, Molecular model of drawing polyethylene and polypropylene, J. Mater. Sci. 6 (1971) 490–508.
[20] Z. Li, B.H. Tan, T. Lin, C. He, Recent advances in stereocomplexation of enantiomeric PLA-based copolymers and applications, Prog. Polym. Sci. 62 (2016) 22–72.
[21] V. Izraylit, O.E.C. Gould, K. Kratz, A. Lendlein, Investigating the phase-morphology of PLLA-PCL multiblock copolymer/PDLA blends cross-linked using stereocomplexation, MRS Advances 5 (14–15) (2019) 699–707.
[22] M.K. Beyer, H. Clausen-Schaumann, Mechanochemistry: the mechanical activation of covalent bonds, Chem. Rev. 105 (2005) 2921–2948.
[23] W. Kuhn, Dependence of the average transversal on the longitudinal dimensions of statistical coils formed by chain molecules, J. Polym. Sci. 1 (5) (1946) 380–388.
[24] H.M. James, Statistical properties of networks of flexible chains, J. Chem. Phys. 15 (9) (1947) 651–668.
[25] G. Ronca, G. Allegra, An approach to rubber elasticity with internal constraints, J. Chem. Phys. 63 (11) (1975) 4990–4997.
[26] B. Erman, P.J. Flory, Relationships between stress, strain, and molecular constitution of polymer networks. Comparison of theory with experiments, Macromolecules 15 (3) (1982) 806–811.
[27] S.F. Edwards, The statistical mechanics of polymerized material, Proc. Phys. Soc. 92 (1) (1967) 9–16.
[28] A. Kloczkowski, J.E. Mark, B. Erman, A diffused-constraint theory for the elasticity of amorphous polymer networks. 1. Fundamentals and stress-strain isotherms in elongation, Macromolecules 28 (14) (1995) 5089–5096.
[29] M. Rubinstein, S. Panyukov, Elasticity of polymer networks, Macromolecules 35 (2002) 6670–6686.
[30] L. Lin, A.S. Argon, Structure and plastic deformation of polyethylene, J. Mater. Sci. 29 (1994) 294–323.
[31] G. Spathis, E. Kontou, Experimental and theoretical description of the plastic behaviour of semicrystalline polymers, Polymer 39 (1998) 135–142.
[32] S. Jabbari-Farouji, J. Rottler, O. Lame, A. Makke, M. Perez, J.-L. Barrat, Plastic deformation mechanisms of semicrystalline and amorphous polymers, ACS Macro Lett. 4 (2015) 147–150.
[33] Z. Bartczak, A. Vozniak, WAXS/SAXS study of plastic deformation instabilities and lamellae fragmentation in polyethylene, Polymer 177 (2019) 160–177.
[34] S. Nikolov, R. Lebensohn, D. Raabe, Self-consistent modeling of large plastic deformation, texture and morphology evolution in semi-crystalline polymers, J. Mech. Phys. Solid. 54 (2006) 1350–1375.
[35] R.N. Haward, Strain hardening of thermoplastics, Macromolecules 26 (1993) 5860–5869.
[36] B.A.G. Schrauwen, R.P.M. Janssen, L.E. Govaert, H.E.H. Meijer, Intrinsic deformation behavior of semicrystalline polymers, Macromolecules 37 (2004) 6069–6078.
[37] K. Hong, A. Rastogi, G. Strobl, A model treating tensile deformation of semicrystalline polymers: quasi-static stress-strain relationship and viscous stress determined for a sample of polyethylene, Macromolecules 37 (2004) 10165–10173.
[38] K. Hong, A. Rastogi, G. Strobl, Model treatment of tensile deformation of semicrystalline polymers: static elastic moduli and creep parameters derived for a sample of polyethylene, Macromolecules 37 (2004) 10174–10179.
[39] R. Hiss, S. Hobeika, C. Lynn, G. Strobl, Network stretching, slip processes, and fragmentation of crystallites during uniaxial drawing of polyethylene and related copolymers. A Comparative Study, Macromolecules 32 (1999) 4390–4403.
[40] S. Hobeika, Y. Men, G. Strobl, Temperature and strain rate independence of critical strains in polyethylene and poly(ethylene-co-vinyl acetate), Macromolecules 33 (2000) 1827–1833.
[41] Y. Men, G. Strobl, Critical strains determining the yield behavior of s-PP, J. Macromol. Sci., Part B: Phys. 40 B (2001) 775–796.
[42] R.N. Haward, G. Thackray, The use of a mathematical model to describe isothermal stress-strain curves in glassy thermoplastics, Proc. R. Soc. London, Ser. A 302 (1471) (1968) 453–472.
[43] V. Crescenzi, G. Manzini, G. Calzolari, C. Borri, Thermodynamics of fusion of poly-β-propiolactone and poly-ε{lunate}-caprolactone. comparative analysis of the melting of aliphatic polylactone and polyester chains, Eur. Polym. J. 8 (1972) 449–463.
[44] H. Tsuji, Poly(lactide) stereocomplexes: formation, structure, properties, degradation, and applications, Macromol. Biosci. 5 (7) (2005) 569–597.

[45] J.H.-V. Seppala, T. M Karjalainen, Biodegradable lactone copolymers. I. Characterization and mechanical behavior of epsilon-caprolactone and lactide copolymers, J. Appl. Polym. Sci. 59 (1996) 1281–1288.
[46] Y. Men, G. Strobl, Critical Strains in Poly(ε -caprolactone) and Blends with Poly (vinyl methyl ether) and Poly(styrene- c o -acrylonitrile), Macromolecules 36 (2003) 1889–1898.
[47] Z. Bartczak, Effect of chain entanglements on plastic deformation behavior of ultra-high molecular weight polyethylene, J. Polym. Sci. B Polym. Phys. 48 (3) (2010) 276–285.
[48] Y. Qiu, J. Wang, D. Wu, Z. Wang, M. Zhang, Y. Yao, N. Wei, Thermoplastic polyester elastomer nanocomposites filled with graphene: mechanical and viscoelastic properties, Compos. Sci. Technol. 132 (2016) 108–115.
[49] F. Deplace, A.K. Scholz, G.H. Fredrickson, E.J. Kramer, Y.-W. Shin, F. Shimizu, F. Zuo, L. Rong, B.S. Hsiao, G.W. Coates, Tough and elastic thermoplastic organogels and elastomers made of semicrystalline polyolefin-based block copolymers, Macromolecules 45 (13) (2012) 5604–5618.
[50] K. Hong, A Model Treating Tensile Deformation of Semi-crystalline Polymers, Faculty for Mathematics and Physics, Albert-Ludwig University of Freiburg, 2005.
[51] Y. Zhao, D. Keroack, R. Prud'homme, Crystallization under strain and resultant orientation of poly(ε-caprolactone) in miscible blends, Macromolecules 32 (4) (1999) 1218–1225.

Supporting information for manuscript

Strain Recovery and Stress Relaxation Behavior of Multiblock Copolymer Blends Physically Cross-Linked with PLA Stereocomplexation

Victor Izraylit[1,2], Matthias Heuchel[1], Oliver E. C. Gould[1], Karl Kratz[1], Andreas Lendlein[1,2*]

[1] Institute of Biomaterial Science and Berlin-Brandenburg Centre for Regenerative Therapies, Helmholtz-Zentrum Geesthacht, Kantstr. 14513 Teltow, Germany

[2] Institute of Chemistry, University of Potsdam, Karl-Liebknecht-Str. 24/25, 14476 Potsdam, Germany

* Correspondence andreas.lendlein@hzg.de

Table S1. Crystalline structure of PLLA-PCL and its PDLA blends.

Sample ID[a]	$\varphi_{c\ PCL}$ [b], wt%	$\varphi_{c\ SC}$ [b], wt%
PLLA-PCL*	30±3	-
PLLA-PCL-SC05	32±3	0.7±0.1
PLLA-PCL-SC1*	31±3	1.1±0.1
PLLA-PCL-SC2*	35±3	1.3±0.1
PLLA-PCL-SC5*	29±3	6±0.6
PLLA-PCL-SC6	33±3	6±0.6
PLLA-PCL-SC7	33±3	6.8±0.7
PLLA-PCL-SC8	30±3	7.4±0.7
PLLA-PCL-SC9	34±3	9.3±0.9
PLLA-PCL-SC10*	27±3	10.7±1.1

[a] Sample code in format PLLA-PCL-SCX, where X stands for the weight ratio of PDLA in a blend; * samples have been reported in [1]; [b] crystallite mass content calculated as ratio between ΔH_m acquired with DSC and the melting enthalpy of 100% crystalline polymer ΔH_m^{100} 135 J·g^{-1} for PCL [2] and 142 J·g^{-1} for PLA stereocomplex [3].

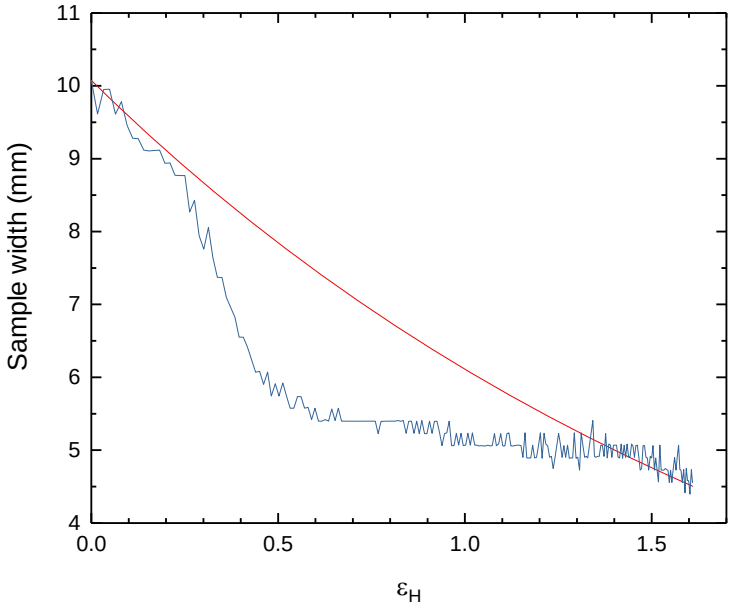

Figure S1. PLLA-PCL-SC10 width in a single elongation experiment measured with DIC (blue) and calculated with an assumption of constant volume of the sample between the tensile machine clamps (red).

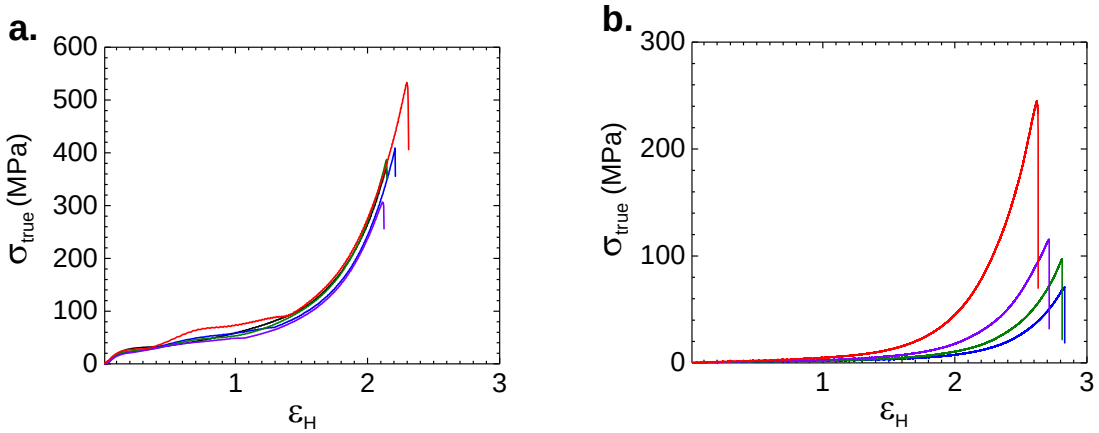

Figure S2. Stress-strain curves at T = 0 °C **(a)** and T = 70 °C **(b)** for sample PLLA15-PCL64 (black), PLLA-PCL-SC1 (blue), PLLA-PCL-SC2 (green), PLLA-PCL-SC5 (purple), and PLLA-PCL-SC10 (red).

Table S2. Mechanical properties of PLLA-PCL and its PDLA blends at 0 °C and 70 °C.

Sample ID[a]	*T*, °C	*E*, MPa[b]	σ_{break}, MPa[c]	ε_{break}[c]
PLLA-PCL	0	241±28	380±73	2.15±0.1
PLLA-PCL-SC1		231±27	410±64	2.21±0.08
PLLA-PCL-SC2		231±11	394±56	2.15±0.06
PLLA-PCL-SC5		256±24	306±114	2.11±0.12
PLLA-PCL-SC10		310±35	534±82	2.3±0.14
PLLA-PCL-SC1	70	1.87±0.13	71±6	2.83±0.08
PLLA-PCL-SC2		1.96±0.1	97±16	2.81±0.15
PLLA-PCL-SC5		3.19±0.15	115±14	2.71±0.11
PLLA-PCL-SC10		5.34±0.21	255±21	2.62±0.7
PLLA-PCL/PLLA10		1.57±0.2	13±7	2.38±0.27

[a] Sample code in format PLLA-PCL-SCX, where X stands for the weight ratio of PDLA in a blend; PLLA-PCL/PLLA10 – control blend with 10 wt% PLLA; [b] Young's modulus, defined as a slope of the initial linear section of the stress-strain curves; [c] stress and elongation at break. The deviation for these measurements was defined as statistical error in 3 measurements.

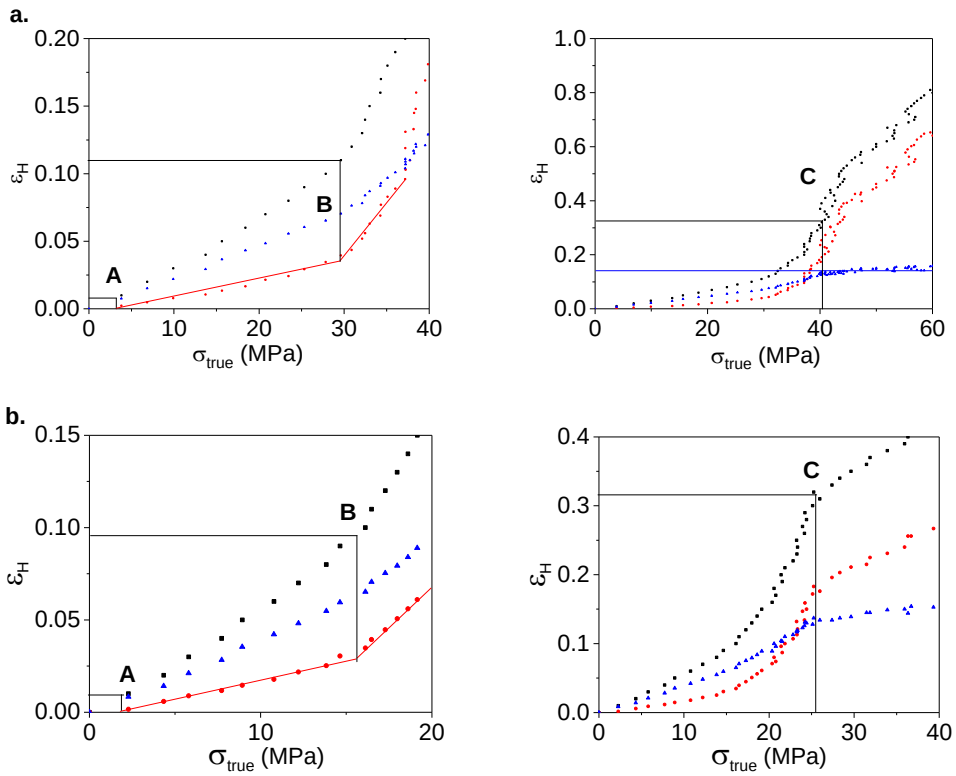

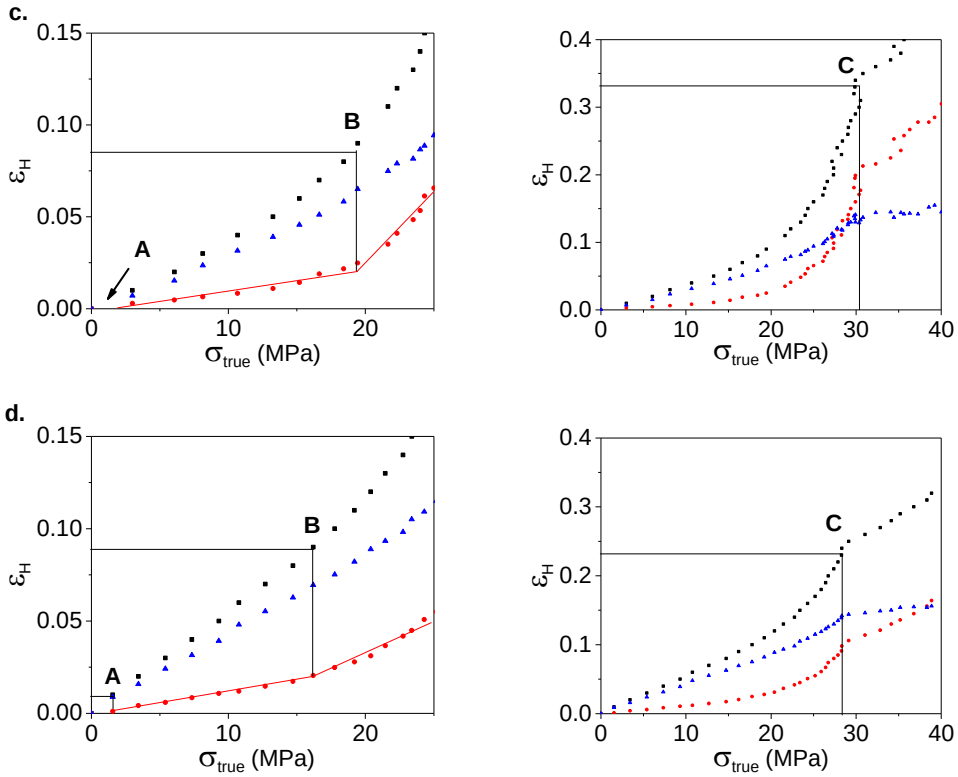

Figure S3. Determination of critical strain points A, B and C from total deformation data (black) at T = 0 °C and their division in plastic (red) and elastic (blue) contribution for samples PLLA-PCL (a), PLLA-PCL-SC1 (b), PLLA-PCL-SC2 (c), and PLLA-PCL-SC10 (d).

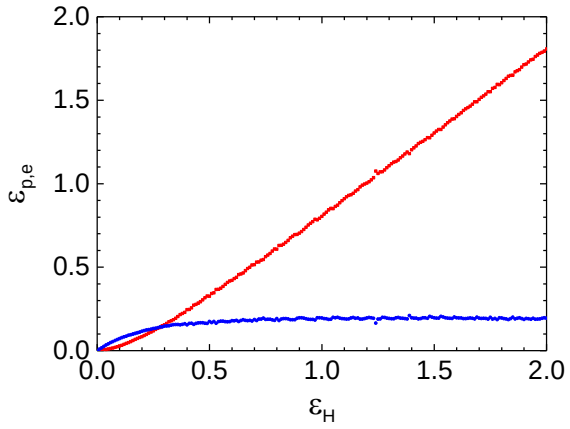

Figure S4. Deformation decomposition $\varepsilon_{p,e}(\varepsilon_H)$ of PLLA-PCL-SC5 at 0 °C. Red – plastic contribution, blue – elastic contribution.

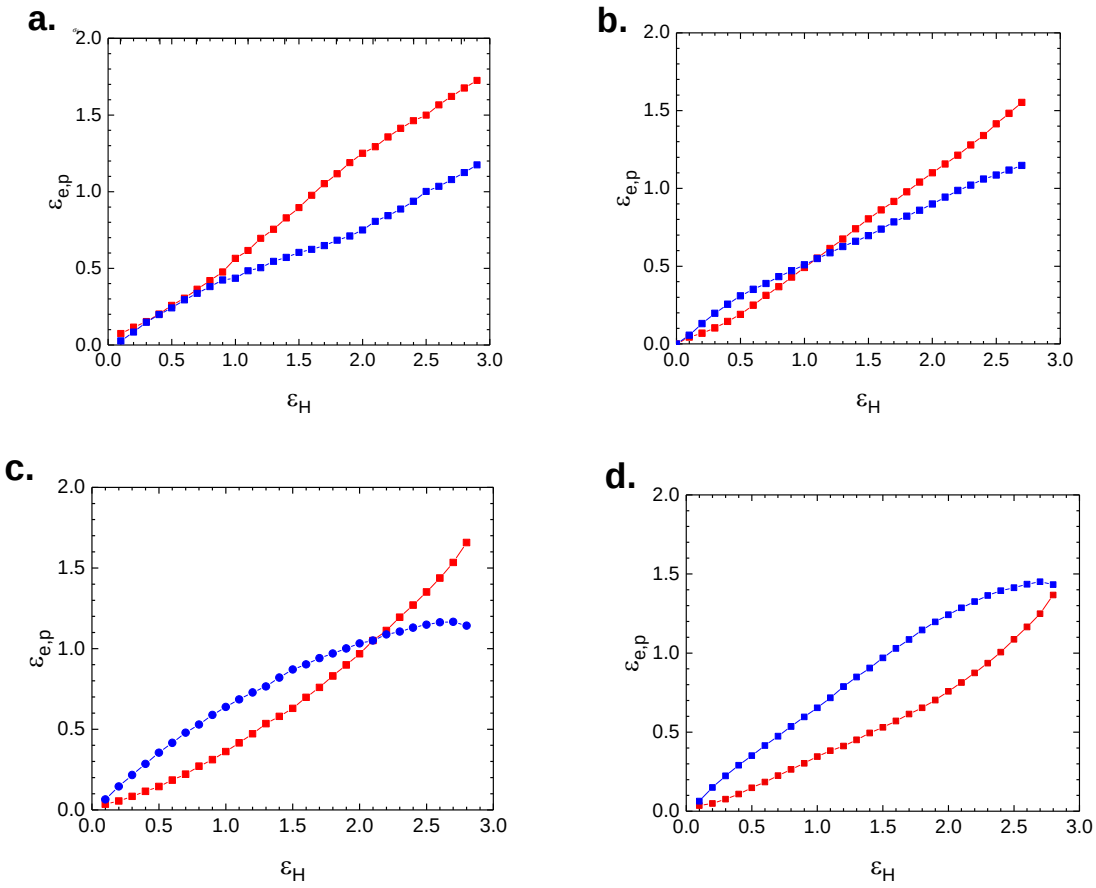

Figure S5. Strain decomposition $\varepsilon_{p,e}(\varepsilon_H)$ in step-cycle experiments at 70 °C for (a) PLLA-PCL-SC2, (b) PLLA-PCL-SC5, (c) PLLA-PCL-SC8 and (d) PLLA-PCL-SC9.

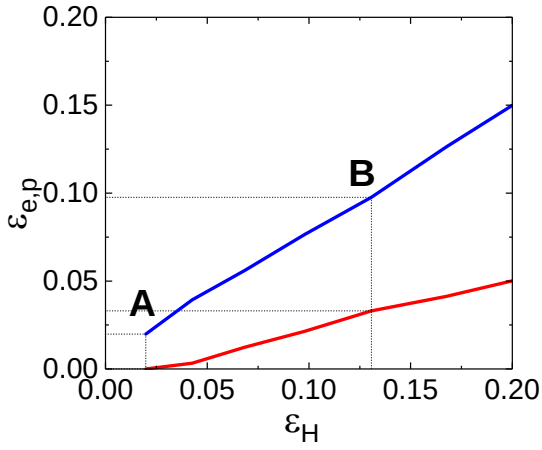

Figure S6. Strain decomposition $\varepsilon_{p,e}(\varepsilon_H)$ in step-cycle experiment at 70 °C for PLLA-PCL-SC1

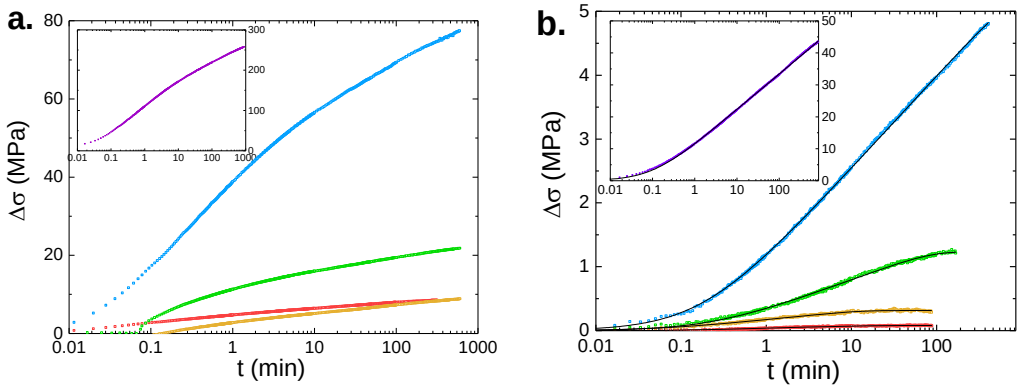

Figure S7. **(a)** Stress relaxation curves (logarithmic scale) of PLLA-PCL-SC10 at T = 0 °C at various ε_0: yellow – ε_H = 0.18, red – ε_H = 0.4, green – ε_H = 0.92, blue – ε_H = 1.8 and purple – ε_H = 2.25. **(b)** Stress relaxation curves of PLLA-PCL-SC10 at 70 °C at various ε_0 yellow – ε_H = 0.18, red – ε_H = 0.4, green – ε_H = 0.92, blue – ε_H = 1.8 and purple – ε_H = 2.4. Black – fitting curves achieved with Hong-Strobl model [4].

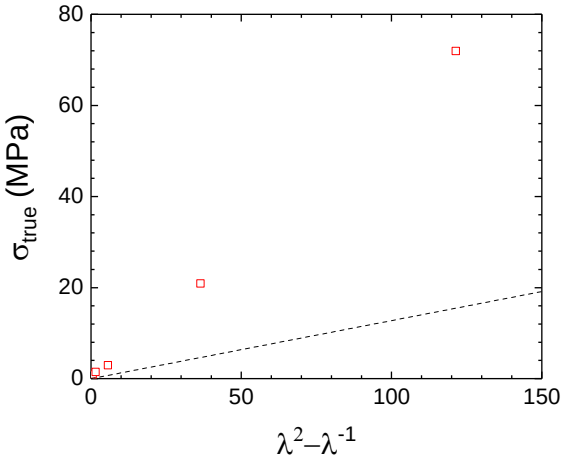

Figure S8. Quasi-static stress-strain relation (red squares) and amorphous network elastic stress contribution (dashed line) for PLLA-PCL-SC10 at 70 °C

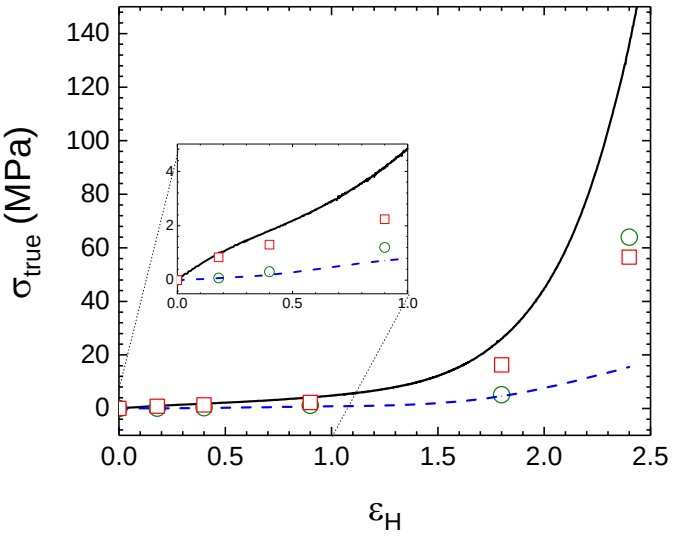

Figure S9. Quasi-static stress decomposition of the stress-strain curve of PLLA-PCL-SC10 at 70 °C (full line) into contributions of viscoelastic (red squares), elastic (dashed line) and elastoplastic (green circles) forces.

References

[1] V. Izraylit, O.E.C. Gould, T. Rudolph, K. Kratz, A. Lendlein, Controlling Actuation Performance in Physically Cross-Linked Polylactone Blends Using Polylactide Stereocomplexation, Biomacromolecules 21(2) (2020) 338-348.
[2] V. Crescenzi, G. Manzini, G. Calzolari, C. Borri, Thermodynamics of fusion of poly-β-propiolactone and poly-ϵ-caprolactone. comparative analysis of the melting of aliphatic polylactone and polyester chains, European Polymer Journal 8(3) (1972) 449-463.
[3] H. Tsuji, Poly(lactide) stereocomplexes: Formation, structure, properties, degradation, and applications, Macromolecular Bioscience 5 (2005) 569-597.
[4] K. Hong, A. Rastogi, G. Strobl, A model treating tensile deformation of semicrystalline polymers: Quasi-static stress-strain relationship and viscous stress determined for a sample of polyethylene, Macromolecules 37(26) (2004) 10165-10173.

Article

Cite This: *Biomacromolecules* 2020, 21, 338−348

pubs.acs.org/Biomac

Appendix III:

Controlling Actuation Performance in Physically Cross-Linked Polylactone Blends Using Polylactide Stereocomplexation

Victor Izraylit,[†,‡] Oliver E. C. Gould,[†] Tobias Rudolph,[†] Karl Kratz,[†] and Andreas Lendlein[†,‡,§,*]

[†]Institute of Biomaterial Science and Berlin-Brandenburg Centre for Regenerative Therapies, Helmholtz-Zentrum Geesthacht, Kantstrasse, 14513 Teltow, Germany

[‡]Institute of Chemistry, University of Potsdam, Karl-Liebknecht-Strasse 24/25, 14476 Potsdam, Germany

[§]Institute of Chemistry and Biochemistry, Freie Universität Berlin, Takustrasse 3, 14195 Berlin, Germany

Supporting Information

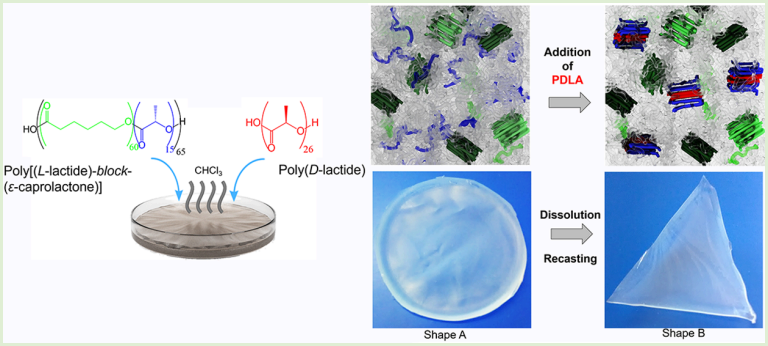

ABSTRACT: Within the field of shape-changing materials, synthetic chemical modification has been widely used to introduce key structural units and subsequently expand the mechanical functionality of actuator devices. The introduction of architectural elements that facilitate *in situ* control over mechanical properties and complete geometric reconfiguration of a device is highly desirable to increase the morphological diversity of polymeric actuator materials. The subject of the present study is a multiblock copolymer with semicrystalline poly(L-lactide) and poly(ε-caprolactone) (PLLA−PCL) segments. By harnessing the stereocomplexation of copolymer chains with a poly(D-lactide) oligomer (PDLA), we provide anchoring points for physical network formation and demonstrate how a blending process can be used to efficiently vary the mechanical properties of a shape-memory actuator. We investigate the effect of molecular structure on the actuation performance of the material in cyclic thermomechanical tests, with a maximum reversible shape change $\varepsilon_{rev}' = 13.4 \pm 1.5\%$ measured at 3.1 wt % of polylactide stereocomplex content in the multiblock copolymer matrix. The thermophysical properties, crystalline structure, and phase morphology were analyzed by DSC, WAXS and AFM respectively, elucidating the structure-to-function relationship in physically cross-linked blended materials. The work demonstrates a one-step technique for manufacturing a polymeric actuator and tuning its performance *in situ*. This approach should greatly improve the efficiency of physically cross-linked actuator fabrication, allowing composition and physical behavior to be precisely and easily controlled.

INTRODUCTION

Polymeric actuator materials are capable of reversibly and repetitively changing their shape in response to an external stimulus. Their actuation behavior can be derived from a wide variety of physical phenomenons, including the swelling/deswelling of hydrogels,[1−3] self-organization of liquid crystallites,[4−6] and oriented crystallization and melting of programmable shape-memory polymers. The nature of the shape transformation can be controlled, and tailored, to a specific function, by altering the physical manifestation of the material or by modifying the macromolecular architecture of key structural components.

A shape-memory polymeric material, capable of free-standing thermoreversible motions, typically consists of three functional elements: (i) actuation units, which undergo oriented crystallization during cooling and melting upon heating, (ii) skeleton units, which define the programmable shape of the actuator as well as the direction of motion, and (iii) netpoints interlinking both actuation and skeleton units.[7] Soft shape-memory polymeric actuators utilizing chemical netpoints,[8−10] and physical netpoints[11−16] have been reported. While covalently cross-linked actuator materials are restricted to shape changes determined at the point of their manufacturing, the reprocessability of physically interlinked

Special Issue: Advances in Functional Polymers for Medicine

Received: September 16, 2019
Revised: November 15, 2019
Published: November 20, 2019

Downloaded via HELMHOLTZ-ZENTRUM GEESTHACHT on March 29, 2021 at 09:43:41 (UTC).
See https://pubs.acs.org/sharingguidelines for options on how to legitimately share published articles.

ACS Publications © 2019 American Chemical Society

DOI: 10.1021/acs.biomac.9b01279
Biomacromolecules 2020, 21, 338−348

networks enables them to undergo complete geometric reconfiguration.[9] This capability for reconfiguration allows for the definition of a new actuation pattern and physical functionality.

A wide variety of intermolecular interactions has been used to generate physical cross-links in polymeric actuator materials. In recent work, hydrogen bonding within directly synthesized poly(3*S*-*iso*butylmorpholin-2,5-dione) networks enabled the creation of stable physical netpoints within a poly(ε-caprolactone) (PCL) matrix.[15] Ionic interactions between sodium ions in a random copolymer of poly[ethylene-*co*-(methacrylic acid)] with 30 wt % methacrylic acid groups neutralized with sodium were used to create physical netpoints.[17] Finally, thermally stable PE crystals within a diblock copolymer of PE and poly(1-octene) have been successfully utilized as physical netpoints during actuation.[18]

However, in these examples, the modification of material composition and subsequent mechanical behavior require costly and time-consuming synthetic alterations of the polymer architecture within the material. The ability to adjust the material composition in physically cross-linked materials through an *in situ* processing method should greatly improve our ability to implement morphological diversity in actuating devices. Controlling the cross-link density of a polymeric actuator material is crucial to both improving its actuation performance and tailoring its physical behavior to a certain application, allowing for the variation of important material characteristics like *E* modulus or elongation at break. In this study, we demonstrate the use of a blending approach to modify the structure of a polymeric material, allowing us to imbue it with a reprogrammable actuation capacity and to efficiently control its actuation performance. By blending a material, which is incapable of actuation in its pure form, with a low molecular weight polymeric additive, we are able to vary the cross-link density and tune the actuation performance by simply adjusting the composition of the blend. Here, unlike in previous work, strong physical netpoints are formed *in situ* during the actuator material processing.

To realize this, we need to design the main component of the blend in such way that all the principal components of the matrix are embedded into its structure. Advances in multiblock copolymer chemistry have made the introduction of multiple functional chemical entities into one macromolecule possible. The potential shape-memory behavior of poly(ε-caprolactone) (PCL) has been widely demonstrated, where the polymer's broad melting transition can be used to provide both skeleton and actuator domains.[19,20] Here, the PCL crystallite population can be bisected by the selection of a suitable actuation temperature, with the more thermally stable fraction providing a rigid backbone, while the less thermally stable fraction drives the actuation. The second requirement of our material is the provision of specific anchoring points for the formation of physical netpoints. To realize a two part blending method for network creation, a polymeric segment capable of forming stable physical netpoints when introduced to an additive compound is required. We have chosen polylactide (PLA) to introduce this function. When combined with a stereoisomer, polylactide stereocomplexation can be used to create thermally and mechanically stable crystallites.[21−23]

As the high molecular weight (number-average molecular weight M_n > 200 kg·mol^{-1}) blend component we synthesized a multiblock copolymer composed of poly(ε-caprolactone) segments with an average segment length of approximately 60 repeating units and poly(L-lactide) segments with an average segment length of approximately 15 repeating units. The segment lengths of all components were designed to ensure the formation of stereocomplex crystallites without latent pure crystallization, to provide sufficient actuation force and to ensure the form stability of the material. While PLA homopolymers have been shown to undergo homocrystallization at average segment lengths of 5−7 repeating units,[24] the decreased flexibility of PLLA segments in a multiblock copolymer should increase the critical segment length for homocrystallization of PLLA.[25,26] As a working principle for the *in situ* generation of physical netpoints, the formation of PLA stereocomplexes was realized by blending the copolymer with poly(D-lactide) (PDLA). This approach is facilitated by developments in synthetic methods to reliably produce oligomeric compounds.[27] The synthesis of PLLA−PCL with a well-defined segment structure was based on the self-polycondensation of diblock macromers.[28−30] Due to an insignificant amount of transesterification reaction, this technique allows the repetitive transfer of the segment structure of the diblock precursor to the multiblock copolymer. This enables the block length of the key structural units to be specified during the diblock synthesis, before scaling up to the high molecular weight multiblock copolymer.

To explore the influence of PLA stereocomplex content in the PLLA−PCL/PDLA blends on the thermal and mechanical properties of the materials, blend samples with varying weight content of PDLA homopolymer component were prepared. By varying the average molecular weight of the PDLA homopolymer component, we gained insight into the molecular weight range where physical network formation is possible. Molecular design and compositional variation were used to modify the phase-structure and thermal properties of the blends, with the aim of generating a physical network which enables functional physical behavior in the form of macroscale reversible actuation. The molecular structure of the samples, determined using NMR and GPC, thermal properties, measured by DSC and DMTA, and crystalline structure, elucidated with WAXS and DSC measurements, were related to physical network formation and actuation function as measured by cyclic thermomechanical testing.

EXPERIMENTAL SECTION

Materials. Chloroform (99.9%, Carl Roth, Karlsruhe, Germany), toluene (99.5%, Carl Roth, Karlsruhe, Germany), methanol (99%, Carl Roth, Karlsruhe, Germany), anhydrous 1-hexanol (99%, Acros Organics, Geel, Belgium), tin(II) 2-hexanoate ($Sn(Oct)_2$) (96%, Alfa Aesar, Massachusetts, USA), dimethylaminopyridine (DMAP) (99%, Sigma-Aldrich, Missouri, USA), *p*-toluenesulfonic acid monohydrate (pTSA) (98.5%, Sigma-Aldrich, Missouri, USA), anhydrous benzylalkohol (BnOH) (98%, Acros Organics, Geel, Belgium), 10% palladium on activated carbon (Alfa Aesar, Massachusetts, USA), deuterated chloroform (99.8% Sigma-Aldrich, Missouri, USA), L,L-dilactide (99.5%, Corbion, Amsterdam, Netherlands) and D,D-dilactide (99.5%, Corbion, Amsterdam, Netherlands) were used as received. Tetrahydrofuran (THF) (99.9% Carl Roth, Karlsruhe, Germany), dichloromethane (DCM) (99.9% Carl Roth, Karlsruhe, Germany) and *N*,*N*′-diisopropylcarbodiimide (DIPC) (98%, Sigma-Aldrich, Missouri, USA) were stored over molecular sieves. ε-Caprolactone (99%, Acros Organics, Geel, Belgium) was distilled before use. Dimethylaminopyridine *p*-toluenesolfonate (DMAP·pTSA) was synthesized as reported elsewhere.[31]

Nuclear Magnetic Resonance Spectroscopy (NMR). ^{1}H NMR spectra were recorded using a DRX Avance 500 MHz spectrometer (Bruker, Rheinstetten, Germany) at room temperature in deuterated

DOI: 10.1021/acs.biomac.9b01279
Biomacromolecules 2020, 21, 338−348

chloroform. Chemical shifts (δ) are reported in parts per million (ppm) relative to residual chloroform at δ 7.26 ppm. Samples were dissolved in $CDCl_3$ at a concentration of 15 mg·mL^{-1}. The spectra were evaluated according to the position and intensity of signals of corresponding groups.[32]

Error values for calculation of molecular weight from ^{1}H NMR data were estimated as a combination of saturation effects, intensity losses due to isotropic sidebands, unevenness of the magnetic field in the sample, and the line shape causing overlapping of the peaks. An estimated error of approximately 12% of the measured value was calculated.

Gel-Permeation Chromatography (GPC). Number-average molecular weights of starting materials and products were determined by high-throughput gel permeation chromatography (GPC), using a Tosoh EcoSEC HLC-8320 gel permeation chromatograph equipped with a refractive index detector (Tosoh Bioscience, Stuttgart, Germany) combined with a PSS Universal Data Center (PSS, Mainz, Germany), a viscometer ETA2010 (PSS, Mainz, Germany), an EcoSEC UV detector 8320 (Tosoh Bioscience), a light scattering detector SLD7100 (PSS, Mainz, Germany), and two HT-GPC columns type PSS SDV analytical linear M 5 μm (PSS, Mainz, Germany) connected in series. For the measurements, by universal calibration, tetrahydrofuran (THF) was used as an eluent (35 °C, flow rate 1.0 mL·min^{-1}) with 0.05 weight content 3,5-di-*tert*-butyl-4-hydroxytoluene as an internal standard in order to determine the hydrodynamic volume as a function of elution volume. Molecular weight and dispersity calculations were performed using WINGPC 6.2 (PSS) SEC software (Polymer Standard Service, Mainz, Germany). The error was considered as 10% of the measured value calculated based on variations in the measurement of polystyrene calibration standards.

Differential Scanning Calorimetry (DSC). DSC experiments were conducted on a Netzsch DSC 204 Phoenix (Nezsch, Selb, Germany) at heating and cooling rates of 10 K·min^{-1}. Samples were weighed directly into hermetic aluminum pans. For the determination of the thermal properties of the polymers and blends, measurements were taken during the first cooling and second heating run in the temperature range from −100 to +200 °C.

The degree of crystallinity (χ_c) of all components was calculated from the obtained melting enthalpies (ΔH_m) according to the equation

$$\chi_c = \frac{\Delta H_m}{\Delta H_m^{100}} \times \frac{1}{W} \times 100$$

where ΔH_m is the experimental melting enthalpy of a fraction, determined as the area under the melting peak. ΔH_m^{100} is the specific melting enthalpy of 100% crystalline polymer, which is 135 J·g^{-1} for PCL[33] and 142 J·g^{-1} for PLA stereocomplex.[34] W is the weight content of the fraction in the copolymer of the blend. The PLA stereocomplex fraction was calculated as the maximal amount of coupling L- and D-lactide units. DSC was used for the measurement of χ_c to enable the characterization of our samples at 0 °C, as opposed to at ambient temperature (25 °C) where the PCL segment of the multiblock copolymer is partially molten. A statistical error of 10% for the measured enthalpy and 1 °C for the peak position provided by the manufacturer was considered for the measurements.

Dynamic Mechanical Thermal Analysis (DMTA). DMTA measurements were performed using an Eplexor 25 N (Gabo, Ahlden, Germany) equipped with a 25 N load cell using a standard test specimen type (DIN EN ISO 527−2/1BB). The applied oscillation frequency was 1 Hz. The measurement was performed in the temperature sweep mode from −100 to 100 °C with a constant heating rate of 1 °C·min^{-1}. The glass transition (T_g) was determined at the peak maximum of the loss modulus (E'') vs temperature curve. Temperature measurements were recorded with a manufacturer-determined accuracy of ΔT = 1 °C.

Wide-Angle X-ray Scattering (WAXS). WAXS measurements were performed with a D8 Discover spectrometer with a 2D-detector from Bruker AXS (Karlsruhe, Germany) in the temperature range of 25−100 °C. The samples of dimensions 2 × 0.5 cm and width 150 μm were fixed at both ends during characterization. Peak position was determined with $\Delta\theta$ = 0.1° error originating from variations in sample thickness and position in the sample holder.

Thermomechanical Testing. All mechanical tests were performed using a thermomechanical tensile tester Zwick Z1.0 (Ulm, Germany) equipped with a thermochamber and a temperature controller. A clamping distance of 10 mm was used in all of the experiments. Elongation at break ε_{break} of the samples was tested by stretching the samples at defined temperatures and a constant deformation rate of 5 mm·min^{-1} until breakage occurred. The actuation capability of the material was characterized by programming, followed by three repetitive actuation cycles. The sample was heated in the thermo-chamber at the programming temperature T_{prog} = 70 °C for 10 min to remove the thermal history in the PCL segments. Then, the sample was elongated to the programming strain ε_{prog} = 300−1250% at 5 mm·min^{-1}. The sample was held at T_{prog} and ε_{prog} for 5 min to allow the initial relaxation processes align the polymer chains along the deformation axis. At the final step of programming, the temporary shape was fixed at 0 °C under constant force. Then the force applied to the sample was reduced to 0.05 N, at which the zero-force reversible shape-memory effect (rbSME) test was carried out. The actuation cycle was performed in a temperature window 0−55 °C, where the minimum temperature of the actuation cycle T_{low} = 0 °C was defined based on DSC data and the maximum temperature of the actuation cycle T_{high} = 55 °C was defined in a rbSME experiment where T_{high} was systematically varied. A sample was programmed at T_{prog} = 70 °C and ε_{prog} = 1000% with shape fixation at T_{low} = 0 °C. An actuation cycle was conducted between T_{low} = 0 °C and a T_{high} which was raised between 50 and 100 °C in 5 °C increments for each consequent cycle. The cycle with the highest ε_{rev}' was used to determine the T_{high} value used in subsequent experiments. Actuation performance ε_{rev}' was calculated as

$$\varepsilon_{rev}' = \frac{l_b - l_a}{l_a} \times 100\% = \frac{\varepsilon_b - \varepsilon_a}{\varepsilon_a + 100} \times 100\%$$

where l_a and ε_a are the length of the sample and its engineering strain at the beginning of the actuation cycle at T_{high} and l_b and ε_b are the length of the sample and its engineering strain at the beginning of the actuation cycle at T_{low}. The ε_{rev}' values were calculated as an average in three subsequent cycles. The process is schematically illustrated in Figure S2.

Atomic Force Microscopy (AFM). AFM measurements were performed on a MFP-3D-BioTM AFM (Asylum Research, Goleta, USA) equipped with a Cooler/Heater controller (Asylum Research, Goleta, USA). Samples were prepared by cutting with a diamond knife. The samples, with an approximate thickness of 100 nm, were placed on a silica grid before imaging, and imaged at 28 °C and at 70 °C. Samples were equilibrated at each investigated temperature for 10 min before measurement. AC mode with a scan rate of 0.5 Hz was used for imaging. AC200TS probes (Olympus, Tokyo, Japan) with a typical driving frequency of approximately 150 kHz (individual variation from 100 to 200 kHz) and a typical spring constant of approximately 9 N·m^{-1} (individual variation from 2.8 to 21 N·m^{-1}) were used. The tip radius and height were 5−10 nm and 14 ± 1 μm respectively, with a three-side shape (front angle of 0 ± 1°, a back angle of 35 ± 1°, and a side angle of 15 ± 1°). A scan size of 1 × 1 μm was used.

Synthesis of Multiblock Copolymer with Poly(L-lactide) and Poly(ε-caprolactone) Segments (PLLA−PCL). A PCL-precursor was synthesized via ring-opening polymerization (ROP) of ε-caprolactone. 100 g ε-caprolactone were put into closed reaction flask under an argon flow and heated to 140 °C with an oil bath. 1300 mg BnOH and 178 mg $Sn(Oct)_2$ were added through a syringe in 50 mg·ml^{-1} dry THF solutions. After 2.5 h the reaction mixture was cooled and dissolved in 500 mL chloroform. Precipitation into methanol gave a white precipitate, which was filtered through a glass filter with average pore size 10−16 μm and dried under vacuum. A yield of 94% was recorded. PLLA−PCL was synthesized via ROP of

DOI: 10.1021/acs.biomac.9b01279
Biomacromolecules 2020, 21, 338−348

L,L-dilactide with PCL as the macroinitiator. Then, 31 g of PCL was dissolved in 150 mL of toluene and dried using a rotary evaporator. The PCL was then placed into a reaction flask with 10 g of L,L-dilactide under argon flux. The vessel was then heated to 140 °C using an oil bath. A 56 mg sample of $Sn(Oct)_2$ was added through a syringe at a concentration of 50 mg·mL^{-1} in dry THF solution. After 4 h, the reaction mixture was cooled and dissolved in 250 mL of chloroform. The reaction mixture was precipitated into methanol, resulting in a white precipitate, which was filtered through a glass filter with average pore size 10−16 μm and dried under vacuum. An 88% conversion of L,L-dilactide was determined by NMR measurements. The benzyl protective group was removed via a hydrogenation reaction. A 30 g sample of PLLA−PCL diblock copolymer was dissolved in 150 mL of THF and put into a Büchi ecoclave reactor. Then 300 mg Pd/C was added. The reaction was left for 36 h at 50 °C under a hydrogen atmosphere. The reaction mixture was precipitated into methanol, and the resulting white precipitate was filtered through a glass filter with average pore size 10−16 μm and dried under vacuum. The final multiblock copolymer was synthesized via self-polycondensation reactions of the PLLA−PCL diblock copolymers. Then 4 g of the multiblock copolymer was dissolved in 100 mL of toluene and dried using a rotary evaporator. The multiblock copolymer was then put into a reaction flask under argon and dissolved in DCM. Here, 8.8 g of DMAP, 35.2 g of DMAP·pTSA, and 85 mg of DIPC were added as DCM solutions. The reaction lasted 3 days at ambient temperature. The reaction mixture was diluted with 100 mL of DCM and precipitated into methanol giving a white precipitate, which was filtered and dried in vacuum. The PLLA−PCL multiblock copolymer used in the study was PLLA15-PCL64, where indexes stand for the average segment length in repeating units, as determined using NMR. The molecular structure of the synthesized multiblock copolymer is presented in Table S1. An exemplary NMR spectrum is presented in Figure S1.

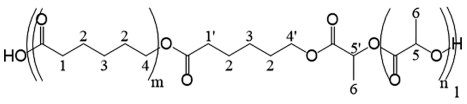

^{1}H NMR (500 MHz $CDCl_3$): δ = 5.15 (q, nH, CH-5); 5.1 (q, H, CH-5′); 4.15 (t, 2H, CH_2-4′); 4.05 (t, mH, CH_2-4′); 2.4 (t, 2H, CH_2-1′); 2.3 (t, mH, $CH_2$1); 1.65 (m, 4(m + 1)H, CH_2-2), 1.6 (d, 3(n + 1)H, CH_3-6), 1.4 (m, 2(m + 1)H, CH_2-3), where m + 1 and n + 1 are the number-average segment lengths of PCL and PLLA, respectively, in the PLLA−PCL multiblock copolymer, and l is the number-average count of PLLA−PCL diblock repeating units in the multiblock copolymer. Signals of the groups marked with a prime originate from monomer (PCL or PLLA) units having an opposite neighboring monomer unit (PLLA or PCL respectively) in the multiblock copolymer chain. m was determined as the ratio of the integral intensities of δ 2.3 and δ 2.4 peaks. n was determined as δ 5.15 and δ 5.1 maxima. The molar ratio of PLLA and PCL in the block copolymers was calculated as the ratio of the integral intensities of the signals in the δ 5−5.2 ppm and δ 5−5.2 ppm regions. To calculate the number-average molecular weight M_{NMR} of the diblock repeating units the ratios were then multiplied by the molecular weight M_{PLA} = 72 kg·mol^{-1} and M_{PCL} = 114 kg·mol^{-1}, respectively.

PDLA was synthesized via $Sn(Oct)_2$ catalyzed 1-hexanol-initiated ROP of D,D-dilactide. A series of PDLA samples with different molecular weight in the range M_n = 0.6−3.5 kg·mol^{-1} were achieved. The exemplary synthesis was performed as following: 15 g of D,D-dilactide was transferred to a closed reaction flask under an argon flow and heated to 140 °C with an oil bath. Then 2.1 g of 1-hexanol and 40 mg of $Sn(Oct)_2$ as a 50 mg·mL^{-1} dry THF solution were added through a syringe. After 45 min, the reaction mixture was cooled and dissolved in 20 mL of chloroform. Precipitation into cold methanol gave a white precipitate, which was filtered through a glass filter with average pore size 10−16 μm and dried under vacuum. A yield of 81% was recorded.

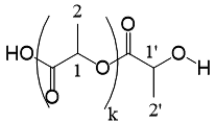

^{1}H NMR (500 MHz $CDCl_3$) δ = 5.15 (q, kH, CH-1); 4.35 (q, H, CH-1′); 1.6 (d, 3kH, CH_3-6), 1.4 (d, 3kH, CH_3-6′), where k + 1 is the number-average segment length of PDLA molecules. Signals of the groups marked with a prime originate from the monomer units located in the end of the polymer chain. k was determined as the ratio of the integral intensities of the signals in δ 5.15 and δ 4.35 regions. The number-average molecular weight M_{NMR} of PDLA was calculated by multiplication of the ratio of intergral intensities by the molecular weight M_{PLA} = 72 kg·mol^{-1} of a repeating unit.

Film Preparation. Films were prepared via solution casting. The components of the blend were dissolved in a predetermined ratio in chloroform. The solution was stirred for 3 h until the polymers were dissolved, before pouring into a PTFE Petri dish, covering with aluminum foil and left to evaporate in ambient conditions for several hours. Dog-bone-shape specimens (length 10 mm, width 3 mm, with an increased grip fixation area) were cut for mechanical testing. To reprocess a prepared sample into an alternative shape, the material was dissolved in chloroform and recast from solution into an alternative mold. Molds in the shape of a circle and triangle were used for the films prepared, shown in Figure 1c.

RESULTS AND DISCUSSION

Design, Synthesis, and Characterization of PLLA−PCL/PDLA Blends. The design of PLLA−PCL and PDLA aimed to maximize the actuation performance of the final blend material by optimizing the property-function ratio on a molecular level. As stated previously, two thermally distinct crystalline domains are required within the material for successful actuation, PCL crystallites to provide actuator and skeleton domains and PLA stereocomplex crystallites to provide the cross-links necessary to ensure the network structure. To prevent the crystallization of PLLA polymer segments before stereocomplexation, their length was reduced to an average segment length of 15 repeating units. This number was experimentally determined as the chain length of PLLA long enough for PLA stereocomplex formation, but too short for the solitary crystallization. While PLA homopolymers have been shown to undergo homocrystallization at average segment lengths of 7 repeating units,[24] the decreased flexibility of PLLA segments in a multiblock copolymer[25,26] explains the observed lack of homocrystallization in the material. For PCL, an average block length of approximately 60 repeating units was chosen to provide a sufficient amount of actuation force during temperature change. A list of prepared samples can be found in Table S1. Further increasing the average PCL segment length led to synthetic complications, originating from steric hindrance during knotting of the polymer chain, reducing the availability of hydroxyl groups during initiation of L,L-dilactide ring-opening polymerization.

GPC analysis (Figure S3) of PDLA homopolymers synthesized with lower number-average chain lengths (3, 6, and 9 repeating units as measured by NMR) showed an increase in polydispersity index ($Đ$) from 1.17 to 1.42 with a decrease in average chain length from 26 to 3 repeating units, as shown in Table S2. This increase of $Đ$, and the overall decrease of molecular weight, was undesirable in this study as it increased the proportion of PDLA homopolymer below the critical average chain length for stereocomplex formation of 7 repeating units as determined in the literature.[24] DSC measurements of samples prepared from PLLA15-PCL64

DOI: 10.1021/acs.biomac.9b01279
Biomacromolecules 2020, 21, 338−348

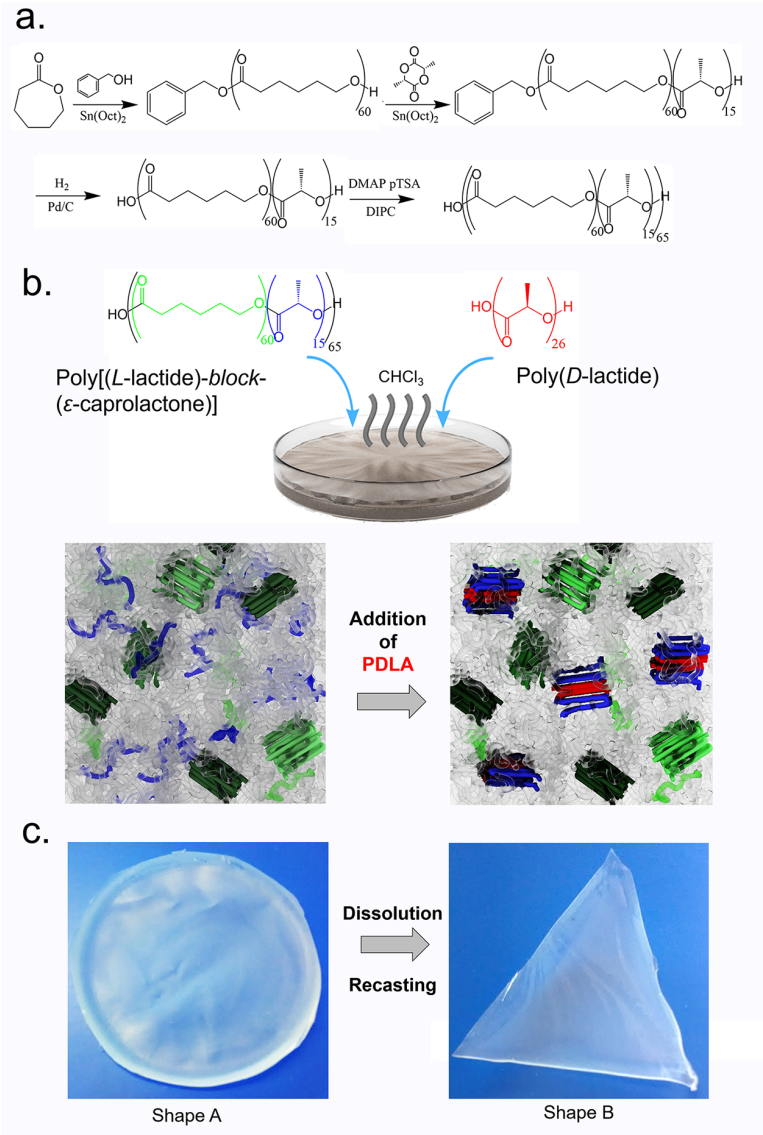

Figure 1. (a) Synthesis of multiblock copolymer containing poly(L-lactide) and poly(ε-caprolactone) segments (PLLA–PCL). Block lengths are number-average values obtained from ^{1}H NMR intergration. (b) Schematic illustrating PLLA–PCL/PDLA blend structural change upon addition of PDLA homopolymer component. PDLA homopolymer (red) and PLLA segments (blue) form PLA stereocomplex crystallites, which act as physical netpoints within the polymer matrix. Crystalline PCL segments of the multiblock copolymer provide skeleton domains (dark green) and actuation domains (light green). (c) Images showing the reprocessing of the blend material via dissolution of form A in chloroform, before using solution casting to generate form B.

Table 1. Thermal Properties of Blend Samples Containing PLLA15-PCL64-SC10 Multiblock Copolymer and PDLA Homopolymer as Measured by DSC

	PCL				PLA stereocomplex			
average PDLA chain length (repeating units)	T_m (°C)[a]	T_c (°C)[a]	ΔH (J·g^{-1})[b]	χ_c (%)[c]	T_m (°C)[a]	T_c (°C)[a]	ΔH (J·g^{-1})[b]	χ_c (%)[c]
3	53 ± 1	18 ± 1	38 ± 4	42 ± 4	130 ± 1	–	1.2 ± 0.1	4 ± 0.4
6	52 ± 1	15 ± 1	43 ± 4	46 ± 4	125 ± 1	–	6 ± 0.6	20 ± 2
9	54 ± 1	17 ± 1	28 ± 3	31 ± 3	148 ± 1	44 ± 1	6.5 ± 0.7	22 ± 2
26	42 ± 1	19 ± 1	34 ± 2	38 ± 2	171 ± 1	55 ± 1	10 ± 2	37 ± 2

[a]Melting and crystallization temperatures determined as the maximum of the respective peaks in the second heating and the first cooling runs. [b]Intrinsic melting enthalpy was determined as the area under the melting peak in the second heating run. [c]Degree of crystallinity, as the ratio between the intrinsic melting enthalpy ΔH_m and the melting enthalpy of a 100% crystalline material ΔH_m^{100}, which is 135 J·g^{-1} for PCL[33] and 142 J·g^{-1} for the PLA stereocomplex.[34]

DOI: 10.1021/acs.biomac.9b01279
Biomacromolecules 2020, 21, 338–348

Table 2. Thermal Properties of PLLA−PCL Multiblock Copolymer and its Blends with PDLA Homopolymer as Measured by DSC

	PCL				PLA stereocomplex			
sample	T_m[a] (°C)	T_c[a] (°C)	ΔH[b] (J·g^{-1})	χ_c[c] (%)	T_m[a] (°C)	T_c[a] (°C)	ΔH[b] (J·g^{-1})	χ_c[c] (%)
PLLA15-PCL64	52 ± 1	13 ± 1	41 ± 4	35 ± 4	–	–	–	–
PLLA15-PCL64-SC1	53 ± 1	15 ± 1	42 ± 4	44 ± 4	172 ± 1	–	1 ± 0.1	35 ± 2
PLLA15-PCL64-SC2	51 ± 1	16 ± 1	47 ± 5	48 ± 5	171 ± 1	51 ± 1	1.9 ± 0.2	28 ± 2
PLLA15-PCL64-SC3	52 ± 1	18 ± 1	36 ± 4	33 ± 3	176 ± 1	59 ± 1	5.9 ± 0.6	71 ± 7
PLLA15-PCL64-SC4	52 ± 1	20 ± 1	29 ± 3	27 ± 3	174 ± 1	61 ± 1	6.5 ± 0.7	58 ± 6
PLLA15-PCL64-SC5	49 ± 1	16 ± 1	39 ± 4	41 ± 4	176 ± 1	49 ± 1	8.5 ± 0.8	60 ± 3
PLLA15-PCL64-SC10	43 ± 1	20 ± 1	37 ± 4	41 ± 4	178 ± 1	78 ± 1	15 ± 2	56 ± 6

[a]Melting and crystallization temperatures determined as the maximum of the respective peaks in the second heating and the first cooling runs. [b]Intrinsic melting enthalpy was determined as the area under the melting peak in the second heating run. [c]Degree of crystallinity, as the ratio between the intrinsic melting enthalpy ΔH_m and the melting enthalpy of a 100% crystalline material ΔH_m^{100}, which is 135 J·g^{-1} for PCL[33] and 142 J·g^{-1} for the PLA stereocomplex.[34]

and PDLA homopolymers with average chain lengths of 3, 6, and 9 repeating units revealed a decrease in PLA stereocomplex crystallinity from 37 ± 2% at an average chain length of 26 repeating units to 4 ± 0.4% at an average chain length of 3 repeating units as shown in Table 1. WAXS measurements indicated stereocomplex formation at PDLA average chain lengths of 6, 9, and 26 repeating units but revealed no stereocomplex formation at a PDLA average segment length of 3 repeating units, as shown by the absence of 2θ = 11° reflection attributed to the PLA stereocomplex (Figure S4). DSC measurements (Figure S5) also revealed that the decrease of the PDLA number-average molecular weight M_n resulted in a reduction in the PLA stereocomplex melt transition maximum from 171 ± 1 to 125 ± 1 °C. Higher average chain lengths than 26 repeating units were experimentally found to reduce the miscibility of the PDLA with the copolymer, reducing the homogeneity of the stereocomplex formation, and increasing the formation of pure PLA crystallites. The high mobility of the low molecular weight PDLA component in solution encourages the formation of stereocomplex crystallites without the need for post processing, e.g., annealing. To maximize stereocomplex crystallinity and retain the high PDLA miscibility associated with low molecular weights, the molecular weight of PDLA was fixed at M_n = 1.9 kg·mol^{-1} or an average chain length of 26 repeating units for the following experiments.

A targeted number-average molecular weight of 200 kg·mol^{-1} was chosen for the copolymer for the following reasons: the stereocomplex, which acts as the physical cross-links of the polymer network, can be destroyed at high deformations of the material during shape-memory effect (SME) programming. While some elongation-induced crystallization is caused by this deformation, the overall loss in network anisotropy hinders the orientated crystallization needed for rbSME. However, some crystal sliding, which causes stereocomplex destruction, is an inevitable process with some stereocomplex crystallites destroyed and reformed. To reduce the effect of this process, the amount of cross-links, i.e., stereocomplex crystallites, per molecule should be increased. This reduces the chance that a certain polymer chain will lose orientational information upon the loss of cross-linking within the material. To increase the amount of stereocomplex crystals per molecule, without changing the blend composition, the chain length of the copolymer must be increased. This molecular weight increase leads to an improved deformability of the material, a higher obtainable molecular orientation, and higher ε_{rev}' values. The multiblock copolymer was produced with a block length and number-average molecular weight measured as PLLA15-PCL64 M_n = 238 kg · mol^{-1}, as shown in Table S1.

With increasing PDLA homopolymer weight content, excess material unable to form a stereocomplex generates pure PDLA crystallites, causing the appearance of additional PLA crystallinity. Decreasing the PDLA content to an equal or lower amount than the PLLA provided by the copolymer removes the pure PDLA crystallinity. This is caused by the energetic preference for PDLA to form stereocomplex over pure crystallites.[34] The highest absolute PLA stereocomplex crystallinity was observed in the PLLA15-PCL64-SC10 sample. Samples with a lower PDLA content were investigated here to minimize any nonstereocomplex associated PLA crystallization. As a result of the low block length of the PLLA segment of the multiblock copolymer, PLLA polymer unoccupied by stereocomplexation with PDLA remained in an amorphous state in the polymer matrix.

The reprocessability of the PLLA−PCL/PDLA physically cross-linked matrix was demonstrated by recasting a film after initial shape formation. The PLA stereocomplex in the PLLA−PCL/PDLA blends were found to be soluble in chloroform, likely as a result of the low molecular weight of its constituents (an average segment length of 15 repeating units for the PLLA segments and average chain length of 26 repeating units for the PDLA oligomer). During this process, the physical network is destroyed and reformed during solvent evaporation with the complete loss of mechanical information within the material. Images of the initial shape and the recasted one are presented in Figure 1c. The WAXS spectra and the DSC curves of the initial and the recasted material are presented in Figure S6. The cross-link density, i.e., stereocomplex crystallite content, was varied by alteration of the ratio of PLLA−PCL/PDLA in the blend. At high molecular weights (M_n > 200 kg mol^{-1}) chain entanglement can affect the mechanical properties of the physically cross-linked matrix. At 70 °C, the PCL crystals are completely molten (Table 2, Figure 2 and Figure S8) and the mechanical strength is derived solely from the PLA stereocomplex and chain entanglement. As expected, the mechanical strength of a sample was found to be dependent on the PLA stereocomplex content of the blend (Figure S9), and at this temperature, the pure PLLA−PCL possessed no mechanical strength. Hence, the contribution of molecular entanglement to the mechanical properties of the samples was deemed to be negligibly low.

DOI: 10.1021/acs.biomac.9b01279
Biomacromolecules 2020, 21, 338−348

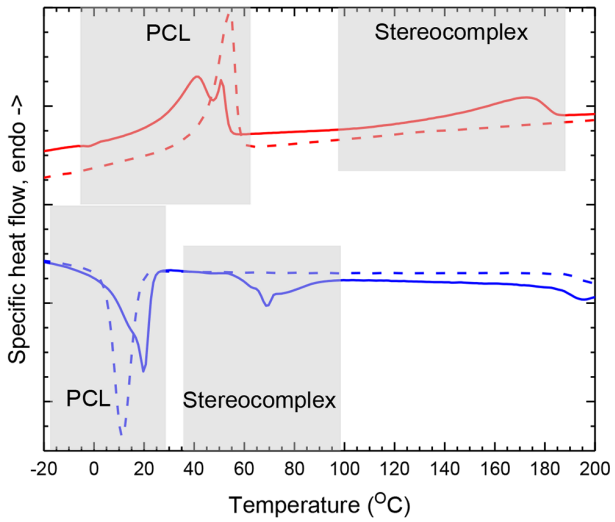

Figure 2. DSC thermograms of samples PLLA15-PCL64 (dashed line) and PLLA15-PCL64-SC10 (solid line) obtained from second heating (red) and first cooling (blue) run.

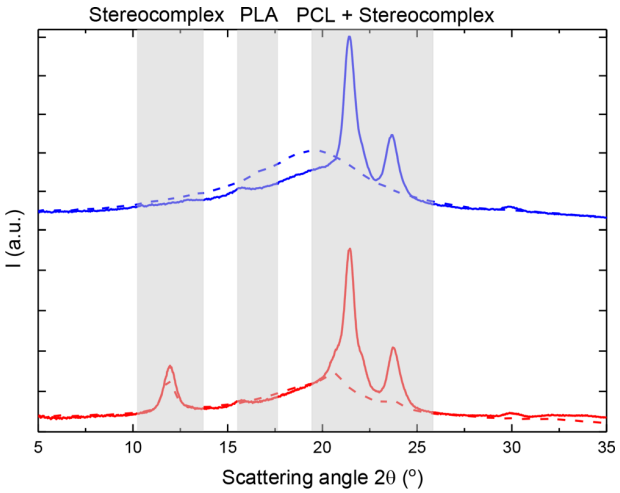

Figure 3. WAXS profiles of PLLA15-CL64 (blue) and PLLA15-CL64-SC10 (red) obtained at 25 °C (solid line) and at 70 °C (dashed line).

Polylactide Stereocomplex Formation in PLLA−PCL/PDLA Blends. Thermophysical data for the analyzed samples are shown in Table 2. The obtained DSC curves for sample PLLA15-PCL64 (Figure 2 and Figure S8) displayed a melting transition with a maximum at 52 ± 1 °C, attributed to PCL. This supports the assumption that the LLA segments of the PLLA−PCL copolymer (with a number-average segment length of 15 repeating units) are too short to undergo isotactic crystallization. A sample from the blended material, PLLA15-PCL64-SC10, displayed a melting temperature range of approximately 100−180 °C with a peak maximum at T_m = 171 ± 1 °C, attributed to PLA stereocomplex, with a melting enthalpy ΔH corresponding to a relative crystallinity of χ_c = 37 ± 2%. The lower measured melting temperature of the PLA stereocomplex, when compared to literature data (>200 °C),[34] is likely the result of the relative short length of the PLA molecules involved in its formation. Data obtained for the sample PLLA15-PCL64-SC10, displayed a decrease in the T_m attributed to PCL crystallites to 42 ± 1 °C with a melt temperature range of approximately 38−58 °C. This is likely the result of interactions between the PLA stereocomplex and PCL crystallites within PLLA−PCL. However, the material's χ_c remained at the same level of 38 ± 2%, demonstrating a sufficient amount of PCL for actuation.

WAXS was used to further elucidate the crystalline structure of the material at two temperatures: 25 and 70 °C. (Figure 3 and Figure S7) At higher temperatures the PCL is molten according to the obtained DSC data (Figure 2 and Figure S8). Nonblended samples, such as PLLA15-PCL64, display signals attributed to PCL (110) and (200) scattering in the region 2θ = 21.5° and 2θ = 24° respectively. At 70 °C, only an amorphous halo can be observed for this material. The measured PCL signals overlap with the scattering from PLA stereocomplex (300), (030) planes at 2θ = 20.5° and (220) at 2θ = 24°. A free-standing (110) PLA stereocomplex maximum at 2θ = 12° is an indicator of its presence at 25 °C. The blend PLLA15-PCL64-SC10 retains a 12° signal at 70 °C, while the molten PCL in the other samples made identification of the signals at 20.5° and 24° difficult. Changes in the crystalline structure of the materials between 25 and 70 °C demonstrate that the PDLA generates a thermostable physically cross-linked matrix.

AFM phase images revealed the presence of hard crystalline areas at room temperature for both PLLA−PCL multiblock copolymers and its blends with 10 wt.% of PDLA (Figure S10). The blend sample displayed more hard areas than the pure PLLA−PCL, due to the presence of additional stereocomplex crystallites. Heating to 70 °C caused a complete disappearance of the hard crystals in the PLLA−PCL. In the blend sample at 70 °C (Table 2; DSC curves are shown in Figure 2 and Figure S8), crystallinity was observed that, due to the absence of crystalline PCL, can only originate from the PLA stereocomplex. PCL crystallinity was restored after cooling the samples to 10 °C.

Actuation Capability. The rbSME performance of a material is dependent on the function of certain key structural units within the polymer matrix. Within the samples presented here, the PLA stereocomplex acts as the physical netpoints of the matrix, providing structural stability and preventing polymer slippage on deformation. By choosing a transition temperature that bisects the PCL crystallite population, it can provide both actuator and skeleton domains. The higher melting fractions stay crystallized, providing the skeleton domain, and maintain network anisotropy with the polymer matrix. The PCL fractions with a lower T_m function as actuator domains, whose melting and crystallization provide the driving force for reversible macroscale shape change. The conceptual schematics of the supramolecular structure transformations during the actuation is depicted in Figure 4a.

The dependency of actuation performance on the programming strain ε_{prog} was investigated for the PLLA15-PCL64-SC1 sample using uniaxial tensile testing. The obtained results are summarized in Table 3. While an increase in the measured value of ε_{rev}' from 11% to 12.6% was observed with a decrease of ε_{prog} from 1250% to 500%, the error values obtained for these measurements (1.3−1.5%) prevent us from inferring a relationship between programming strain and ε_{rev}'. rbSME experiments where ε_{prog} was varied in the range of 1000 to 500% for samples PLLA15-PCL64-SC10, PLLA15-PCL64-SC2, PLLA15-PCL64-SC3, PLLA15-PCL64-SC4, and PLLA15-PCL64-SC5 also showed no correlation between

DOI: 10.1021/acs.biomac.9b01279
Biomacromolecules 2020, 21, 338−348

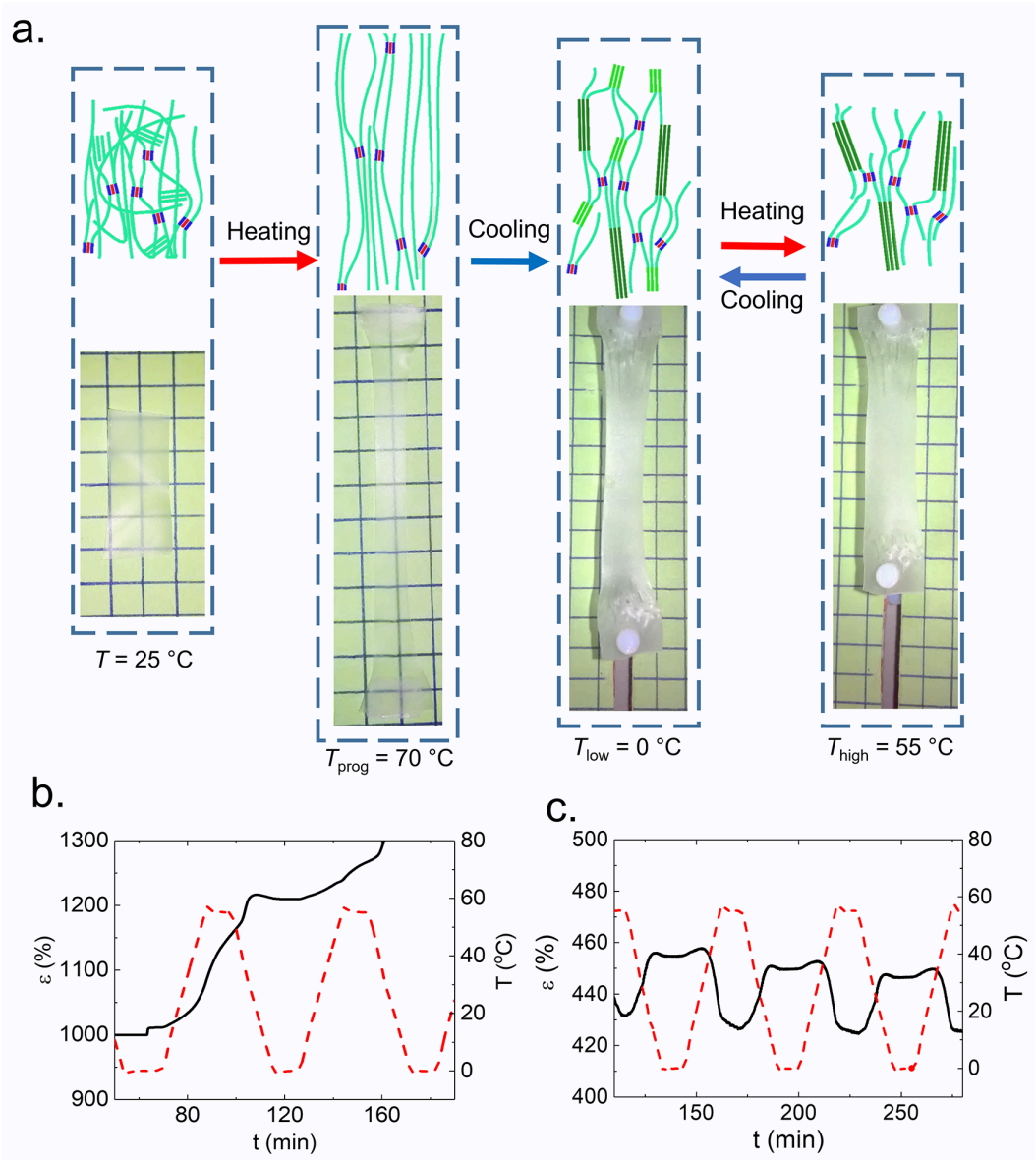

Figure 4. (a) (Top) Schematic illustration of structural changes within PLLA−PCL multiblock copolymer blends during actuation. The orientation of the polymer chains is kept by the PCL skeleton domains (dark green) while the network is cross-linked by PLA stereocomplex (blue − PLLA, red − PDLA). Crystallization and melting of the PCL actuator domains (light green) drives the actuation. (a) (Bottom) Image series showing shape change of a film sample during programming and actuation with no external stress applied. (b) rbSME curves of PLLA15-PCL64 and (c) PLLA15-PCL64-SC10 as measured by cyclic thermomechanical testing. The black line shows the strain change during the experiment as the sample is exposed to a cyclic temperature change (red dotted line).

ε_{prog} and ε_{rev}' (Table S3). At ε_{prog} = 300% no rbSME was observed. We propose that here the variation in deformation mechanism in different strain regions plays an important role. Literature reports have demonstrated that a semicrystalline polymeric material undergoes structural changes upon tensile deformation in a series of different deformation modes.[35,36] This restructuring follows different mechanisms depending on the applied strain. At the lowest elongation the deformation is purely elastic and the crystallites undergo no structural changes. Furthermore, before the elastic limit, crystalline sliding takes place in a random manner, and with increase of the strain over the elastic limit, this movement becomes coordinated. An increase in strain beyond this point causes crystalline lamellae fragmentation through fibrillation, which can be observed as strain hardening. At the highest deformation the amorphous network disentangles and the material loses any memory of the initial structure. The deformation mechanism of stereocomplex containing blends will be studied at greater length in following work. A programming strain of ε_{prog} = 1000% was chosen for further experiments.

As the PCL segments provide both the skeleton and the actuator domains, the skeleton/actuator ratio can be varied by modifying the temperature profile of the rbSME process.[7] In contrast to material systems where geometry-determining and actuation domains have different chemistry and structure, the

DOI: 10.1021/acs.biomac.9b01279
Biomacromolecules 2020, 21, 338−348

Table 3. Measurement of ε_{rev}' in PLLA−PCL Blend Samples with Variation of Weight Content of PDLA Homopolymer and Programming Strain ε_{prog}

sample	ε_0[a] (%)	χ_c stereocomplex[b] (%)	stereocomplex content[c] (wt %)	ε_{rev}'[d] (%)
PLLA15-PCL64-SC10	1000	37 ± 2	7.5 ± 0.2	5.3 ± 0.5
PLLA15-PCL64-SC5	1000	60 ± 3	6 ± 0.2	7.7 ± 0.5
PLLA15-PCL64-SC4	1000	58 ± 6	5 ± 0.3	10 ± 0.7
PLLA15-PCL64-SC3	1000	71 ± 7	3.1 ± 0.2	13.4 ± 1.5
PLLA15-PCL64-SC2	1000	28 ± 2	1.1 ± 0.1	12 ± 1.2
PLLA15-PCL64-SC1	1250	35 ± 2	0.7 ± 0.1	11 ± 1.5
PLLA15-PCL64-SC1	1000	35 ± 2	0.7 ± 0.1	11.4 ± 1.5
PLLA15-PCL64-SC1	750	35 ± 2	0.7 ± 0.1	11.8 ± 1.3
PLLA15-PCL64-SC1	500	35 ± 2	0.7 ± 0.1	12.6 ± 1.5

[a]Programming elongation used for shape-memory experiments. [b]Degree of crystallinity of PLA stereocomplex determined with DSC as a ratio of melting enthalpy of PLA stereocomplex (integral intensity of the melting peak) to the melting enthalpy of 100% crystalline PLA stereocomplex ΔH_m^{100} = 142 J·g^{-1} normalized by the PLA content in the blend (Table 1).[30] [c]Calculated from the melting enthalpy of PLA stereocomplex and PLA content of the blends as measured by DSC. [d]Actuation performance measured in the shape-memory experiments, as calculated from $\varepsilon_{rev}' = \frac{l_b - l_a}{l_a} \times 100\% = \frac{\varepsilon_b - \varepsilon_a}{\varepsilon_a + 100} \times 100\%$, where l_a and ε_a are the length of the sample and its engineering strain at the beginning of the actuation cycle at T_{high} and l_b and ε_b are the length of the sample and its engineering strain at the beginning of the actuation cycle at T_{low}.

variation of skeleton/actuator ratio in the described PLLA−PCL/PDLA blends can be performed by modifying T_{high} of a rbSME. To determine the optimum T_{high} an actuation cycle was conducted between T_{low} = 0 °C and a T_{high} which was raised between 50 and 100 °C in 5 °C increments for each consequent cycle with sample PLLA15-PCL64-SC10. The cycle with the highest ε_{rev}' was used to determine the T_{high} value used in subsequent experiments. The highest value of ε_{rev}', 7.9 ± 0.5%, was measured for the sample PLLA15-PCL64-SC10 at T_{high} = 55 °C (Figure S11). As a result the temperature range for each actuation cycle was set as 0−55 °C. The actuation performance of PLLA−PCL/PDLA blend samples was measured over three cycles. The mixed glass transition of the multiblock copolymer was determined by DMTA as T_g = −40 ± 3 °C for all samples. This transition lies outside of the rbSME temperature range and subsequently does not interfere with the actuation performance of our samples.

PLLA15-PCL64 samples without stereocomplexation show no rbSME (Figure 4b). Without stereocomplex crystallites the material is not able to generate sufficient network anisotropy on deformation. However, samples blended with PDLA (PLLA15-PCL64-SC10) display a sustained actuation performance (Figure 4c), due to the presence of PLA stereocomplex induced cross-linking. The shape transformation of an axially programmed PLLA15-PCL64-SC10 strip during programming and actuation is shown in Figure 4a.

To determine the dependency of ε_{rev}' on the molecular weight of the PDLA homopolymer component of the blends, cyclic thermomechanical testing was performed on blend samples containing PDLA homopolymer with average chain lengths of 3, 6 and 9 repeating units as determined by NMR. Testing revealed that the variation in actuation performance ε_{rev}' with the reduction of PDLA homopolymer average chain length from 26 to 7 repeating units was below the margin of error calculated $\Delta\varepsilon_{rev}'$ = 1.5% for the measurements. However, samples prepared from PDLA homopolymer with an average segment length of 3 showed no actuation capability, consistent with the relatively low stereocomplex crystallinity value, 4 ± 0.4%, obtained in DSC measurements of this sample.

A reduction of PDLA weight content in the blends was observed to lead to an increase of ε_{rev}'. With the decrease of PDLA26 in the matrix from 10 wt % to 1 wt % the ε_{rev}' increased from 5.9 ± 0.5% to 12.5 ± 0.5%, where the stereocomplex content was measured using DSC. The observed effect can be understood in comparison with traditional covalently cross-linked rbSME-matrices, where the actuation performance is highly dependent on the cross-link density. If the cross-link density of the network is too high, deformation causes breakage of the intermolecular interactions providing cross-linking before a change in molecular orientation occurs. If the cross-link density is too low, deformation of the material causes slippage of the polymer chains without a corresponding change in molecular orientation. At large number-average molecular weights (M_n > 200 kg·mol^{-1}) and a number-average molecular weight of the PLLA−PCL diblock repeating unit of approximately 8 kg·mol^{-1} (average block lengths of 64 hydroxyhexanoate repeating units and 15 L-lactide repeating units), a stereocomplex content of 0.8 ± 0.1 wt % was sufficient to ensure a rbSME.

Changing the weight ratio of PLLA−PCL and PDLA in the blends directly leads to the variation of PLA stereocomplex content. The effect of PLA stereocomplex crystallite content, i.e., cross-linking density, on the magnitude of the rbSME in experiments with identical programming parameters (ε_0 = 1000%, T_{prog}= 70 °C) is shown in Figure 5. rbSME performance increased with an increase in PLA stereocomplex concentration to a content of 3.1 ± 0.2 wt %, after which a drop off of ε_{rev}' is observed.

CONCLUSION

In this paper, we demonstrate how the stereocomplexation of a poly(L-lactide) and poly(ε-caprolactone) (PLLA−PCL) multiblock copolymer with a poly(D-lactide) oligomer (PDLA) can be used to provide anchoring points for physical network formation. The ability to introduce physical cross-linking via a blending process enabled the efficient variation of mechanical properties of a shape-memory actuator. Cyclic thermomechanical testing was used to investigate the effect of blend composition on the actuation performance of the material, with a maximum actuation performance of ε_{rev}' = 13.4 ± 1.5% measured. This method, capable of the realization of such actuation behavior in a reprocessable material, presents significant advantages over similar shape-changing materials, which are often limited to a single postprocessing form. With

DOI: 10.1021/acs.biomac.9b01279
Biomacromolecules 2020, 21, 338−348

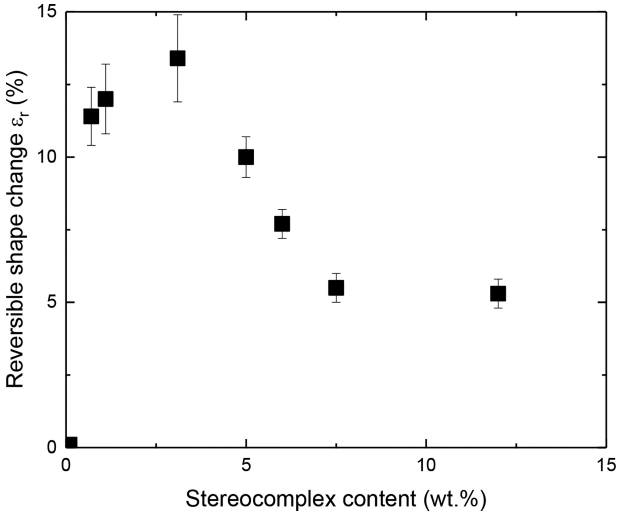

Figure 5. Reversible shape change (ε_{rev}') of PLLA−PCL/PDLA blend samples with varying PLA stereocomplex content. ε_{rev}' was determined using cyclic thermomechanical testing; stereocomplex content was determined by DSC.

this work, we demonstrate a powerful and efficient method to modify material composition, and subsequent mechanical behavior, without the synthetic modification of polymer architecture. Such methods to adjust the network structure of physically cross-linked materials through *in situ* processing should provide a platform for the creation of low cost reconfigurable devices in robotics and biomedicine.

■ ASSOCIATED CONTENT

Supporting Information

The Supporting Information is available free of charge at https://pubs.acs.org/doi/10.1021/acs.biomac.9b01279.

Figure S1, NMR spectra of PLLA15-PCL64 multiblock copolymer; Table S1, molecular structure of PLLA15-PCL64; Figure S2, schematic illustrating thermomechanical treatment procedure; Figure S3, molecular weight distributions of PDLA oligomers; Figure S4, WAXS spectra of blend samples containing PLLA15-PCL64-SC10; Figure S5, DSC traces of blend samples containing PLLA15-PCL64-SC10; Table S2, molecular structure of PDLA; Figure S6, WAXS spectra and DSC traces of PLLA15-PCL64-SC10; Figure S7, WAXS profiles of PLLA15-PCL64-SCX at 25 °C; Figure S8, DSC traces of PLLA15-PCL64-SCX; Figure S9, stress−strain curves of PLLA−PCL−PDLA blends; Figure S10, AFM phase images of sample blends; Table S3, effect of ε_{prog} variation on ε_{rev}'; and Figure S11, RbSME in PLLA15-PCL64-SC10 with T_{high} variation (PDF)

■ AUTHOR INFORMATION

Corresponding Author

*(A.L.) E-mail: andreas.lendlein@hzg.de.

ORCID

Oliver E. C. Gould: 0000-0002-8034-5724

Andreas Lendlein: 0000-0003-4126-4670

Notes

The authors declare the following competing financial interest(s): A.L. and K.K are co-inventors on patent applications in the field of PLA stereocomplexes.

■ ACKNOWLEDGMENTS

This work was financially supported by the Helmholtz-Association of German Research Centers (through programme-oriented funding, and through the Helmholtz Graduate School of Macromolecular Bioscience [MacroBio], grant no. VH-GS-503). The authors thank Ms. Susanne Schwanz for the WAXS and DSC measurements and Ms. Manuela Keller for the AFM experiments.

■ REFERENCES

(1) Yoshida, R.; Uchida, K.; Kaneko, Y.; Sakai, K.; Kikuchi, A.; Sakurai, Y.; Okano, T. Comb-type grafted hydrogels with rapid deswelling response to temperature changes. *Nature* **1995**, *374*, 240−242.

(2) Yuk, H.; Lin, S.; Ma, C.; Takaffoli, M.; Fang, N. X.; Zhao, X. Hydraulic hydrogel actuators and robots optically and sonically camouflaged in water. *Nat. Commun.* **2017**, *8*, 1−12.

(3) Yew, Y. K.; Ng, T. Y.; Li, H.; Lam, K. Y. Analysis of pH and electrically controlled swelling of hydrogel-based micro-sensors/actuators. *Biomed. Microdevices* **2007**, *9*, 487−499.

(4) Lagerwall, J. P. F.; Scalia, G. A new era for liquid crystal research: Applications of liquid crystals in soft matter nano-, bio- and microtechnology. *Curr. Appl. Phys.* **2012**, *12*, 1387−1412.

(5) Yu, H.; Ikeda, T. Photocontrollable liquid-crystalline actuators. *Adv. Mater.* **2011**, *23*, 2149−2180.

(6) Kularatne, R. S.; Kim, H.; Boothby, J. M.; Ware, T. H. Liquid crystal elastomer actuators: Synthesis, alignment, and applications. *J. Polym. Sci., Part B: Polym. Phys.* **2017**, *55*, 395−411.

(7) Behl, M.; Kratz, K.; Zotzmann, J.; Nöchel, U.; Lendlein, A. Reversible bidirectional shape-memory polymers. *Adv. Mater.* **2013**, *25*, 4466−9.

(8) Lendlein, A. Fabrication of reprogrammable shape-memory polymer actuators for robotics. *Sci. Robot.* **2018**, *3* (18), No. eaat9090.

(9) Zhao, Q.; Qi, H. J.; Xie, T. Recent progress in shape memory polymer: New behavior, enabling materials, and mechanistic understanding. *Prog. Polym. Sci.* **2015**, *49*−*50*, 79−120.

(10) Hu, J.; Zhu, Y.; Huang, H.; Lu, J. Recent advances in shape-memory polymers: Structure, mechanism, functionality, modeling and applications. *Prog. Polym. Sci.* **2012**, *37*, 1720−1763.

(11) Lendlein, A.; Gould, O. E. C. Reprogrammable recovery and actuation behaviour of shape-memory polymers. *Nat. Rev. Mater.* **2019**, *4*, 116−133.

(12) Guo, Q.; Bishop, C. J.; Meyer, R. A.; Wilson, D. R.; Olasov, L.; Schlesinger, D. E.; Mather, P. T.; Spicer, J. B.; Elisseeff, J. H.; Green, J. J. Entanglement-Based Thermoplastic Shape Memory Polymeric Particles with Photothermal Actuation for Biomedical Applications. *ACS Appl. Mater. Interfaces* **2018**, *10*, 13333−13341.

(13) Gu, X.; Mather, P. T. Entanglement-based shape memory polyurethanes: Synthesis and characterization. *Polymer* **2012**, *53*, 5924−5934.

(14) Zhou, S.; Zheng, X.; Yu, X.; Wang, J.; Weng, J.; Li, X.; Feng, B.; Yin, M. Hydrogen bonding interaction of poly(D, L-lactide)/hydroxyapatite nanocomposites. *Chem. Mater.* **2007**, *19*, 247−253.

(15) Yan, W.; Rudolph, T.; Noechel, U.; Gould, O.; Behl, M.; Kratz, K.; Lendlein, A. Reversible Actuation of Thermoplastic Multiblock Copolymers with Overlapping Thermal Transitions of Crystalline and Glassy Domains. *Macromolecules* **2018**, *51* (12), 4624−4632.

(16) Dolog, R.; Weiss, R. A. Shape memory behavior of a polyethylene-based carboxylate ionomer. *Macromolecules* **2013**, *46*, 7845−7852.

(17) Lu, L.; Li, G. One-Way Multishape-Memory Effect and Tunable Two-Way Shape Memory Effect of Ionomer Poly(ethylene-

DOI: 10.1021/acs.biomac.9b01279
Biomacromolecules 2020, 21, 338−348

co-methacrylic acid). *ACS Appl. Mater. Interfaces* **2016**, *8*, 14812−14823.
(18) Gao, Y.; Liu, W.; Zhu, S. Polyolefin Thermoplastics for Multiple Shape and Reversible Shape Memory. *ACS Appl. Mater. Interfaces* **2017**, *9* (5), 4882−4889.
(19) Farhan, M.; Rudolph, T.; Nöchel, U.; Kratz, K.; Lendlein, A. Extractable free polymer chains enhance actuation performance of crystallizable poly(ε-caprolactone) networks and enable self-healing. *Polymers* **2018**, *10* (3), 255.
(20) Kolesov, I.; Dolynchuk, O.; Borreck, S.; et al. Morphology-controlled multiple one- and two- way shape-memory behavior of cross-linked polyethylene/poly(ε-caprolactone) blends. *Polym. Adv. Technol.* **2014**, *25* (11), 1315−1322.
(21) Tsuji, H.; Ikada, Y. Stereocomplex formation between enantiomeric poly (lactic acids). 9. Stereocomplexation from the melt. *Macromolecules* **1993**, *26*, 6918−6926.
(22) Tsuji, H. Poly(lactic acid) stereocomplexes: A decade of progress. *Adv. Drug Delivery Rev.* **2016**, *107*, 97−135.
(23) Yang, D. D.; Liu, W.; Zhu, H. M.; Wu, G.; Chen, S. C.; Wang, X. L.; Wang, Y. Z. Toward Super-Tough Poly(l-lactide) via Constructing Pseudo-Cross-link Network in Toughening Phase Anchored by Stereocomplex Crystallites at the Interface. *ACS Appl. Mater. Interfaces* **2018**, *10* (31), 26594−26603.
(24) de Jong, S. J.; van Dijk-Wolthuis, W. N. E. E.; Kettenes-Van Den Bosch, J. J.; Schuyl, P. J. W. W.; Hennink, W. E. Monodisperse Enantiomeric Lactic Acid Oligomers: Preparation, Characterization, and Stereocomplex Formation. *Macromolecules* **1998**, *31*, 6397−6402.
(25) Loo, Y. L.; Register, R. A.; Ryan, A. J. Polymer crystallization in 25-nm spheres. *Phys. Rev. Lett.* **2000**, *84* (18), 4120−3.
(26) Huang, P.; Zhu, L.; Cheng, S. Z. D.; Ge, Q.; Quirk, R. P.; Thomas, E. L.; Lotz, B.; Hsiao, B. S.; Liu, L.; Yeh, F. Crystal Orientation Changes in Two-Dimensionally Confined Nanocylinders in a Poly(ethylene oxide)-b-polystyrene/Polystyrene Blend. *Macromolecules* **2001**, *34* (19), 6649−6657.
(27) Lendlein, A.; Neuenschwander, P.; Suter, U. W. Hydroxy-telechelic copolyesters with well defined sequence structure through ring-opening polymerization. *Macromol. Chem. Phys.* **2000**, *201* (11), 1067−1076.
(28) Jikei, M.; Suga, T.; Yamadoi, Y.; Matsumoto, K. Synthesis and properties of poly(L-lactide-co-glycolide)-b-Poly(ε-caprolactone) multiblock copolymers formed by self-polycondensation of diblock macromonomers. *Polym. J.* **2017**, *49*, 369−375.
(29) Jikei, M.; Takeyama, Y.; Yamadoi, Y.; Shinbo, N.; Matsumoto, K.; Motokawa, M.; Ishibashi, K.; Yamamoto, F. Synthesis and properties of Poly(L-lactide)-Poly(ε-caprolactone) multiblock copolymers by the self-polycondensation of diblock macromonomers. *Polym. J.* **2015**, *47*, 657−665.
(30) Jikei, M.; Yamadoi, Y.; Suga, T.; Matsumoto, K. Stereocomplex formation of poly(L-lactide)-poly(ε-caprolactone) multiblock copolymers with Poly(D-lactide). *Polymer* **2017**, *123*, 73−80.
(31) Moore, J. S.; Stupp, S. I. Room temperature polyesterification. *Macromolecules* **1990**, *23*, 65−70.
(32) Perego, G.; Vercellio, T.; Balbontin, G. Copolymers of L- and D, L-lactide with 6-caprolactone: synthesis and characterization. *Makromol. Chem.* **1993**, *194*, 2463−2469.
(33) Crescenzi, V.; Manzini, G.; Calzolari, G.; Borri, C. Thermodynamics of fusion of poly-β-propiolactone and poly-ε{lunate}-caprolactone. comparative analysis of the melting of aliphatic polylactone and polyester chains. *Eur. Polym. J.* **1972**, *8*, 449−463.
(34) Tsuji, H. Poly(lactide) Stereocomplexes: Formation, Structure, Properties, Degradation, and Applications. *Macromol. Biosci.* **2005**, *5* (7), 569−597.
(35) Hiss, R.; Hobeika, S.; Lynn, C.; Strobl, G. Network Stretching, Slip Processes, and Fragmentation of Crystallites during Uniaxial Drawing of Polyethylene and Related Copolymers. A Comparative Study. *Macromolecules* **1999**, *32*, 4390−4403.
(36) Hong, K.; Rastogi, A.; Strobl, G. A model treating tensile deformation of semicrystalline polymers: Quasi-static stress-strain relationship and viscous stress determined for a sample of polyethylene. *Macromolecules* **2004**, *37*, 10165−10173.

DOI: 10.1021/acs.biomac.9b01279
Biomacromolecules 2020, 21, 338−348

Supporting information

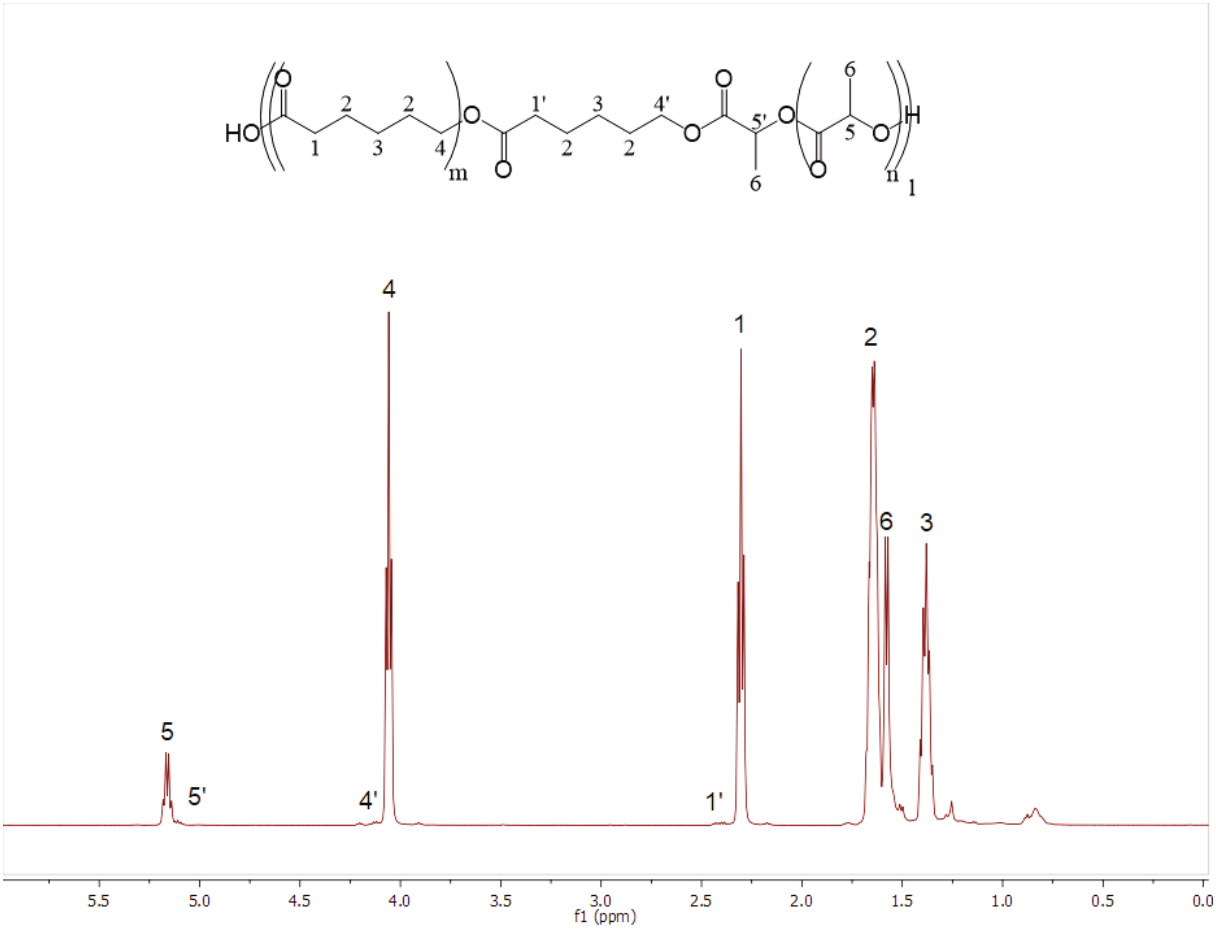

Figure S1. 500 MHz ^{1}H NMR spectra of PLLA15-PCL64 measured in $CDCl_3$ solution.

Table S1. Molecular structure of the reported PLLA-PLC and their precursors.

Sample[a]	M_{NMR}[b], kg·mol^{-1}	M_n[c], kg·mol^{-1}	M_w[c], kg·mol^{-1}	Đ[c]	PLA/ PCL[d]	PCL block length, repeat units[e]	PLA block length, repeat units[e]
PCL64	9.7	12	20	1.6	-	85	-
PLLA15-PCL64 diblock precursor	12.2	17	25	1.48	16/84	65	27
PLLA15-PCL64	-	238	483	2.03	17/83	64	15

[a] The sample name PLLAX-PCLY, where X indicates the PLLA average block length of the end product PLLA-PCL multiblock copolymer determined with ^{1}H-NMR and Y indicates the PCL number average block length of the end product PLLA-PCL multiblock copolymer determined with ^{1}H-NMR.

[b] Determined with ^{1}H-NMR as ratio of the integral intensity of a quadruplet in the 5.2 region attributed to CH-signal of a chain unit of PLLA segments and a quadruplet in the 4 ppm region attributed to PCL CH_2-signal of a chain unit (Figure S1) to the integral intensity of a quadruplet in 4.4 ppm region attributed to PLLA carboxyl end group for the block copolymer samples and a quadruplet in 3.8 ppm region attributed to PCL carboxyl end group for the PCL homopolymer. The ratios were then multiplied by the molecular weight M_{PLA} = 72 kg · mol^{-1} and M_{PCL} = 114 kg · mol^{-1} respectively.

[c] Number and weight-average molecular weight and polydispersity index. Determined with a multidetector GPC setup against universal calibration using tetrahydrofuran as eluent with a flow rate of 1 mL · min^{-1} equipped with a light scattering detector. Where Đ was calculated as a ratio of weight and number average molecular weight.

[d] Calculated from ^{1}H-NMR spectra as the ratio of the integral intensities of a quadruplet in the 5.2 region attributed to CH-signal of a chain unit of PLLA segments and a quadruplet in the 4 ppm region attributed to PCL CH_2-signal of a chain unit (Figure S1).

[e] Determined with ^{1}H-NMR as a ratio of the integral intensities (quadruplet in the 5.2 region attributed to CH-signal of a chain unit of PLLA segments and a quadruplet in the 4 ppm region attributed to PCL CH_2-signal of a chain unit (Figure S1)) of the main peak and its right or left shoulder for PLLA and PCL respectively. Where the main peak is attributed to the repeating units having the same neighbor and the shoulder having the same multiplicity is attributed to the repeating units having a different neighbor in the multiblock copolymer chain.

The error of GPC was considered as 10% of the measured value according to deviations in the calibration curve achieved for the machine with polystyrene standards.

The deviation of ^{1}H-NMR data was considered as combination of saturation effects, unevenness of the magnetic field in the sample and the line shape causing overlapping of the peaks. The last element has the highest input into the calculation error resulting total deviation of approx. 12%.

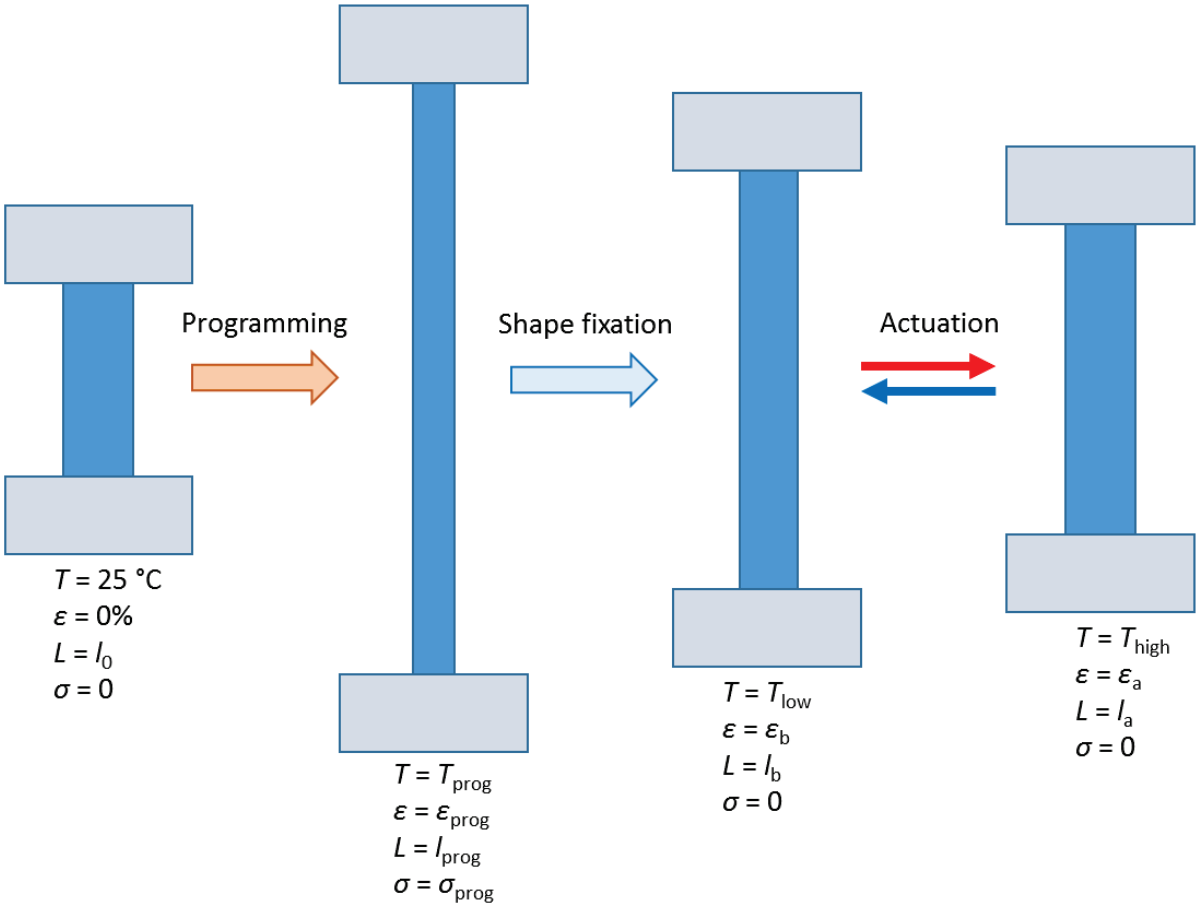

Figure S2. Schematic illustration of thermomechanical treatment in rbSME experiments. A dog-bone shaped sample is fixed in a tensile testing machine in an undeformed (no strain ε applied to the sample and its length $L = l_0$) not loaded state ($\sigma_0 = 0$) at the room temperature T = 25 °C. The sample is programmed by deformation at T_{prog} to the programming strain ε_{prog}. In the following step the shape is fixed by cooling the sample to T_{low} before reduction of the applied stress σ to 0. The actuation cycle is performed by subsequent changing the temperature in the thermo chamber of the tensile machine between T_{low} and T_{high}, which causes changes in sample length due to crystallization-induced elongation and melting-induced contraction.

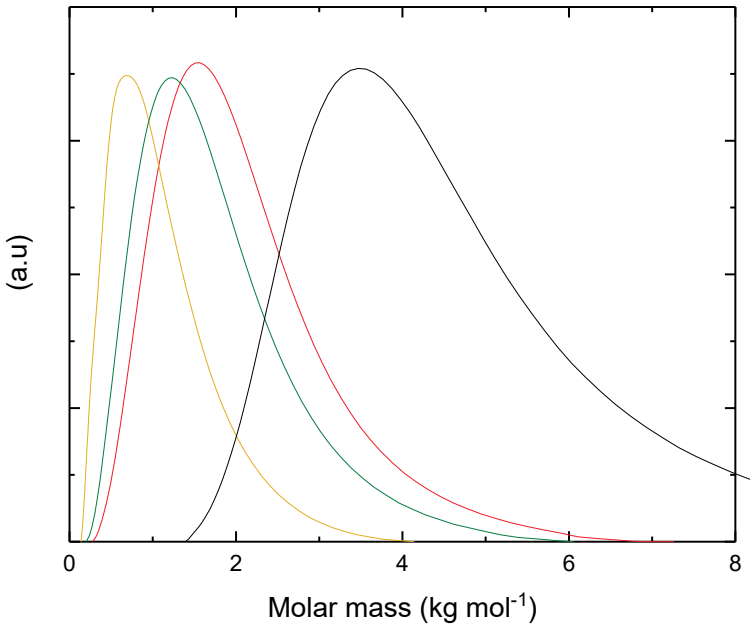

Figure S3. Molecular weight distributions of PDLA oligomers PDLA3 (yellow), PDLA6 (green), PDLA9 (red) and PDLA26 (black). Measurements were performed on a multidetector GPC setup against universal calibration in THF and an eluent flow rate of 1 mL·min^{-1}.

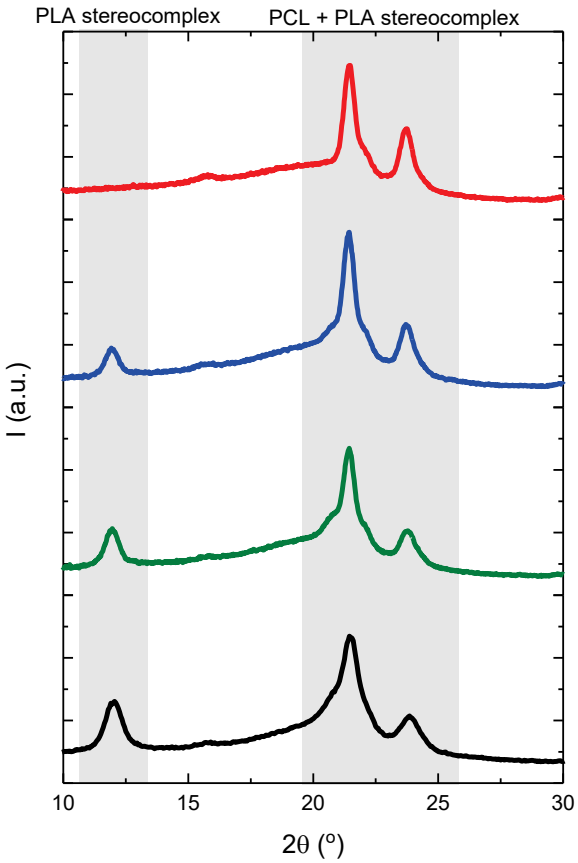

Figure S4. WAXS spectra at the ambient temperature of blend samples containing PLLA15-PCL64-SC10 multiblock copolymer with PDLA homopolymers of different number average lengths: 3 (red), 6 (blue), 9 (green) and 26 (black) repeating units determined with ^{1}H NMR.

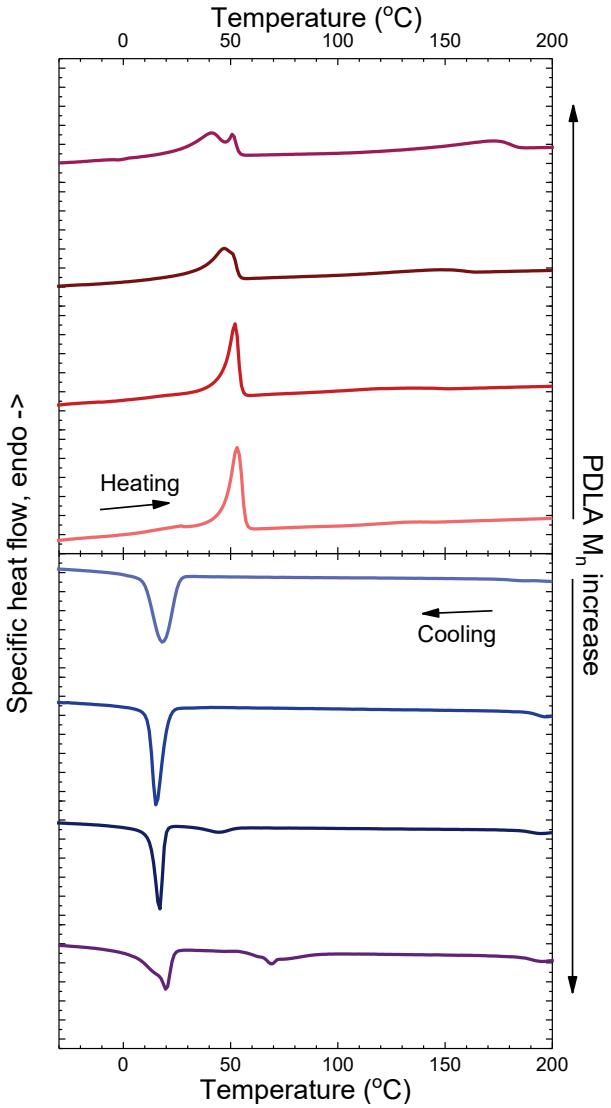

Figure S5. DSC traces of blend samples containing PLLA15-PCL64-SC10 multiblock copolymer with PDLA homopolymers of different number average lengths in order starting from the central x-axis: 3, 6, 9 and 26 repeating units determined with ^{1}H NMR. The second heating (red curves) and the first cooling (blue curves) runs at 10 °C heating/cooling rate.

Table S2. Average molecular weight and polydispersity of PDLA homopolymers.

Sample[a]	Segment length, repeating units[b]	M_n, kg · mol^{-1} [c]	M_w, kg · mol^{-1} [c]	Đ[c]
PDLA3	3	0.6	0.8	1.42
PDLA6	6	1	1.4	1.35
PDLA9	9	1.3	1.7	1.31
PDLA26	26	3.5	4.1	1.17

[a] The sample name PDLAX where X indicates the PDLA segment length determined with ^{1}H-NMR. [b] Determined with ^{1}H-NMR as ratio of the integral intensity of a quadruplet in the 5.2 region attributed to CH-signal of a chain unit of PDLA and a quadruplet in the 4.4 ppm region attributed to PLLA carboxyl end group. [c] Number and weight-average molecular weight and polydispersity index. Determined with GPC against universal calibration using tetrahydrofuran as eluent with a flow rate of 1 mL · min^{-1} equipped with a light scattering detector. Where Đ was calculated as a ratio of weight and number average molecular weight.

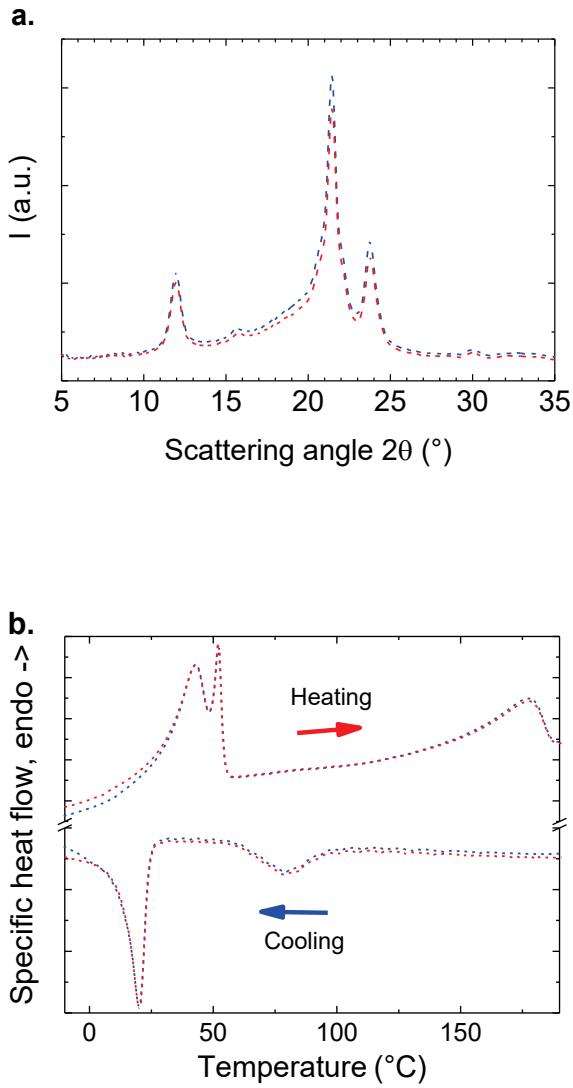

Figure S6. (a) WAXS spectra and (b) DSC traces of PLLA15-PCL64-SC10 initial sample (blue) and re-casted physical network (red), here the second heating and first cooling traces with 10 °C min^{-1} rates are shown.

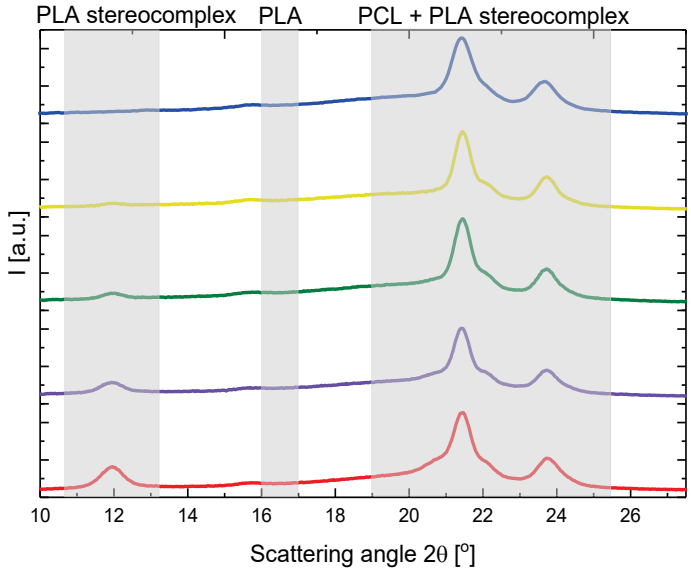

Figure S7. WAXS spectra of PLLA12-PCL58 (blue), PLLA15-PCL64-SC1 (yellow), PLLA15-PCL64-SC2 (green), PLLA15-PCL64-SC5 (purple) and PLLA15-PCL64-SC10 (red) at 25 °C

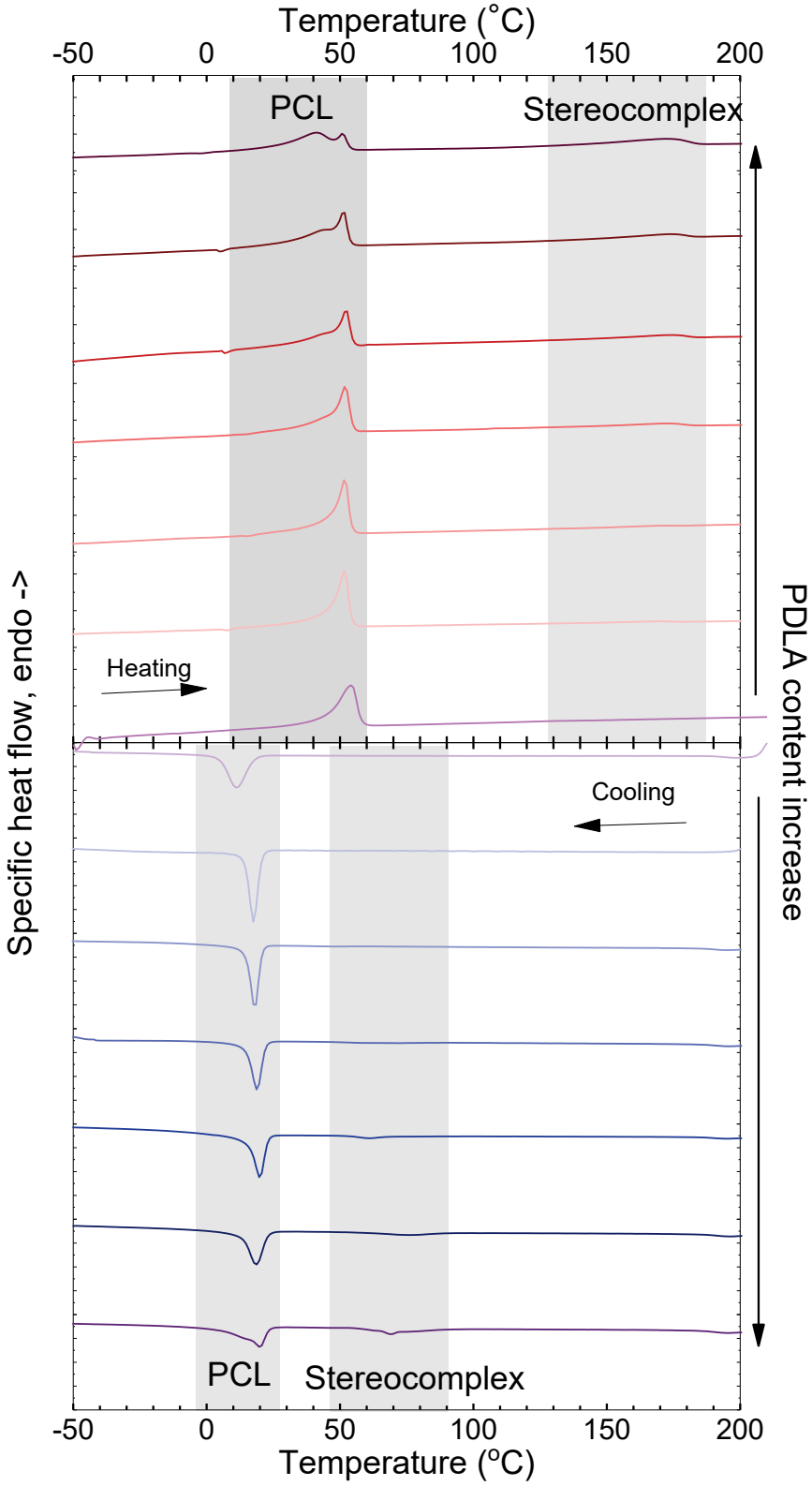

Figure S8. DSC traces of PLLA-PCL / PDLA blends with different PDLA content in order starting from the central x-axis: PLLA15-PCL64, PLLA15-PCL64-SC1, PLLA15-PCL64-SC2, PLLA15-PCL64-SC3, PLLA15-PCL64-SC4, PLLA15-PCL64-SC5, PLLA15-PCL64-SC10. The second heating and the first cooling runs at 10 °C heating/cooling rate.

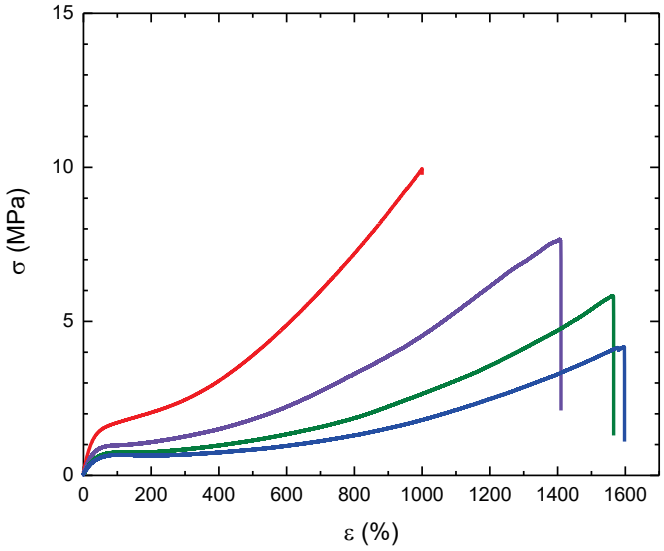

Figure S9. Stress-strain curves at 70 °C and deformation rate 5 mm min-[1] of PLLA15-PCL64 blended with different amounts of PDLA. Blue – PLLA15-PCL64-SC01, green – PLLA15-PCL64-SC02, purple PLLA15-PCL64-SC05, red – PLLA15-PCL64-SC10

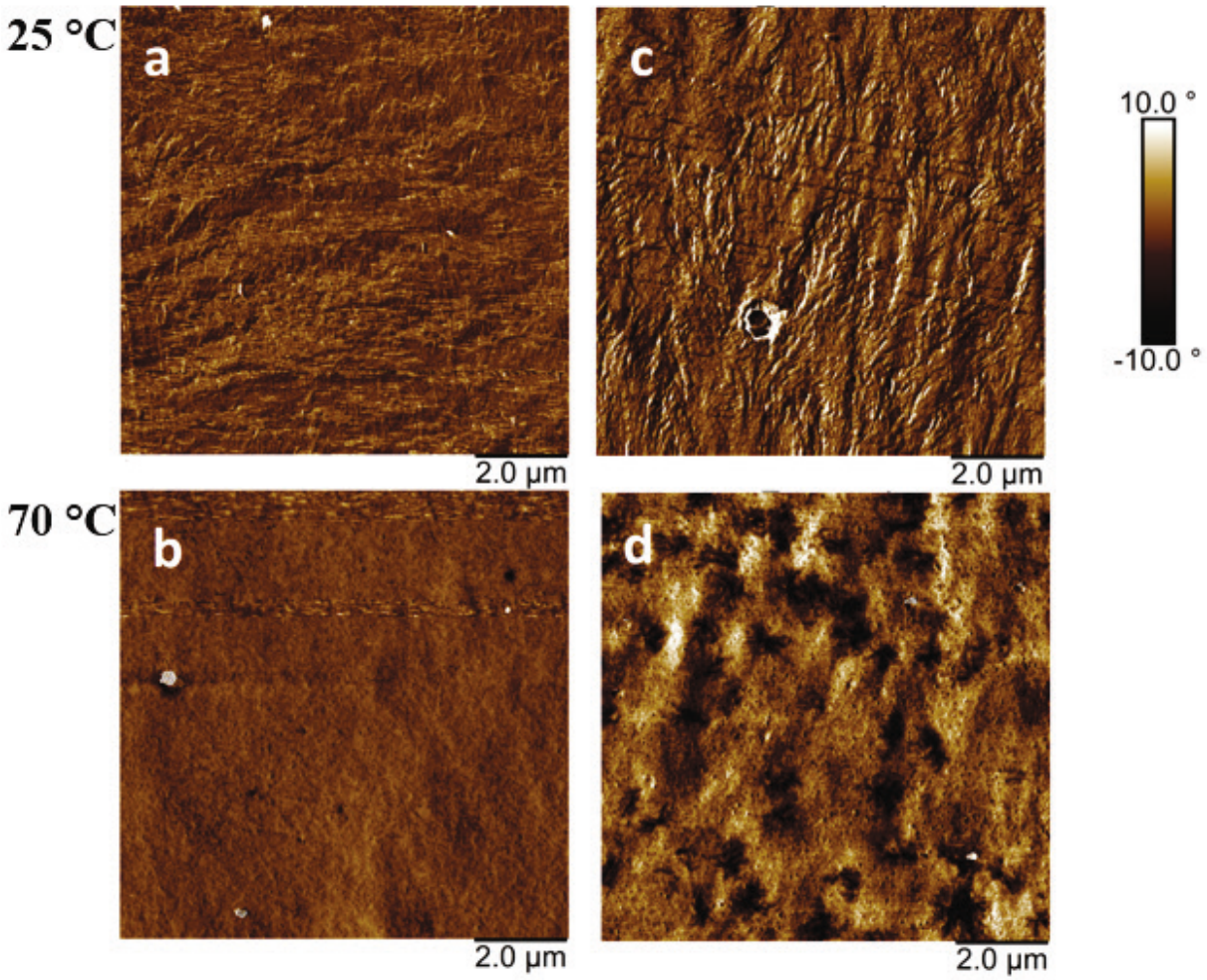

Figure S10. AFM phase image of PLLA-PCL multiblock copolymer at 25 °C (a) and 70 °C (b) and its blend with 10 wt.% of PDLA at 25 °C (c) and 70 °C (d)

Table S3. Effect of the programming strain ε_{prog}, on the actuation performance ε'_{rev} of PLLA-PCL / PDLA blends.

Sample name[a]	ε_{prog}, %[b]	ε'_{rev}, %[c]
PLLA15-PCL64-SC10	750	5.3±0.5
	1000	5.3±0.5
PLLA15-PCL64-SC5	500	8.9±1.2
	750	6.1±0.5
	1000	7.7±0.5
PLLA15-PCL64-SC2	500	10±1.5
	750	10±0.9
	1000	12±1.2
PLLA15-PCL64-SC1	500	12.6±1.5
	750	11.8±1.3
	1000	11.4±1.5
	1250	11±1.5

[a] The sample name LLAX-CLY-SCZ, where X and Y indicate the block length of PLLA and PCL respectively determined with ^{1}H-NMR, and Z indicates, the weight content of PDLA in the blend. [b] Programming elongation of the rbSME experiment. [c] Reversible actuation performance determined as the ratio of the change in the sample length in an actuation cycle to its length in the beginning of the cycle at T_{high}

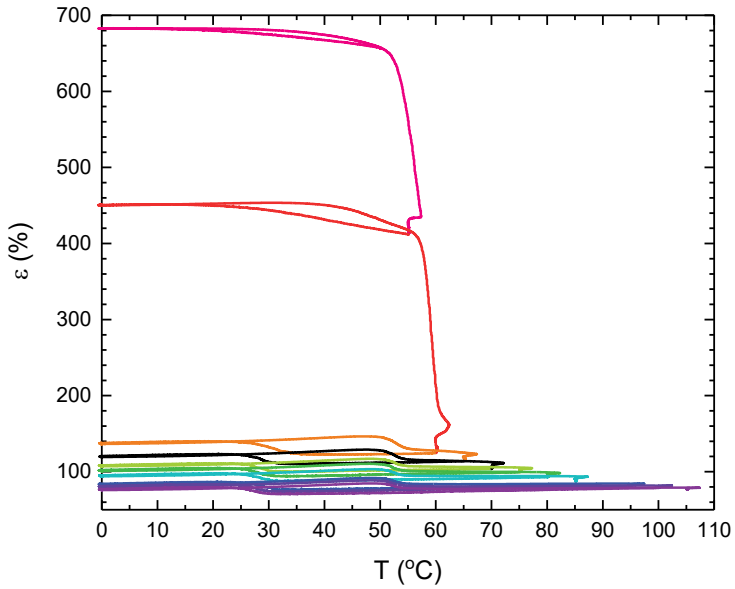

Figure S11. Reversible elongation change of PLLA15-PCL64-SC10 with a variation of T_{high}, as measured by cyclic thermomechanical testing.